Kinetics of the Degradation of Type 316 Stainless Steel by Liquid Lithium

D.G. Bauer

June 1980

UWFDM-363

Ph.D. thesis.

FUSION TECHNOLOGY INSTITUTE

UNIVERSITY OF WISCONSIN

MADISON WISCONSIN

Kinetics of the Degradation of Type 316 Stainless Steel by Liquid Lithium

D.G. Bauer

Fusion Technology Institute
University of Wisconsin
1500 Engineering Drive
Madison, WI 53706

http://fti.neep.wisc.edu

June 1980

UWFDM-363

Ph.D. thesis.

KINETICS OF THE DEGRADATION OF TYPE 316 STAINLESS STEEL BY LIQUID LITHIUM

BY

DONALD GEORGE BAUER

A thesis submitted in partial fulfillment of the requirements for the degree of

DOCTOR OF PHILOSOPHY

(Chemical Engineering)

at the

UNIVERSITY OF WISCONSIN--MADISON

1980

ABSTRACT

KINETICS OF THE DEGRADATION OF

TYPE 316 STAINLESS STEEL BY LIQUID LITHIUM

Donald George Bauer

Under the Supervision of Professor Warren E. Stewart

A forced convection loop is used to study the corrosion of type 316 stainless steel by liquid lithium at temperatures relevant to fusion reactors. Weight loss data are reported for tubular samples located in the hot zone of the loop. Temperatures of 440C and 490C have been used in the hot zone with temperature differences of 100C to 200C between the hot and cold zones. The effect of lithium velocity on local mass transfer rates is examined by simultaneously exposing stainless steel samples to parallel streams of lithium at velocities ranging from 40 to 130 cm/s. The loss rates become essentially steady after one month of exposure. The rates agree substantially with rates reported by previous workers, but are one to two orders of magnitude smaller than the rates predicted by boundary layer theory, using an extrapolation of the available solubility data for iron in lithium. It is presumed that particles of iron circulate in the lithium and by their dissolution and precipitation act as a buffer to reduce the wall fluxes.

The loss rate increases with lithium velocity in a manner suggestive of liquid-phase controlled mass transfer. The velocity dependence is weaker than expected for flows in the range of Reynolds numbers studied. This may reflect a significant interfacial resistance to the dissolution.

The mass loss rates at 440C are reduced when the temperature difference between the hot and cold zones is reduced. The rates during the first 1000 hours are three to four times higher at 490C than at 440C. The dissolution rate at 490C decreases markedly after 1000 hours. The transformation of the steel surface to a ferritic phase may cause the reduction in the rate.

Date:_____ Signed:_____

Warren E. Stewart
Professor of Chemical Engineering

To my Family

"If the Lord does not build a house,
then in vain do the builders labor."

* * * * *

an adaptation of Psalm 127

TABLE OF CONTENTS

LIST OF FIGURES

LIST OF TABLES

TABLE OF APPENDICES

[NOTE: The appendices to this work have been published separately in a companion document, UWFDM-364.]

TABLE OF APPENDICES (CONTINUED)

LIST OF FIGURES IN APPENDICES

Also, additional illustrations by the author.

LIST OF TABLES IN APPENDICES

ACKNOWLEDGEMENTS

I have been blessed in this work through the friendship and help of many people. There are more than I can name here whose cheerful, ready support made this research pleasant and helped me to grow mentally, socially, and spiritually during the past six years.

I thank Professor Warren Stewart, Dai-Kai Sze, and Igor Sviatoslavsky, my advisors, who gave me guidance which added polish to my efforts. Their help and friendship made the long road easier.

I am grateful to Professor R.W. Conn and the Fusion Design Program for supporting the lithium loop project; to J.H. DeVan for his advice, interest, and overall assistance; to W.R. Hundley for helping us to obtain equipment; and to J.E. Strain, C. Bagnall, and E.D. Glover for their help in the lithium analyses, scanning electron microscopy work, and electron microprobe analyses.

I thank the staff of the UW Physical Sciences Lab, who did a tremendous job in building the loop and in providing ready assistance in its maintenance and supply. I also thank the staffs of the Chemical and Nuclear Engineering Departments and the Instrumentation Systems Center for their efficient and friendly help each day.

I have made many good friends among my fellow students. I have special thanks for Chien Chun Wang, who helped outfit the lithium loop, and for Mark and Catherine Bolme, for our longtime friendship and much pleasant conversation, and for their thoughtful hospitality.

God has blessed me in many ways here. I cherish the fellowship I shared and the inspiration I received from the community at St. Paul's Chapel, and from the Prayer Group. I especially thank Father John Schmitz for his advice and friendship.

I thank all the teachers who showed me the way since I was very young. I am grateful to the relatives and friends who have taken an interest in my studies through the years.

Finally, I thank my brothers and sisters, and most of all our Father and Mother, for their constant encouragement and love. With my family I share this achievement; to them I dedicate this thesis.

* * * * * * * * *

This research was funded by the Wisconsin Electric Utilities Research Foundation and the United States Department of Energy. Graduate fellowships were provided by the National Science Foundation and by the Wisconsin Alumni Research Foundation. Computer time was provided through the National Magnetic Fusion Energy Computer Center.

The author is grateful for this support.

CHAPTER I. INTRODUCTION

INTRODUCTION

Liquid metals, because of their low vapor pressure and high thermal conductivity, are excellent heat transfer fluids. Their stability under radiation makes them expecially attractive for nuclear reactor applications.

Fusion reactors operating on the D-T cycle must have lithium in the blanket region around the burning plasma in order to be self sufficient with respect to tritium. The lithium can be provided in elemental form, or as a eutectic or compound. For liquid systems, such as we consider in this research, the problems of corrosion and mass transfer have to be addressed.

There are two major concerns related to corrosion and mass transfer in a fusion reactor:

1 - Corrosion or dissolution of the liquid metal containing structure, and consequent change in its mechanical properties.

2 - Deposition of radioactive corrosion products in the cold zones of the loop, with consequent heat exchanger fouling and other related problems.

In the early days of conceptual fusion design studies it was generally believed that the first generation of fusion power reactors would have stainless steel as the structural material in the blanket and first wall. Experience with fission reactors had provided a wealth of data on 316 stainless steel, especially with respect to radiation damage. The ductility loss due to radiation damage would apparently limit the service life of the first wall to 2 or 3 years if 10% cold-worked 316 stainless steel were used in a fusion reactor with a wall loading of 3-4 MW per square meter.

Many of the early conceptual designs had pure lithium as the coolant and breeding material (Badger, et al., 1973, 1976). At that time there were no long-term, high temperature data on the corrosion of type 316 stainless steel by liquid lithium under forced convection conditions. Short term tests (Gill, 1961) gave extremely high corrosion rates, which implied that tons per year of corrosion products would be transported within the primary coolant loop. Furthermore, little was known about the effects of velocity on the corrosion process.

For the present research, a forced convection, thermal gradient loop was built to investigate the long-term corrosion of type 316 stainless steel at conditions relevant to fusion reactors. Construction of the loop started in early 1976; testing began in August 1978 and has continued to the present time.

CHAPTER II. BACKGROUND INFORMATION AND LITERATURE REVIEW

STAINLESS STEEL METALLURGY (Mack,1975; Parr, 1965)

Iron alloyed with a small fractional percentage of carbon and approximately 11% chromium gives a "stainless" steel capable of forming a surface layer of chromium oxide which will protect the underlying metal from much of the corrosion which would attack unalloyed iron. Additional chromium may be used to modify the basic alloy for better resistance to corrosion or for special properties. Generally, the stainless steels are stronger than their pure component metals.

Metallic iron exists in several crystalline forms, depending on the temperature and the amount of alloying elements present. Between 910C and 1400C it exists in a face-centered cubic (fcc) lattice, as "gamma iron," or austenite, which has an equilibrium carbon content of 2%. At lower temperatures, the stable crystalline form is a body-centered cubic (bcc) phase called ferrite, or "alpha iron." Ferrite has an equilibrium carbon content of .02%, much less than that for austenite.

The austenite form of iron is more easily worked and is tougher than ferrite. Addition of nickel to a stainless steel stabilizes the austenite so that it persists at lower temperatures. In particular a combination of 8% nickel with 18% chromium (in iron with some carbon and minor alloying elements) produces a class of stainless steels known as "18-8." Type 304 stainless is a well-known "18-8" alloy. This steel is only metastably austenitic at room temperature. Cold working

or deep freezing will convert it to its stable ferritic form.

Molybdenum can also be added to the stainless alloy. It confers additional resistance to chloride solutions, which otherwise can cause pitting and degradation in the regular 18-8 stainless steels. The best known molybdenum-bearing stainless steel is type 316 stainless steel, which has 2 to 3 percent molybdenum. Molybdenum tends to stabilize ferrite, as does chromium. To offset this tendency, the nickel content is raised to between 10 and 12% in type 316 stainless steel.

The crystal form and metallurgical properties of stainless steel are strongly dependent on the composition of the alloy. Metastable austenitic forms are made by quenching the steel from a high temperature at which the carbon solubility is 2 percent. At room temperature the solubility of carbon is only .02 percent in ferrite. Perturbations such as cold working or loss of nickel from the lattice cause the alloy to revert to the more stable ferritic form. The carbon, present in excess at the lower temperature, may migrate to the grain boundaries and form carbides there. Such carbides are typically of the form $M_{23}C_6$, in which the metal is usually chromium.

Between 430C and 820C, carbide precipitation on the grain boundaries of metastable austenitic stainless steels such as types 304 and 316 is a special problem. In this temperature range, the thermodynamics and kinetics are both favorable to the formation of grain boundary carbides. Carbon migrates to the grain boundaries from

throughout the metal grains, which are supersaturated with this element. Chromium also diffuses to the boundaries. However, since the diffusivity of chromium is much less than that of carbon, the chromium needed for the formation of grain boundary carbides tends to come from the regions immediately adjacent to the grain boundaries. These areas become depleted of chromium, causing "sensitization," or loss of corrosion resistance. Sensitization is peculiar in that it opens the way for preferential dissolution of the grain boundary areas, where corrosion can be very severe. Sensitization is worst at 650C. Sensitization can be minimized by the use of low-carbon stainless steels, by adding small amounts of niobium or titanium to form carbides (thereby sparing chromium from that role), or by long-time annealing. Annealing allows the chromium to diffuse into the depleted areas around the grain boundaries, so that some of the corrosion resistance is restored. Cold working, and solution heat treatment, also reduce the chance of sensitization. Solution heat treatment entails a cold water quench from high temperatures, where austenite is stable. Cold working provides precipitation sites other than the grain boundaries, so that carbides are more evenly distributed in the alloy matrix. Cold working, however, may open the way for galvanic interactions in the alloy, since the cold worked metal is anodic to annealed metal.

SOLUBILITIES OF METALS AND NON-METALS IN LITHIUM

Transition metal solubilities in lithium at 540C are apparently around 10 to 100 ppm (Mausteller, 1967). The available solubility data seem inconsistent. Minushkin (1961) reported the solubility of iron in lithium at 760C was 85 ppm. Leavenworth (1961) gave a value of 42 ppm, and Sand reported 120 ppm, including a blank of 60 to 80 ppm.

The data on solubility and enthalpy of solution for transition metals in lithium are quite varied (McKisson, 1966). Enthalpies ranging from 5 to 50 kcal/mol are reported. McKisson et al. commented that oxygen and perhaps nitrogen were contributing factors in the dissolution of other metals in lithium.

Strauss (1958) correlated enthalpies of solution with the ratio of the atomic radii of the solute and solvent metals in a variety of liquid metal systems. Leavenworth's (1961) data fit Strauss' correlation; the data are shown on Figure II.1. Additional data show that nitrogen in lithium increases the solubilities of several of the solute metals.

In most solubility tests, the solute metal is dissolved in a small container of the alkali metal. Such tests are called "static" or "capsule" tests. Measurement errors can occur in capsule tests where the solute metal is supplied from an alloy, or where the capsule metal is different than the solute. Small solubilities

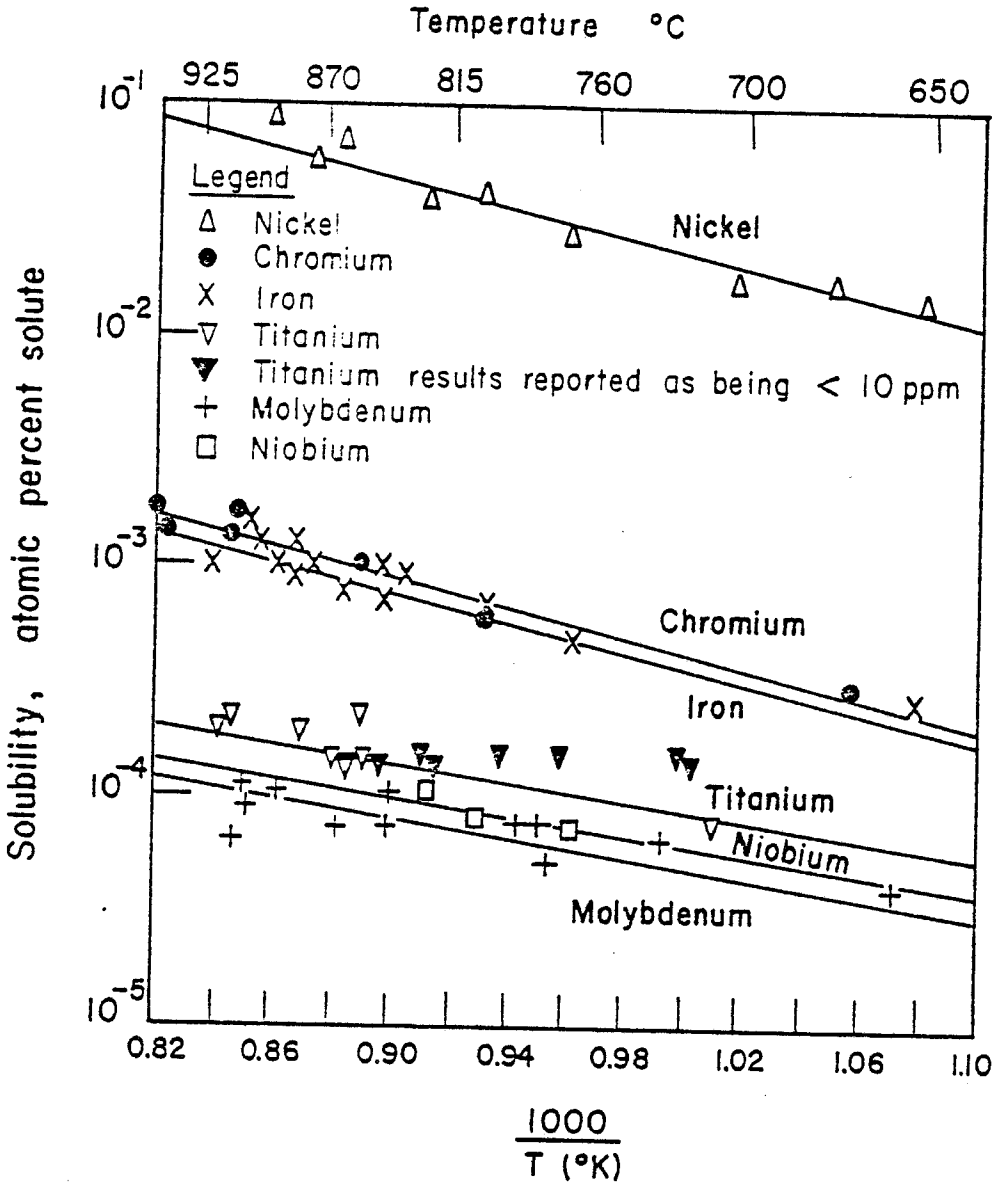

FIGURE II.1 SOLUBILITIES OF METALS IN LITHIUM
(Leavenworth and Cleary, 1961)

can also lead to errors. The solubility of a transition metal might be around 10 ppm, while an analytical test for the metal might be precise only to 5 ppm. Furthermore, particles present in solubility melts may give apparent solubilities which are high.

In research similar to the work reported here, Gill used the iron solubility data of Sand (1958) and the nickel solubility data of Bagley and Montgomery (1958). In later work (1961), Gill also had access to the iron, chromium and nickel data of Leavenworth(1961).

The solubilities of non-metals, especially nitrogen, oxygen, carbon, and hydrogen in lithium are also important. Small amounts of these elements in lithium may increase its corrosiveness (although only nitrogen seems particularly suspect in this regard). In addition to corrosion, non-metallic impurities may cause other engineering problems--for example, the solubility of hydrogen in lithium would affect the handling of tritium generated in the blanket of a fusion reactor.

The solubility of nitrogen in lithium is shown on Figure II.2. It appears to be near 1000 ppm at the melting point of lithium (182C) but experiments often operate with lithium having lower nitrogen levels. Lithium delivered from the producer can have less than 100 ppm of nitrogen. Titanium and zirconium are effective gettering agents for "hot trapping" nitrogen from lithium above 600C.

Gettered lithium can have as little as 10 ppm of nitrogen (ORNL notes, 1975).

Figure II.3 shows the solubility of oxygen in lithium. The solubility is 10^{-3} mole % Li_2O (6 wppm O) at 200 C. Cold trapping alone might not reduce the oxygen to this level. Filters with pores two microns or smaller in size might be needed to remove oxides properly from lithium (Yonco, 1979). Zirconium and yttrium are also suitable getters of oxygen from lithium; levels of around 100 ppm oxygen can be achieved (ORNL notes, 1975).

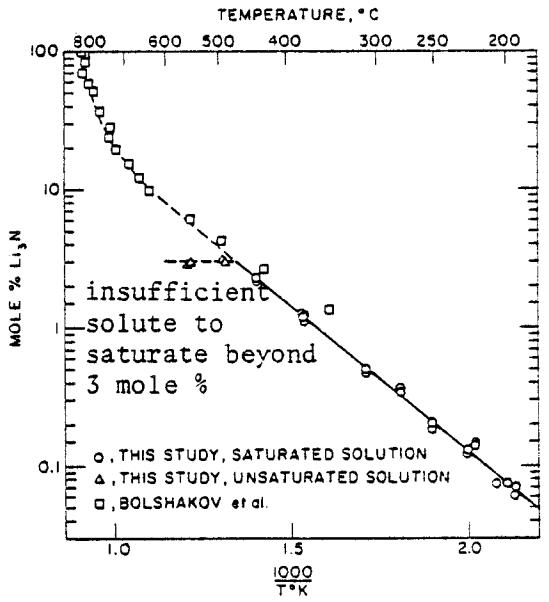

FIGURE II.2 Solubility of Nitrogen in Lithium (from Yonco et al., 1973; includes data from Bolshakov et al.,1959)

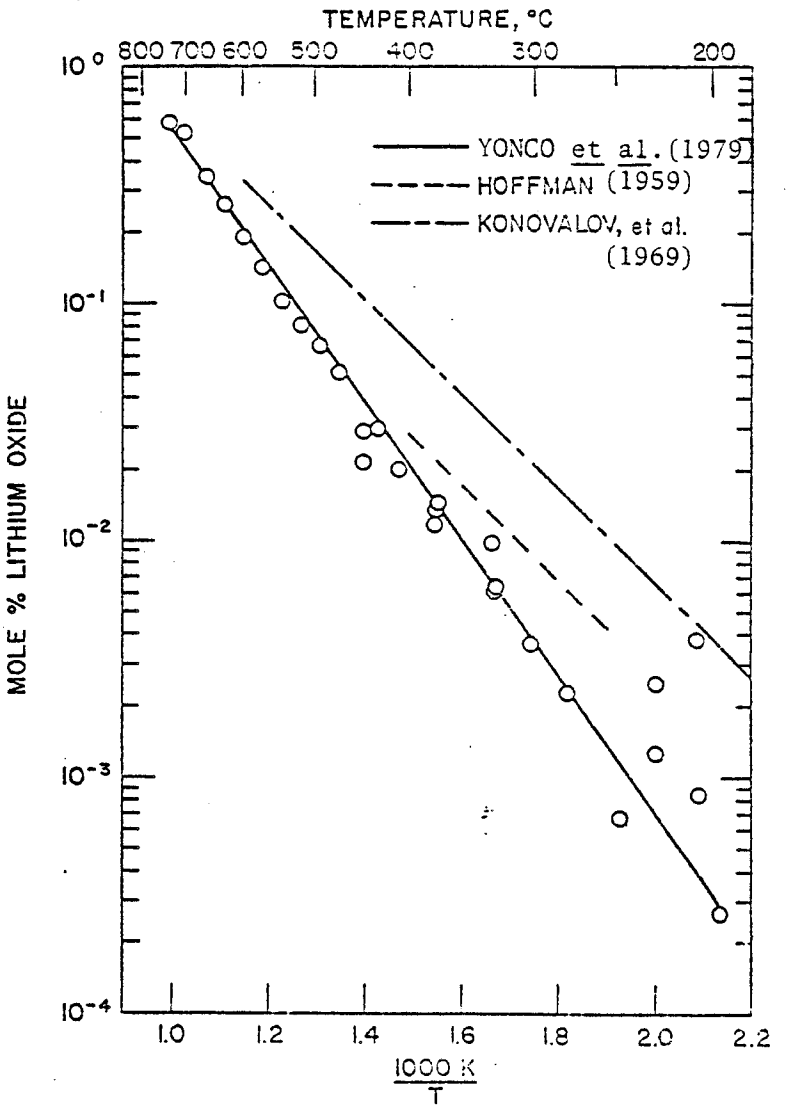

FIGURE II. 3 Solubility of Oxygen in Lithium (from Yonco et al., 1979).

LIQUID METAL CORROSION OF STAINLESS STEEL

The following survey covers previous work on the effects of major variables--temperature, liquid metal velocity, and solute concentration. The effects of selective mass transfer in the stainless steel and in the alkali metal are then examined. Grain boundary corrosion and stream transport are discussed briefly.

Corrosion of stainless steels by liquid metals has been studied for more than 20 years, at temperatures from 400C to 1000C, and under a variety of flow conditions, including both natural and forced convection. Much work has been done with sodium; recently more attention has been given to lithium. The following paragraphs and Table II.1 summarize lithium experiments to date.

Hoffman (1960) noted that alkali metal corrosion can proceed by six different modes of attack: solution, alloying, intergranular penetration, impurity reaction, temperature gradient mass transfer, and concentration gradient (dissimilar metal) mass transfer. In the present research, dissolution and subsequent temperature-gradient mass transfer are particularly important. Under certain conditions intergranular penetration and impurity reactions may be important. Lithium apparently does not alloy with stainless steel, and by proper design dissimilar-metal mass transfer can be minimized.

TABLE II.1 INVESTIGATIONS OF CORROSION OF STAINLESS STEEL BY LIQUID LITHIUM

LAB	MATERIALS	T max	T diff	VELOCITY	TIME	CORROSION RATE OR AMOUNT
Oak Ridge (Hoffman,1960)	310 SS 347 SS	732 C 538 C	280 C 212 C	2.4-3 m s^{-1} 2 cm s^{-1}	23-53 hrs 3000 hrs	1000 ug m^{-2} s^{-1} (high) 75 microns irregular
Col. Schl. Mines (Olson, 1974-5)	304L SS	800 C	static test	static test	150 hrs	0.7 ug m^{-2} s^{-1}
Oak Ridge (DeVan,1975-9)	316 SS	600 C	200 C	natural convection	2500-7500 hrs	3 ug m^{-2} s^{-1}
Syracuse U. (Gill, 1960-1)	304 SS	420-612 C	10-212 C	.16-.85 m s^{-1}	100 hrs	4 ug m^{-2} s^{-1} @ 500C
JAERI (Nihei,1974)	316 SS	600 C	100 C	natural convection	2500 hrs	3 ug m^{-2} s^{-1} @ 600C
Westinghouse (Whitlow,1979)	316 SS	538 C	165 C	1.82 m s^{-1}	900 hrs	8 ug m^{-2} s^{-1}
University of Wisconsin --current-- (nominal conditions)	316 SS	450 C	195 C	.4-1.4 m s^{-1}	4000 hrs	1.8-2.9 ug m^{-2} s^{-1}
		450 C	110 C	.4-1.4 m s^{-1}	3900 hrs	0.6-0.9 ug m^{-2} s^{-1}
		500 C	175 C	.4-1.4 m s^{-1}	1300 hrs 2900 hrs	~10 ug m^{-2} s^{-1} 0.8-1.5 ug m^{-2} s^{-1}

Corrosion rates are given in each case for coupons located in the hot zone of the loop.

Hoffman's study, one of the earliest on lithium - stainless steel systems, gave "negligible" corrosion rates (less than 0.4 ug $m^{-2}s^{-1}$) at 500C. "Slight" degradation (about 0.4 ug $m^{-2}s^{-1}$) was noted at 600C. These results were for isothermal static systems. In non-isothermal flow systems, the attack was still slight below 550C. Moderate attack occurred between 550C and 650C. At higher temperatures the attack was generally severe enough to make stainless steels impractical for prolonged containment of lithium. The overall temperature difference and/or associated thermal convection velocity in the flow systems were shown to affect the corrosion rate.

Hoffman gathered a large amount of data on lithium - stainless steel corrosion, under a wide variety of conditions, but it is difficult to summarize his results concisely.

Non-flow tests have more recently been performed by Olson and Bradley (1974, 1975). Stainless steel samples were exposed to lithium at temperatures from 600C to 1000C for times up to 250 hours. Results were reported in terms of grain boundary penetration depth and weight loss. The extent of corrosion seemed to be proportional to the square root of the exposure time. The penetration depth was 125 microns after 200 hours at 600C. (Patterson, 1975; Schlager, 1978).

DeVan and coworkers at Oak Ridge National Laboratory have extensively studied thermal convection mass transfer of type 316 stainless steel in lithium (ORNL notes, 1975, 1979; personal communications

1975-1980). Hot and cool zone temperatures of 600C and 400C were used in most of these experiments. Results indicate that diffusion in the lithium boundary layer controls the corrosion, that the temperature distribution around the loop probably has an important effect, and that the effect of nitrogen on thermal gradient mass transfer is insignificant or may be masked by a tendency for the stainless steel itself to remove nitrogen from the lithium (For [N] less than 1000ppm).

An early forced-convection loop system was studied at Syracuse University by Gill (1960). Mass transfer of type 304 stainless steel by liquid lithium was measured for a range of conditions as shown in Table II.1. Notable features of this research were the rather short run times of 100 hours, the use of flat plate coupons (metal samples), and the analysis of both hot and cool-zone coupons. For subsequent research, Gill used tubular coupons (1961). In comparison to Gill's system, the present loop operates with run times of several thousand hours, using tubular coupons which are located in the hot zone only.

Gill reported that the solution rate could be represented as an Arrhenius function of the hot zone temperature. Hot zone rates implied some type of solid-phase control; cold zone rates made it appear that liquid phase diffusion controlled there. Gill's results predict a hot zone corrosion rate of about 15 microns a year(0.6mil/yr) at 500C. A thermal convection loop system studied for 2500 hours of operation by Nihei (1974) of JAERI gave approximately the same rate, 12 microns per year(0.5 mil/yr) for type 316 stainless steel

in lithium at 600 C.

Most recently, Whitlow and coworkers at Westinghouse (1979) reported a corrosion rate of 30 microns per year (0.8 ug m^{-2} s^{-1}) for stainless steel after 1000 hours in lithium at 538C. Types 304 and 316 stainless steel were corroded at essentially equal rates in their forced convection loop.

EFFECT OF MAXIMUM TEMPERATURE

Gill (1960, 1961) studied the corrosion of type 304 stainless steel by lithium and reported that the solution rate was an Arrhenius-type function of the maximum temperature, with an activation energy of 24 kcal/mol. Researchers at General Electric assumed an Arrhenius temperature dependence for their statistical analyses of mass transfer in a sodium loop. The calculated activation energy was also about 24 kcal/mol (Jaech, 1965; Young, 1967).

For comparison with the activation energies found by these workers, typical activation energies for diffusion in solid and liquid metals are shown below:

Iron in alpha iron--60 kcal/mol		(Borg, 1960)
Nickel in alpha iron	59	(Hirano, 1961)
Nickel and iron in stainless steel	60	(Perkins, cited by Hill, 1974)
Nickel and iron on grain boundary	30	(Perkins)
Liquid metal diffusion	10	(Epstein, 1957)

Strauss et al.'s correlation (1958) predicts heats of solution of about 14 kcal/mol for iron, chromium and nickel in lithium; Leavenworth's data (1961) support this value.

DeVan and Sessions (1967), working with lithium in a natural convection, refractory alloy (Nb- 1%Zr) loop, deduced that the rate-

limiting step in this system was the chemical solution of metal in the hot zone, rather than its deposition in the cool zone. The highest corrosion rate was at the exit of the heater.

EFFECT OF TEMPERATURE DIFFERENCE

Hot and cold zones exist in any liquid-coolant heat removal system. Since the solubilities of the containment metals are temperature dependent, the containment metal is continuously transferred from the hot zone to the cool zone. Hoffman (1960) remarked that mass transfer driven by a temperature difference is one of the most troublesome of corrosion forms. It is difficult to observe in static tests. Even in non-isothermal systems, its effect may be detected only after long times.

Dillon (1975) of Battelle Northwest noted that the maximum deposition rate in a non-isothermal sodium loop occurred at the point where the temperature began to fall. For high nickel alloys, the mass transfer rate was dependent on temperature difference. Dillon cited work by Thorley showing that temperature differences greater than 50 degrees C up to at least 400 degrees C do not further affect the corrosion rate of iron by sodium.

Stang (1970) in a Battelle review report commented on General Electric studies (Jaech, 1965; Young, 1967) noting that corrosion rates were comparable for sodium loops with temperature differences of 139 degrees C and 278 degrees C.

EFFECT OF VELOCITY

Hopenfeld (1970), Thorley and Tyzack (cited by Kolster, 1975), Schrock (1974), and Bagnall and Jacobs (1975) generally found that corrosion rates of stainless steel by sodium were linear with velocity below approximately 3 m s^{-1}, but were not affected by further increases beyond this velocity. The rate of corrosion for pure nickel in sodium is linearly dependent on velocity up to 12 m s^{-1}(Dillon, 1975).

Hoffman (1960) reported a velocity effect in his lithium-stainless steel (type 316) loop, but the apparent effect was probably confounded with a temperature effect, since the loop was driven by thermal convection. Recently researchers at Oak Ridge have devised a mechanical means of varying the flow resistance in their thermal convection loops, thereby allowing the velocity to be somewhat independent of temperature difference (Tortorelli, 1979). However, the maximum velocity in any thermal convection loop is quite small compared to typical velocities in forced-convection loops.

In Gill's forced-convection loop (1960) an array of flat-plate coupons was used. Their corrosion rates were plotted against the length Reynolds number$(D\langle v\rangle\rho/\mu)(x/D)$. The rates varied with downstream position (x/D)--an entrance effect--but the data did not permit a ready determination of the possible effect of flow velocity. In later work (1961) Gill used tubular coupons. In both cases, the

lithium velocity was varied from run to run, but the temperature was varied simultaneously and its effect might mask an effect of velocity.

Gill's data show that the "j factor" for deposition in the cold zone was apparently proportional to the 0.8 power of the length Reynolds number, when flat-plate coupons were used. Later work with tubular coupons indicated a 0.89 power dependence of the j factor for deposition, on Reynolds number ($D\langle v\rangle\rho/\mu$). The results in both of these cases are what would be expected for turbulent boundary layer diffusion control of the deposition. Gill concluded that the solution in the hot zone of the loop was controlled by both liquid and solid phase resistances. The solution rates depend on position (x/D), but not so strongly as expected for mass transfer controlled solely by liquid phase boundary layer diffusion.

Jaech (1964) reported that the corrosion rate in sodium loops was proportional to the 0.88 power of the velocity. A revision of the analysis (Young, 1967), reconsidering and slightly modifying the rate model, gave an exponent of 0.43 for the velocity. A caveat was added: only two velocities--2.1 and 6.6 m s^{-1}--were studied. The higher velocity is in the range (above 3 m s^{-1}) where velocity reportedly has no further effect on corrosion rate (Hopenfeld,1970; Schrock, 1974; Bagnall and Jacobs, 1975).

FLOW EFFECTS OTHER THAN VELOCITY MAGNITUDE

Young (1967a) noted an entrance effect in the mass transfer of type 316 stainless steel in a sodium loop; statistical analyses by Jaech(1964) and Young (1967b) confirmed a small entrance effect. Whitlow (1970) noted that surface heat fluxes may make it appear that there is a velocity effect. If the temperature at the exit of a heater is set at a certain value, then an increase in the liquid metal velocity will require an increased heat flux, which would presumably raise the temperature of the wall and might therefore increase the local corrosion rate.

Hoffman (1960) as well as Murback and Atkins (1970) reported increased mass transfer at flow disturbances in loop systems. Dillon (1975) stated that mass transfer increased at points of disturbed flow.

Schwarz and Rajakovics (1973) noted another flow effect. They reported grain boundary corrosion of stainless steel by sodium at low flow velocities; at higher velocities sodium attacked the surface of the stainless grains as well.

Wozadlo and Pohl (1969) showed that the corrosion rate of type 316 stainless steel in sodium fell from 9.8 microns per year at the beginning of an isothermal 650 C zone to 3.7 microns per year some 130 cm downstream. Dillon (1975) reported that the deposition rate also fell off with increasing downstream distance.

Kolster and Bojers (1971) reported that an exponential position dependence (predicted by their first order equation for the dissolution of stainless steel in sodium) fit data satisfactorily. Schwarz and Rajakovics (1973) also chose an exponential although a parabolic downstream function fitted some of their data better.

DeVan and Sessions (1967) did not find a measurable downstream effect in a niobium - 1% zirconinum loop. This lithium loop operated at 1200 C with a temperature difference of 150 degrees C between the hot and cold zones. A recent study by Whitlow et al. (1979) found a slight entrance effect in the corrosion of stainless steel by lithium. The effect was a 2% reduction in the rate between (x/D) values of 100 and 150 for type 316 stainless steel. The reduction was 20% for type 304 stainless steel.

Weeks and Isaacs (cited by Dillon,1975) consider that the downstream effect may be catalytic in nature. Schwarz and Rajakovics pointed out that the effect becomes less with time and that it is dependent on the nickel content of the steel and the sodium in a loop. They concluded that the downstream effect was due to selective mass transfer effects.

In considering the so-called downstream effect, it is important to make a distinction between the usual entrance effect and any additional effect (such as a catalytic effect, saturation of the liquid metal as it flows through the test zone, etc.) which might be reflected in the local corrosion rate. It is not clear that this distinction has always been made. The entrance effect should not depend strongly on chemical factors. The so-called downstream effect, particularly when the term is applied to sodium systems, may be chemically caused.

A true entrance effect should have a power function dependence on downstream position (x/D). The exponential dependence reported by some researchers may reflect the fact that an exponential decay is somewhat similar to a negative-power function of (x/D), and might provide a satisfactory fit to the limited data available in some corrosion experiments. As noted above, Schwarz and Rajakovics (1973) chose to fit their data with an exponential but admitted that a parabolic downstream function provided the best fit for some of their data. The data were generated in an entrance flow following a sharp-edged inlet.

SELECTIVE MASS TRANSFER AND IMPURITY EFFECTS

The solubility of nickel in lithium is at least an order of magnitude greater than that of iron and chromium (Leavenworth, 1961). (See Figure II.1.)Therefore, nickel should be more readily removed from the stainless steel matrix. In particular, regions near grain boundary $Cr_{23}C_6$ carbides might be corroded faster than the alloy as a whole, since these regions are richer in nickel.

The fate of all the solute metals in the liquid metal stream is of interest. The liquid phase has been studied by many investigators, including Gurinsky (1969), Roy (1970), Jaech (1965) Young (1967), Wozadlo (1967), Stang (1970), Seebold (1960), and DeVan (1967). The majority of these studies involved sodium rather than lithium.

Roy and Gurinsky found that nickel is apparently, and chromium possibly, transported in sodium as an atomic species. Roy found that nickel may nucleate in the sodium stream before depositing in an austenitic crystal form in hot regions. A different crystalline form of nickel was found in cold regions. Stang, Roy, and Kolster's works indicated that oxygen in the sodium might influence the transport of chromium, either by forming a compound with the chromium or by catalyzing its dissolution. Such a compound might nucleate in the high temperature regions of a loop and deposit after reaching a critical size, according to Roy.

The dissolution rate of iron, according to Kolster, is proportional to the square of the oxygen content in sodium. Kolster postulated an "active oxygen" generated by the combination of two molecules of sodium chromite ($NaCrO_2$) or sodium ferrite ($Fe[Na_2O_2]$). Gurinsky reported that oxygen in the sodium increased the corrosion rate, and possibly formed a complex with the sodium and iron. Roy assumed that iron would deposit atomically from the sodium. Jaech and Wozadlo reported corrosion rates of stainless steel to be proportional to the 1.2 power of the oxygen content. Isaacs' study (cited by Dillon,1975) agreed with the 1.2 power dependence.

Young found that the chromium and nickel content of the hot zone surfaces in a stainless steel loop decreased while the relative amounts of these two metals increased in the cool zone deposits. After 3000 hours in sodium flowing at a velocity of 2.93 m s^{-1} the chromium content of the hot zone (700 C) surfaces had decreased from 16.9% to 6.2%. The nickel content dropped from 13.2% to 1.1% in the hot zone surfaces. Meanwhile, the cold zone at 100C now had three to six microns of deposits with chromium and nickel enrichments from the original alloy composition to new percentages of 44% and 29% respectively.

Seebold tested type 304 stainless steel in a non-isothermal pipe (not a loop) system with a maximum temperature of 815C in lithium contaminated with 0.36% air. These conditions are rather severe; after 72 hours, metallic deposits in the cool zone had plugged the 2.3 cm ID pipe. Chromium, not nickel, was selectively removed

from the hot zone. The lithium in the coldest part of the pipe contained as much as 25% chromium. Seebold concluded that a non-isothermal forced convection lithium loop would circulate chromium and would deposit nickel and iron in the cooler regions. His chromium concentrations probably indicate particles were present, since the solubility of chromium in lithium is far below the concentrations he found.

DeVan's thermal convection tests with lithium in stainless steel loops show that the hot zone dissolution of stainless steel is not selective, at least at times longer than 2000 hours, but that separate deposition zones exist in the cooling regions. Deposition possibly depends on local temperature and surface area (personal communication, 1979).

PARTICLES

"Calculations of corrosion rates (in sodium) from solubility measurements have been orders of magnitude too high, especially for iron alloys", stated one review of the liquid sodium corrosion work (Dillon, 1975). One reason for this might be particles circulating in the liquid metal. The nickel content of sodium in a loop is usually somewhere between the solubilities at the extreme temperatures, indicating that nickel is transferred as an atomic species rather than as a compound. Iron and chromium, however, are found in the sodium in amounts greater than their solubilities should allow, indicating that particles may be present.

DeVan and Sessions (1967) deduced that particles were present in the lithium of their niobium alloy loop by comparing the net mass losses with known solubilities. Epstein (1957) listed the possible fates of particles: deposition and adhesion in the cold zone; circulation and agglomeration to plug regions other than the cold zone; or fortuitous circulation and redissolution in the hot zone, which would protect to some extent the containment metal there (Detman, 1970).

Weeks and Isaacs (1973) report on a computer model for particle mass transfer. The particles would have to be sub-micron in size (given the very low levels of solute measured in loops) in order to make significant contributions to the overall mass transfer.

GRAIN BOUNDARY ATTACK, AUSTENITE-FERRITE TRANSFORMATION

According to Ray (1970) the mechanical properties of stainless steel are affected by general corrosion, that is, uniform dissolution, by the transformation of austenite to ferrite, and by interstitial depletion or grain boundary attack. The rate of general corrosion, hopefully, can be predicted, or at least fairly well bracketed by weight loss measurements. The austenite-ferrite transformation and grain boundary attack cannot be studied merely by weight change, but require metallographic, microscopic, and metallurgical tests.

The austenite-ferrite transformation is useful to gauge how deeply the alloying elements have been removed from metals such as type 316 stainless steel. The diffusivities of the alloying elements in the two different phases may be different enough to affect corrosion rates if solid phase processes control the corrosion.

Grain boundary attack, the third effect mentioned above by Ray, is unpredictable, occurs to significant depths in the stainless steels, and is probably the most influential factor affecting the mechanical properties of the steel. Schrock (1970) commented that non-uniform removal of the stainless steel by intergranular attack, and the removal of interstitial elements, will ultimately be of more concern to the reactor designer than the average (uniform dissolution) transfer rates of the metallic elements.

Hoffman (1960) found that grain boundary penetration of stainless

steel by lithium was particularly severe when there were carbides precipitated in the grain boundaries. The lithium in Hoffman's work, as well as that in some recent studies by Patterson (1975) had a high nitrogen content; the lithium used by Patterson contained up to 10,000 ppm. In this lithium, type 304L (low carbon) stainless steel was penetrated to a depth of 100 microns after 100 hours at 600 C. Patterson and his coworkers found that the rate controlling step for grain boundary penetration was grain boundary diffusion of lithium through a complex corrosion product. (Studies included lower temperatures and lithium with lower nitrogen content.)

The selective transport of chromium and nickel from the grain boundaries and surface of stainless steel caused a transformation of austenite to ferrite in sodium experiments by Young et al (1968, also cited by Stang, 1970). For type 316 stainless steel, the ferrite thickness was 6 microns after 2800 hours at 650 C in sodium of low oxygen content. Type 304 steel showed a 50 micron ferrite layer. Dillon (1975) reported a 15 micron ferrite layer on type 316 stainless steel after 10,000 hours in sodium at 700C. Such "well leached" stainless was said to behave like a low alloy iron for temperature gradient mass transfer.

With tests 100 hours long using type 304 stainless steel in flowing lithium, Gill (1960) reported that the degree of ferrite formation was greater at elevated temperatures where the mass transfer was more severe. He attributed the austenite - ferrite transformation to preferential loss of nickel and to the precipitation of carbon on the

grain boundaries. Leavenworth and Gregory (1962) noted that the ferrite depth agreed with calculations using the diffusivity of nickel rather than that of nitrogen or carbon, the other austenite stabilizers in stainless steel.

At the very high temperature of 1000 C, Hoffman (1960) found that the austenite - ferrite transformation was already apparent after 400 hours. The weight percentage of chromium at the surface of the metal had dropped, whereas the nickel content remained fairly constant. The iron content was increased at the surface (as expected for ferrite).

DeVan's tests with thermal convection loops showed an apparently constant ferrite thickness of 10 microns for type 316 stainless steel after 3000 hours in lithium at 600 C (personal communication, 1978). Beyond the ferrite layer the stainless was depleted from its initial composition for another 10 microns further into the steel. The constant ferrite thickness might correspond with the onset of a steady state corrosion rate.

Various phases may also be present in the deposition zone in a liquid metal loop. Roy (1970) reported that deposition at 575C in a sodium - stainless steel loop was largely austenitic, due to a high percentage of nickel. At 320C austenite was still a strong minor phase, but ferrite was the predominant deposit. At lower temperatures ferrite became the only evident phase.

Schwarz and Rajakovics(1973) reported seeing new grain boundaries and Brehm(1970) noted an increase in grain size in their sodium loops. Both effects were attributed to the austenite-ferrite transformation.

TIME DEPENDENCE OF CORROSION

Since the solubilities of the individual metal constituents of stainless steel are not equal, the surface composition of the alloy may change with time in a corrosion loop. Young et al (1971) showed that the rate of nickel removal from stainless into sodium was constant for a time and then eventually dropped to a lower steady value. Chromium dissolution from the stainless steel dropped exponentially with time to a steady value; the steady state appeared to be reached in 1000 hours. As mentioned previously, DeVan suggested that steady state occurred when a ferrite layer of constant thickness had been formed in the lithium - stainless steel thermal convection loops at Oak Ridge (personal communications, 1978). At 600C there were indications of an approach to steady state after 500 to 1000 hours. Steady state was definite by 2500 hours. A steady state might ultimately be reached when the more soluble nickel and chromium had first been rapidly removed from the stainless surface, causing the surface to be transformed into ferrite. Subsequent "steady state" corrosion would correspond to the removal of the surface ferrite and smaller amounts of nickel and chromium which must diffuse through a relatively "thick" ferrite layer. Ultimately the resistances would build up so that the iron, chromium and nickel were all removed at at relative rates equal to their original proportions in the steel.

Alloy composition changes are not the only possible cause for changes in the mass transfer rate. Rates may change because of changes in impurity levels in the liquid metal phase (Detman, 1970).

SOLID PHASE MASS TRANSFER

Patterson (1975), using static tests, found that surface grains broke off stainless steel in high-nitrogen lithium after an initial delay period during which the degradation rate in high-nitrogen lithium was equal to that in titanium-gettered lithium. The plot of temperature against delay time was a C-shaped curve characteristic of a nucleation process taking place in the penetrated grain boundaries. The lithium's nitrogen content was several thousand parts per million; at this high level unusually severe corrosion might be expected.

Klueh (1974) initially assumed that grain boundary diffusion of lithium was controlling the corrosion rate of his niobium coupons. The diffusion model which he used predicted a penetration depth X

$$X = \sqrt{\frac{2\ \mathcal{D}_{Li,gb}\ [Li]\ t}{\phi\ [O]}} \qquad (1)$$

where $\mathcal{D}_{Li}$ is the diffusivity of lithium in the grain boundaries, [Li] is the interfacial content of lithium in the niobium, [O] is the original oxygen content of the niobium, t is the time, and ϕ is the ratio of lithium to oxygen in the hypothetical corrosion product formed in the grain boundaries. This diffusion model, Klueh stated, did not explain corrosion increases with increased oxygen content, and failed at large values of X, the penetration depth. It did not

explain the cessation of corrosion at low temperatures.

Klueh therefore proposed that a corrosion product formed a growing wedge which penetrated the grain boundaries. The velocity of the lithium into a grain boundary would then be

$$V = \frac{w \sigma \cos\theta}{4 \mu x} \qquad (2)$$

where σ is the lithium surface tension, θ is its contact angle with the niobium, μ is the lithium viscosity, and w and x are the width and depth of the grain boundary crack, respectively.

Sessions and DeVan (1970) derived an error function relation for the mass transfer of zirconium out of a niobium alloy into lithium at 1200C and 1300C. Solid - phase diffusion control was indicated by the agreement of gradients in the niobium-zirconium alloy with the predictions of the error function relation.

While grain boundary corrosion is in some (often severe) conditions very important, general dissolution will probably be the major mode of mass transfer from any acceptable containment system. Such dissolution would be either completely stoichiometric, with no changes occurring from the original containment alloy composition, or else the corrosion would be selective, with one or more constituents of the alloy being removed in non-stoichiometric proportions. Such selective removal would not continue indefinitely

in an acceptable containment system, although due to unequal solubilities some initial selective removal is likely. The probable long-term corrosion behavior will be stoichiometric removal, after the more soluble components are depleted from the steel surface and dissolve more slowly by diffusion through the depleted layer.

Regardless of the exact mechanism of corrosion, if solid-phase behavior controls the overall corrosion process, the diffusivities of the various metal constituents may have to be known or determined from the data in order to analyze the corrosion process. Pertinent diffusivities are listed below. Others may be important as well.

SELECTED SOLID PHASE DIFFUSIVITIES

Fe in ferrite	118 exp(-67.2/RT) $cm^2 s^{-1}$	(Borg,1960)
Ni in ferrite	1.4 exp(-58.7/RT)	(Hirano,1961)
Ni in austenite	.77 exp(-67 /RT)	(Hirano,1961)
Fe in 316 SS	0.2 exp(-65.1/RT)	(Hill,1974)
Ni in 316 SS	.009exp(-60 /RT)	(Hill,1974)
C in 316 SS	.19 exp(-37.4/RT)	(cited:Snyder,1973)
C in 316 SS	41 exp(-49.6/RT)	(Ray,1973)
Cr in 316 SS @704C	3×10^{-14}	(Brehm,1970)
N in 316 SS @650C	$.7 \times 10^{-9}$	(Ray, 1971)

in grain boundaries of type 316 stainless steel:

Fe in 316 SS gb	$2. \times 10^{-8}/w$	(Hill, 1974)
Ni in 316 SS gb	$3.7 \times 10^{-9}/w$	(Hill,1974)

w is width of grain boundary in cm

LIQUID PHASE MASS TRANSFER

Epstein (1957) stated an equation for static corrosion

$$C = C_0 \left(1 - \exp\left(\frac{-\alpha A}{V} t\right)\right) \qquad (3)$$

where A/V is the surface to volume ratio of the container, t is the time, and C and C_0 are the present (at time t) and initial concentration of solute in the solvent. For boundary layer diffusion controlling the mass transfer, α would be proportional to some power of the diffusivity of the solute in the solvent. Otherwise α would depend on chemical factors and not on diffusivity. For iron dissolving in lithium, Leavenworth (1961) determined a value of 0.009 cm s^{-1} for α. The experimental temperature was 800C in this case.

Epstein's simple equation (3) does not describe the behavior of flow systems, which have velocity and temperature gradients in addition to the concentration effects encountered in static tests.

For flow systems, Epstein outlined the solution of the differential equation

$$\frac{dC}{dx} = \frac{4k\,(C_w - C)}{D\,V} \qquad (4)$$

where C and C_w are the concentration of solute at position x in the bulk stream and at the wall, respectively; k is the liquid phase mass transfer coefficient, D is the channel diameter, and V is the

average velocity of the solvent through the channel. Epstein solved equation (4) by assuming the term 4k/DV to be constant throughout the loop. This enabled him to use the standard integrating-factor method. Gill (1960) used a similar approach. Both Epstein and Gill reported order-of-magnitude agreement between their calculations and actual corrosion data, although in Gill's experiment the agreement held only for deposition and not for dissolution.

The first order differential equation (4) requires one boundary condition, which Gill supplied by assuming that the lithium leaving a filter in the loop would be saturated with solute at that point, that is, the lithium would be in equilibrium with the local stainless steel surface in the filter. The equilibrium point in a loop might be better defined as the point where the mass flux is zero; this point could be determined from weight loss measurements (DeVan, 1975). The lithium leaving a filter might not be in equilibrium with the local surface. Only rapid deposition kinetics and a fine-pore filter could ensure equilibrium at the filter exit.

Since corrosion loops are closed systems, at steady state in the fluid all the solute dissolved in the loop must be balanced by an equal amount of solute being deposited elsewhere in the loop. The mass balance must close. At steady state, any point in the system will have a fluid composition which

does not vary with time. In particular, after the lithium has circulated around a loop and comes back to an arbitrary location or origin anywhere along the length of the loop, the lithium composition will be identical to the composition when last the lithium passed that location. This simple fact can be used to obtain the steady state solution directly.

One may assume a concentration of solute(s) in the liquid metal at an arbitrary origin. A stepwise integration around the loop, as by a Runge-Kutta method, or by a superposition integral, gives the concentration of the solute(s) after one cycle around the loop. If this resulting concentration does not agree with the assumed concentration, a new concentration is assumed and the integration is performed again. A few iterations suffice to determine the solute level at which the steady-state mass balance closes. This method of solution might formerly been quite difficult; present computers facilitate it. With stepwise integration, it is not necessary to assume that the term 4k/DV is constant around the loop.

The solution of the mass transport equation requires knowledge of the solubilities of any metals being transported. Since the available solubility data shows much variation, it would be helpful if an experiment could generate solubility estimates along with mass transfer data. With enough reliable data taken over a range of temperatures, a carefully planned and analyzed experiment could give internal estimates of the

solubilities. A van t'Hoff form seems to be a likely function for the solubility, and it would agree with the solubility data given by Leavenworth and Cleary (1961).

DeVan and Sessions (1967) suggested that the local liquid phase concentration could be found by integrating the wall flux, found by weight loss measurements, around the loop--provided that steady state is reached and there is no formation of particles in the liquid. However, the wall flux can be experimentally determined at all points only if coupons are positioned around the entire loop. Often a loop must be sacrificed entirely in order to determine the wall flux at all points.

Instead of placing coupons at all points in their loop, Gill et al. (1960) analyzed weight-change data from the hot zone and cold zone for experimental runs made over a range of temperatures. In subsequent analyses of the data, it was assumed that the local dissolution rate,at any point where the flux could not be directly measured, would be the flux determined for hot-zone coupons in an experimental run for which the hot zone had been at the local temperature. In other words, solution rates were assumed to depend only on the local temperature. The validity of this assumption is questionable.

Velocity and temperature difference probably play a role in the solution process. Gill's data did not show any effect of these two factors, but an effect could have been masked by the effect of maximum temperature.

Because of the magnitude of mass transfer coefficients calculated for cold zone deposition in his loops, Gill concluded that deposition was liquid diffusion controlled. The effect of Reynolds number also seemed to support this conclusion. Mass transfer coefficients calculated for dissolution in the hot zone were 1000 times lower than the values expected from j-factor correlations. Later work (1961) showed an apparent entrance effect in both the hot and cold zones, indicating the importance of fluid diffusion in the dissolution as well as deposition processes. Some solid phase effect still seemed likely in the dissolution process.

The dissolution and deposition fluxes seem to be approximately equal in magnitude in Gill's loops. The 1000-fold ratio of transfer coefficients between the hot and cold zones may be due to the assumptions (described above) made in calculating the local concentration and hence the local concentration driving force. The driving force in the hot zone was calculated to be about 1000 times larger than that in the cold zone, leading thence to the calculation of much smaller mass transfer coefficients for solution than for deposition.

Kolster (1971) noted that analyses of stainless steel corrosion can be simplified by considering only iron to be transferred, since it is the major component of stainless steel. However, it is improbable that all the components--nickel, chromium, iron (and molybdenum)--in stainless steel will transfer independently or in stoichiometric proportions, according to Bagnall and Jacobs (1975). It is also unlikely, they comment, that one component will control the corrosion process. But if an iron-rich surface ferrite layer is formed --as found by Tortorelli and DeVan (1979)--after an initial leaching of nickel and possibly chromium, the important long term corrosion behavior of the stainless steel might be amenable to simpler analytical treatments than otherwise could be used.

DISSIMILAR METAL TRANSFER

A common form of "concentration gradient mass transfer" is the transport of metal solutes between dissimilar alloys or dissimilar pure metals. Roy (1970) placed pure iron next to type 316 stainless steel in the hot zone of a sodium loop and observed that the nickel content at the surface of the iron rose to 6% and the chromium to 3%. The percentages dropped slightly to 11% and 13% for the same metals on the stainless steel surface. Hoffman (1960) noted extensive grain boundary attack on austenitic stainless steel coupons when these were tested in lithium contained in Armco iron capsules at 1000C. The attack was much less when dissimilar metal transfer was eliminated by used stainless steel for the capsules as well as for the coupons.

Weeks (cited by Stang, 1970) advised against mixing containment alloys unless their major constituents are insoluble and the activities of nitrogen, carbon, hydrogen and oxygen have been equalized by gettering.

ANALYSIS OF COUPONS

The following section describes possible pretreatments for corrosion coupons as well as describing analytical methods which have been used by other researchers. Each subject gives a short survey of available techniques followed by a brief statement or description of the method(s) used in the present research.

Coupon pretreatment

Specimens are often specially prepared before placement in a loop. Hoffman (1960) polished the coupons mechanically and chemically. After degreasing, the coupons were annealed in hydrogen. Burrs were removed. The coupons were examined metallographically before exposure to lithium.

Patterson (1975) and coworkers annealed their coupons at 900 C for four hours. The average grain diameter of the specimens was then 45 microns.

Ray (1972) used coupons that were solution annealed, sensitized, Garofalo treated, and 20% cold-worked as received. Cold-worked stainless steel had a higher corrosion rate in sodium than did annealed stainless, with increased diffusion through the grain boundaries.

The coupons in the University of Wisconsin lithium loop are

machined to the required length by surface grinding. The ends are deburred, and the coupons are cleaned with alcohol and a hot detergent solution. Before being put into the loop the coupons are oven-dried and weighed. No special metallurgical treatment has yet been given to any of the coupons, except for four coupons which were welded before placing them in the loop.

Coupon cleaning

The coupons must be cleaned after removing them from the lithium. Schwarz and Rajakovics (1973) cleaned the sodium from their coupons with alcohol followed by distilled water. The coupons were stored in a dessicator until analyses by X-ray spectrometer. These coupons were then returned to the sodium loop.

Liquid ammonia has been used at Oak Ridge National Lab to clean alkali metal from loop coupons (DeVan, 1975). Ammonia is faster-acting than alcohols. It is also non-flammable but has the disadvantage of requiring a refrigeration system. Both alcohol and ammonia can leave an oxide on the coupons. Ammonia may hydrogen-embrittle the coupons. Alcohol can carburize metals cleaned with it (Whitlow, 1970).

Lithium is less reactive than sodium; therefore water can safely be used for cleaning in the present research. Lithium-covered parts, sometimes while yet quite hot, are immersed in large amounts of lukewarm to hot tap water. To minimize stresses in the metal parts

the stainless / lithium assembly is sometimes cooled below the boiling point of water before immersion. Adequate ventilation is provided for the removal of hydrogen generated during cleaning. The lithium hydroxide solution formed by the cleaning is thoroughly rinsed from the parts with hot water and distilled water. Immersion in water for more than the necessary time for dissolving the lithium leads to rusting of the stainless steel which has been corroded. Coupons not returned to the loop are stored in methanol or isopropanol.

Weight change measurements

Weight change data collected by Wozadlo (1967) for a sodium experiment, and data in a Japanese study (JAPFNR, 1972) were reported to be precise to 10-50 micrograms. Hopenfeld (1970) reported that 40 micrograms was the 99% confidence limit on the precision of his coupon weight change measurements. Hopenfeld's data included weight changes of from 2 to 1000 micrograms, with 70% being more than 30 micrograms. For the most part, accuracies of 20% were achieved.

The coupons in the present research at the University of Wisconsin weigh about 4 grams and lose from 1 to 10 milligrams per month (depending on the lithium temperature and velocity). This weight change can be easily followed on an analytical balance reading to the (estimated) nearest microgram. Weighings repeated after half an hour differ by from less than 10 micrograms up to

50 micrograms. This reproducibility is in agreement with Hopenfeld's confidence limits.

Metallography

Optical microscopy is used to examine some of the coupons in the present research. Ray (1970) suggests etching procedures. A combination of glycerine, hydrochloric, and nitric acids works well on type 316 stainless steel (Mack, 1980).

Non-Optical Microscopy and Spectroscopy of Coupons

The electron microprobe is used with a "line scan" to measure the relative composition gradients in the stainless steel coupons. An area scan can be used to measure average compositions. Coupons examined by the microprobe are polished, so that surface compostions cannot be very well determined by the probe.

Ray (1971), and Sessions and DeVan (1970) used the electron microprobe to measure composition changes in coupons. The one micron electron beam enables analysis with a sensitivity of 2 to 4 percent (Young, 1968). The lattice composition is usually measured quite accurately. Precision movement of the probe sample stage can give an incremental scan across a metal sample.

The surfaces of a few coupons from the present research were studied using the scanning electron microscope and energy dispersive x-ray analysis (EDAX).

LITHIUM SAMPLING AND ANALYSIS

The impurity levels in a liquid metal loop are quite low and the liquid metal sampling apparatus must be very clean to ensure representative samples. Gurinsky (1968) reported that the outer surface of a 1/2 inch sampler tube could contain 1 or 2 micrograms of contaminant per cm of length. Although in most cases this would only contribute a few parts per million to the impurity levels measured, any such contamination should be minimized. Since the levels of metallic impurities in lithium or sodium are on the parts per million level, sample tube contamination could lead to erroneous analyses. Some workers grit-blast sample tubes before proceeding with the analysis of oxygen in sodium (oxygen is more important in sodium than in lithium). Sample tubing can be sandpapered and wiped with solvent before it is sectioned for analyses. Methods (such as the micro-Kjeldahl for nitrogen) which dissolve the alkali metal out of the sampling tubing may introduce contaminants from the tubing outside surface.

Wet chemical methods are often used to determine the bulk composition of alkali metal samples. Methods are reported in the literature and Mausteller (1967) gives a summary of them.

Probably the most important wet chemical analysis of lithium is the microKjeldahl method for the nitrogen determination. The lithium sample, without ever being exposed to atmospheric nitrogen, is dissolved in water and the ammonia produced by the hydrolysis of

lithium nitride is distilled off, collected, and measured titrimetrically, colorimetrically, or electrochemically (see Appendix N). Precisions range from a reported 1 part per million (Goldman and McKee, 1969) for a sample having an absolute nitrogen content of 10 ppm, up to several hundred ppm when the nitrogen was present in more than 1000 ppm, as is sometimes the case when nitrogen is deliberately added to the lithium. Generally, precision runs about 10 percent of the nitrogen content. The amount of lithium in the sample is determined by titrating the hydroxide solution left after the ammonia has been distilled out.

Wet chemical methods for the determination of metals in lithium often require a tedious separation prior to quantitative analysis of a single element. Spectrographic methods are not so demanding. DC arc spectrography was reported by Gurinsky (1968) to be sensitive at the 0.1 ppm level, and is used at Oak Ridge to analyze lithium for metallic solutes. Atomic absorption spectrometry was reportedly less sensitive but more precise than DC arc spectroscopy (Gurinsky).

Neutron activation analysis has been used to determine the composition of liquid metal samples. Neutron activation analyses would be difficult in a "swimming-pool" reactor such as the University of Wisconsin reactor. The chance of lithium reacting with the blanket water would make special containers necessary. Also, lithium has a high neutron cross-section and would require special standards (Cashwell 1975). A sample of lithium from the current University of Wisconsin lithium work was analyzed for oxygen by neutron activation analysis

at Oak Ridge, where a special neutron generator makes such analyses more practical (Yonco et al, 1979).

Oxygen and nitrogen analyses at Oak Ridge make use of a high-purity atmosphere (using argon) glove box for sectioning samples, and vacuum stopcocks for transferring samples to a special reactor vessel for nitrogen analyses (or a sealed mason jar to transfer the lithium sample to the oxygen measuring equipment: ORNL notes). In the University of Wisconsin lab, smaller, inexpensive "glove bags" were tested as an alternative to a glove box. These probably provide as good an atmosphere as some large glove boxes and are more convenient to evacuate due to their smaller volume and collapsibility. Vacuum stopcocks can be used to transfer samples from the glove bags to the Kjeldahl distillation reactor flask. (Further information on the Kjeldahl method is given in Appendix N.)

As an alternative to glove box or glove bag handling, the lithium may be deep frozen in liquid nitrogen to allow sectioning of the sample tube and its transfer to the Kjeldahl apparatus without contaminating the lithium surfaces with atmospheric nitrogen. The nitride reaction, judging from the bright appearance of the very cold lithium, is apparently quite slow at liquid nitrogen temperatures.

CHAPTER III. DESCRIPTION OF EQUIPMENT

The lithium loop was built to study the corrosion of type 316 stainless steel by liquid lithium at temperatures up to 500C and velocities up to 2 m s^{-1}. The loop is part of the University of Wisconsin Nuclear Engineering Department's Fusion Engineering Program.

Construction of the loop began in early 1976. During that year, the containment system (piping), support structures and frame, and a protective enclosure were built at the U W Physical Sciences Laboratory near Stoughton, Wisconsin. In 1977 the wiring, insulation, and auxiliary equipment were added to the loop after it had been moved to the liquid metal laboratory in the Engineering Research Building on the University of Wisconsin Madison Engineering Campus. Final preparations for operation of the loop were made in the first half of 1978. Operation began in August 1978 and continues to date.

This section describes the design of the lithium loop. The appendices at the end of the thesis contain details of the construction and operation of the loop and suggest remedies for typical operating and equipment problems which have been encountered.

FUNCTIONS AND DESIGN REQUIREMENTS OF LITHIUM LOOP[1]

The lithium loop was built for the Fusion Engineering Program to evaluate type 316 stainless steel as a material for a lithium-cooled fusion reactor. The conceptual tokamak reactor, UWMAK-I, is typical of first-generation deuterium-tritium (D-T) fusion reactor designs which employ a natural lithium blanket as the coolant and breeding material. Lithium is known to corrode stainless steel. The lithium loop is used for further study of the corrosion at typical controlled thermonuclear reactor blanket temperatures and at lithium velocities up to 2 m s^{-1}.

Removable type 316 stainless steel coupons can be taken from the loop for inspection. The coupons can be removed without sacrificing any containment piping. Ball valves and freeze plugs at each of four test stations (placed in parallel flows at one point in the loop) can under suitable precautions be opened to remove the coupons from the lithium loop. Coupon inspections take place bimonthly or oftener; lithium samples are taken at longer intervals. The lithium is sampled at a flow bypass across the electromagnetic pump.

The lithium loop is designed for long-term continuous operation. It is unattended at night and on weekends, as well as for long periods of time on weekdays. Automatic protection circuits "scram" the loop to safe standby conditions if abnormal conditions threaten. In a scram, the University Police Department is automatically notified and alerts one or more of the operators responsible for the lithium loop. The police also

help check the laboratory in case of a scram alarm.

The loop containment piping for lithium was built by expert welders. All welds are full-penetration and were x-rayed and helium leak-tested. A heavy sheet metal enclosure around the loop provided extra safety. In the event of a pipe rupture the enclosure would shield the operators.

The lithium corrosion loop is in the liquid metal laboratory, Room 1408, of the Engineering Research Building of the University of Wisconsin at Madison. The laboratory was designed for liquid metal work and has suitable ventilation. There are no windows. The laboratory has two exits. In addition to the electrical power available in the room initially, several circuits were added for the electromagnetic pump and for some of the heaters.

---

[1]Notes are explained at the end of the chapter.

Operating conditions

All parts of the lithium containment system are type 316 (or in a few cases, type 304) stainless steel.

The maximum pressure in the system is approximately 3 x 10^4 N m^{-2} (5 psi) gauge, at the outlet of the electromagnetic pump. The maximum temperature is 500C at the main heater outlet. The average lithium velocity is 0.6 m s^{-1} with the maximum lithium velocity in a test zone being 2 m s^{-1}. These velocities correspond to a lithium flow rate of .05 kg s^{-1} (10^{-4} m^3 s^{-1}) and a system pressure drop of about 1.5 x 10^4 N m^{-2} (2.5 psi). The lithium velocity can be increased with a consequent increase in pressure drop.

Instrumentation and control

Instrumentation and control systems are designed to keep loop conditions safe at all times. The systems put the loop on standby condition if unsafe conditions threaten. Such conditions include overheating, high or low lithium level in the expansion tank, or loss of electrical power.

The output of electromagnetic flowmeters and selected thermocouples is logged on strip chart recorders. Additional thermocouples and electrical meters can be logged manually. The lithium level in the expansion tank is read manually from a monitor.

Details of Lithium Loop System

The lithium loop is shown in Appendix B, and, simplified, on the following two pages. A General Electric conduction type alternating current electromagnetic pump circulates the lithium at a flow rate of .05 kg s^{-1} (10^{-4} $m^3 s^{-1}$, nominal flow rate; nominal or design values are used here and below for flow rates, temperatures, etc.) The piping which connects the loop components is 1.6 cm ID x .21 cm wall (1/2" Sc 40; .622" ID x .083" wall). With the exception of the main heater and the four test sections, most of the loop pipes have a hydraulic diameter of from 2 to 2.5 cm. The surface-to-volume ratio of the loop is 1.6 cm^{-1}.

From the pump[2] the lithium flows into a 10 kilowatt main heater where its temperature is raised by 20 degrees C. The lithium leaving the heater is then delivered through a manifold into four parallel flow paths at velocities individually set by flow control valves. The parallel paths are each equipped with permanent-magnet type electromagnetic flowmeters. Within a vertical test zone in each parallel path is placed a removable stringer (holder) for corrosion coupons (samples of stainless steel). The parallel piping paths are also designated as "test sections," and ideally should be isothermal.

The lithium leaving the four test sections recombines in a manifold near the top of the loop. An expansion tank is connected to this upper manifold and serves as a high point of the loop. It is located in the upper left corner of the frame-enclosed space surrounding the loop. This expansion tank is partly filled with lithium under a cover gas of

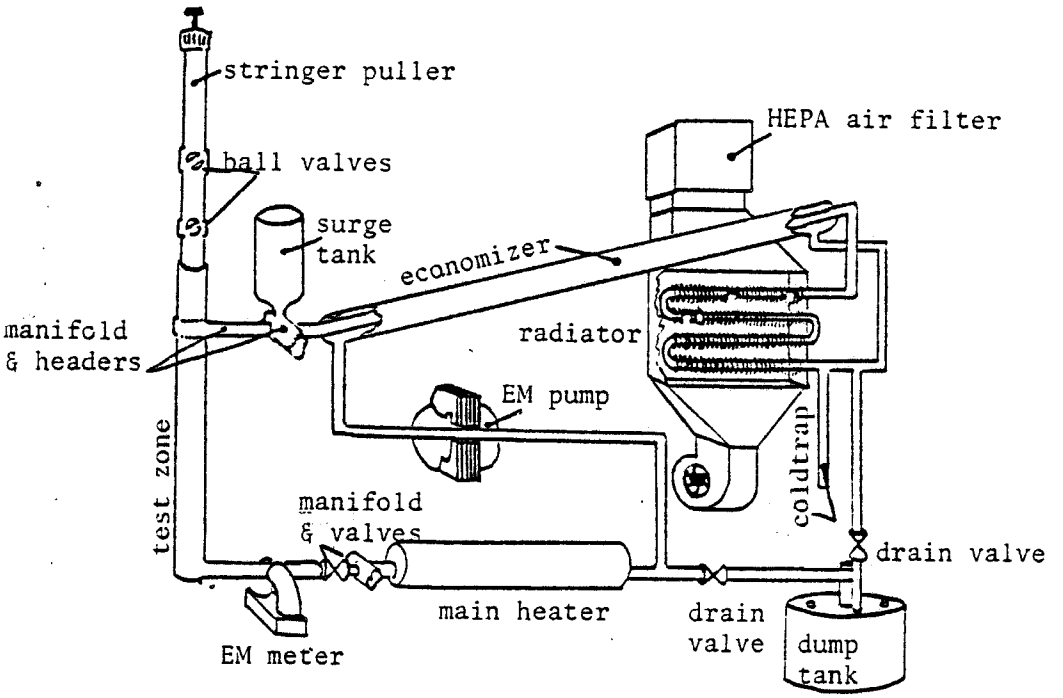

FIGURE III.1a LITHIUM LOOP

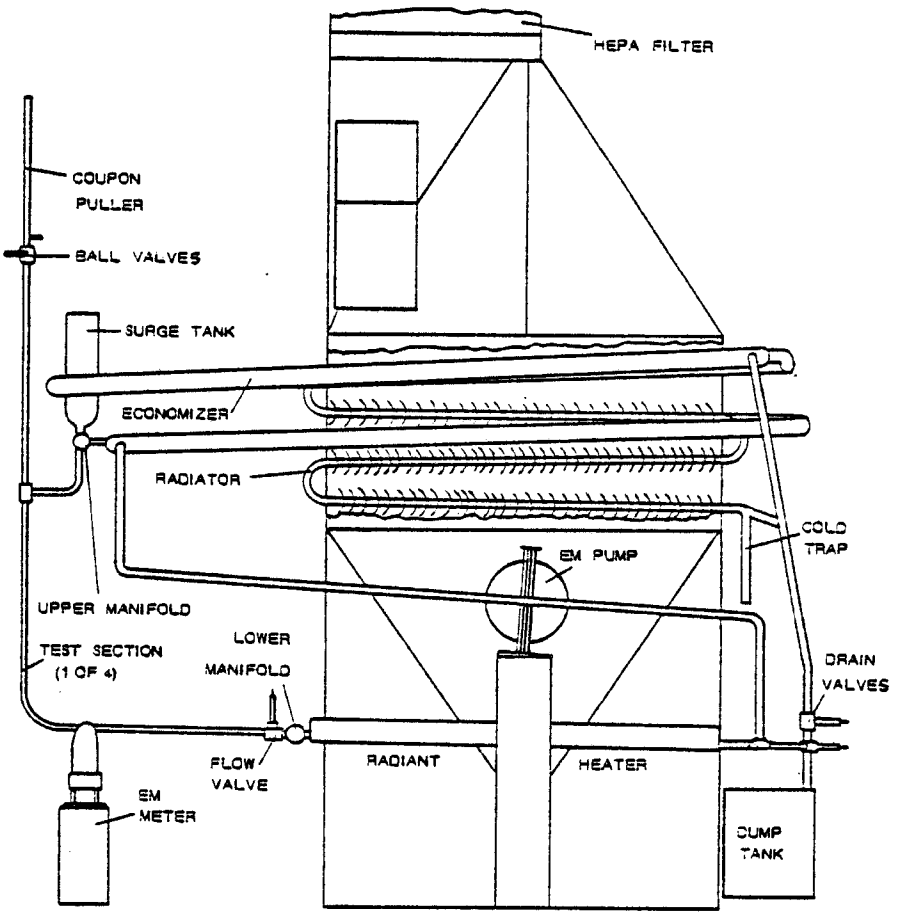

FIGURE III.1b LITHIUM LOOP
Drafting by H. Fack

Airco Grade 5 high purity argon. The expansion tank accomodates thermal expansion of the lithium.

The lithium flows from the upper manifold to the inside pipe of a countercurrent double pipe heat exchanger. The temperature of the lithium falls 180 degrees C from 500 C to 320 C during its transit through the inner pipe of the heat exchanger.

From the inner pipe of the heat exchanger the lithium goes through a finned-pipe radiator where heat is rejected to air, cooling the lithium an additional 20 degrees C to 300 C. The air in the radiator can be allowed to circulate by free convection in the dampered radiator ductwork, or in extreme cases air may be blown through the radiator with a fan provided for that purpose.

To reduce energy costs and system size, the lithium is passed back through the outer pipe of the double pipe heat exchanger. It is thereby reheated approximately 180 degrees C and exits the heat exchanger outer pipe at 480 C. Since the heat exchanger saves energy it is also designated as an "economizer." The economizer is designed to transfer 90 kilowatts when operated with a temperature difference of 20 degrees C between the countercurrent lithium streams. From the economizer the lithium, reheated nearly to the maximum operating temperature, is moved through the electromagnetic pump for another pass around the loop.

The lithium temperature varies with position around the loop. This temperature variation simulates the conditions which would be found in a power generation system such as

that of UWMAK-I where the lithium transfers energy from the reactor blanket to a steam generation system. The temperature variation causes thermal gradient mass transfer. The containment material, here 316 stainless steel, will dissolve in the hotter parts of the loop and deposit in the cooler parts.

Mass transfer test coupons (samples of stainless steel) in the lithium loop are placed in the parallel test sections in stringers (holders) which can be lifted out of the loop through ball valves. While the specimens are being removed, the lithium level in the loop may be lowered slightly, but the loop is not drained completely. During flow operation, frozen plugs of lithium are allowed to form in the standpipes above each test section (and just below the ball valves) to provide extra containment security. During coupon removal or replacement operations, these plugs of lithium are melted and the lithium level in the "freeze pipes" is equal to that in the nearby expansion tank.

There are two low points in the loop system. These are at the main heater inlet and the radiator outlet. Two valved pipes (from these low points to the "dump tank") allow draining and filling of the loop. To facilitate draining of the the loop, most of the piping and components are installed with at least a 3% slope toward the low points.

The loop contains "low-sodium" natural lithium supplied by the Lithium Corporation of America. The properties of the lithium are listed in Table III.1. The flow behavior is similar to that of water. Lithium is half as dense as water. The thermal conductivity is much higher than that of water. At the design temperatures and flow rate,

TABLE III.1 PROPERTIES OF LITHIUM (Maroni,1973)

Property	Value
Melting point	180.6°C
Boiling point	1342°C
Heat of Fusion	717 cal/g-atom
Heat of Vaporization	37.7 Kcal/g-atom
Volume Change on Melting	1.5% of Solid Volume
Property	(Equation; t = °C, T = °K)
Density, d, g/cm^3	$d = 0.515 - 1.01 \times 10^{-4}(t-200)$ (200-1600°C)
Vapor Pressure P, Torr	$\log_{10}P = 10.2788 - 8283.1/T - .7081 \log_{10}T$ (800-1400°C)
Viscosity, centipoise μ	$\log_{10}\mu = 1.4936 - 0.7368 \log_{10}T + 109.95/T$ (185-1000°C)
Thermal Conductivity, λ, cal/(sec m °C)	$\lambda = 10.1 + 2.94 \times 10^{-3}t$ (250-950°C)
Electrical Resistivity, ρ, μohm-cm	$\rho = 18.33 + 3.339 \times 10^{-2}t - 6.795 \times 10^{-6}t^2$ (200-1000°C)

the pressure drop around the loop should be less than 1.5×10^4 N m^{-2} (2.5 psi; see Appendix P.) A setting of 10% on the electromagnetic pump (50 volts, 6 amperes) is enough to sustain the design flow rate of .05 kg s^{-1} (10^{-4} m^3 s^{-1}).

A typical temperature profile of the lithium loop is given in Figure III.2. Temperatures are taken with thermocouples placed around the loop. These represent the temperatures on the outside of the pipe walls. The estimated inside wall temperatures are also shown; these are the appropriate values to use when considering mass transfer. (See also Appendix P.).

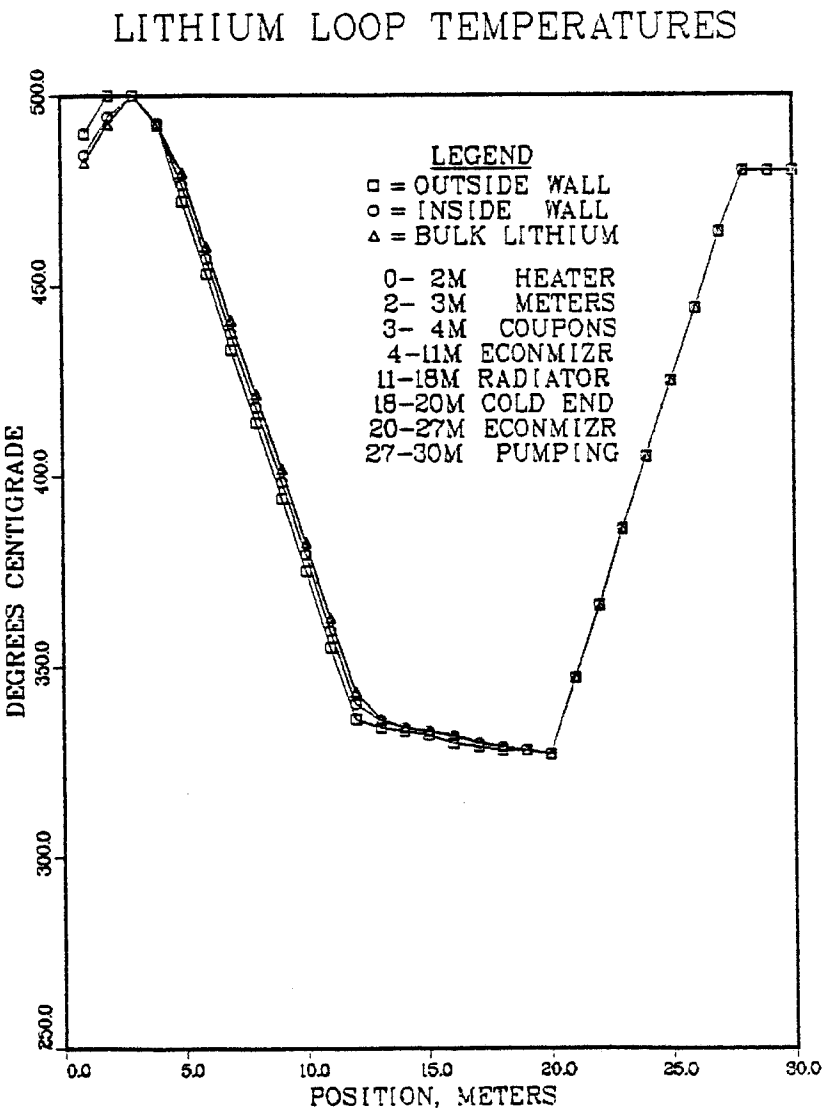
LITHIUM LOOP TEMPERATURES
LEGEND
□ = OUTSIDE WALL
o = INSIDE WALL
△ = BULK LITHIUM
0- 2M HEATER
2- 3M METERS
3- 4M COUPONS
4-11M ECONMIZR
11-18M RADIATOR
18-20M COLD END
20-27M ECONMIZR
27-30M PUMPING
DEGREES CENTIGRADE
500.0
450.0
400.0
350.0
300.0
250.0
0.0
5.0
10.0
15.0
20.0
25.0
30.0
POSITION, METERS

FIGURE III.2

Electromagnetic pump

A General Electric conduction type, alternating current electromagnetic pump moves the lithium through the loop(General Electric,1955). Although the pump is rated for 30 amperes maximum primary coil current, this would be too high for the lithium loop, as settings above 20% cause undesirable vibration of the pump. A 10% setting (6 amps, 50V) is sufficient to sustain a design flow rate of .05 kg s^{-1} ($10^{-4} m^3 \cdot s^{-1}$).

The efficiency of this type of pump is low. Mausteller (1967) gives values of 5% to 20%.

The pump is controlled through a 15 kilovolt-amp variable transformer with a maximum single phase input of 30 amperes at 480 volts. The power is conditioned with a .5 farad capacitor to offset the pump inductance. The manufacturer quotes an impedance of 6.6 ohms plus 6.8 henries. The maximum current in the pump secondary (cell current) is 1000 amperes at about 6 volts.

Control of lithium flow rates through the four individual test sections is by a flow control valve in each test section just downstream of the lower (inlet) lithium manifold. These valves are stainless steel, liquid metal type with bellows seals. Their settings are never changed except during flow calibration tests.

The test sections, made of thin-wall tubing, are bent apart from each other downstream of the valves to make room for electromagnetic flowmeters (described later). The test sections converge toward each other again before entering the isothermal oven.

Surge tank

This tank, near the top of the loop, provides an expansion space for the lithium. It is joined to the upper manifold of the parallel test sections. The joint is a short piece of 1.6 cm ID x .21 cm wall (1/2" Schedule 40) pipe. There is no net flow of lithium to or through the surge tank during loop operation, except as caused by thermal expansion or natural convection of the lithium, or when lithium is transferred back and forth between the loop and the dump tank.

The surge tank, unlike many of the other loop components, is not braced. Care should be taken not to exert force on the tank or on its fittings, since the only support is the pipe joint to the manifold.

Four Swagelok fittings penetrate the surge tank. Two are 1.27 cm (1/2") fittings for single-point level probes.* A third fitting is .8 cm (5/16") for a continuous-type level probe located in the center of the tank. The fourth fitting is .95 cm (3/8") for a stainless steel tube which goes to a stainless-steel-wool filled demister pipe and thence to a gas manifold on top of the loop enclosure.

The inside of the surge tank is 10.7 cm in diameter, and the tank is 41 cm deep. The axis of the tank is vertical; the top end is closed with a flat disk and the lower end is hemispherical. The tank and all probes are stainless steel. The probes are not necessarily type 316 or 304 steel, due to difficulty in obtaining the proper material. A type 300 stainless steel, however, should be used.

* The "single-point" probes can also be used as continuous probes, although the resistor in some spark-plugs is undesirable.

Mass transfer coupons

Mass transfer coupons (stainless steel samples) are located at the hot zone of the loop. Four coupon holders, called "stringers", are held there in separate pipes with different lithium flow velocities in each pipe. The test zone pipes, or "test sections", are in parallel between an entrance (lower) manifold, fed from the main heater, and an exit (upper) manifold, which empties into the double pipe heat exchanger. The lithium temperature in the entrance manifold is controlled so that the temperature in the test sections is nominally 500C although some drop in temperature occurs between the manifold and the coupons. The temperature is normally steady within about 2 degrees C in a given test section and within 5 degrees C between the sections.

Each of the four test sections has provision for insertion and removal of a 45 cm long split-tube stringer which has an outside diameter of 1.27 cm and which holds 16 tubular flow-through coupons coaxially. Each coupon is made of type 316 stainless steel cut from 0.62cm ID tubing with a wall thickness of 0.9 mm. The coupons are held in a jig and machine-ground to a length of 2.54 cm.

The stringers are inserted into and pulled from the lithium through a pair of ball valves above each test section. The stringers are held shut by type 316 stainless steel wire (.5 mm in diameter) recessed in 6 grooves machined around each stringer. The coupons fit snugly into the stringers. A snug fit ensures a continuous smooth inside wall when the coupons have been assembled in the stringers, so

that lithium turbulence due to wall discontinuities will be minimized.

The lithium in the "freeze pipe" standpipe above a test section must be melted during stringer removal or insertion. During normal flow operation of the loop, the lithium here is cooled and plugs the freeze section between the test zone and the ball valves above it. This frozen zone does not interfere with lithium flow through the test zone, since a tee diverts the lithium flow below the frozen zone into the upper manifold. The ball valves above the frozen lithium in the standpipe form a safety barrier and a gas lock to minimize contamination of the lithium by air, especially during coupon servicing (at which times, of course, the standpipes are not plugged by frozen lithium.)

During insertion or removal of the stringer, the lithium within the loop is not drained, but the flow through the loop is stopped by turning off the pump. A small amount of lithium is drained from the loop to lower the level of lithium in the expansion tank and freeze standpipes. This reduces the chance of getting lithium on the ball valves during the stringer servicing. A small amount of lithium is likewise refilled into the loop after the stringers have been replaced. This raises the lithium in the freeze pipes so that it will form a more effective fin and develop a better freeze plug. Also, should the frozen surface of the lithium in the standpipe become nitrided by air leakage, it can be cleaned only if the surface is quite close to the top of the standpipe.

Lithium transfers during stringer servicing are to the dump tank.

Dump tank

This tank is a lithium reservoir and is located at the lowest point of the loop, in the bottom right corner of the protective enclosure. The loop was initially filled from this tank, which itself had been filled from a shipping tank in which the lithium was delivered from the producer. The dump tank receives lithium drained from the loop when the lithium level is temporarily lowered during stringer servicing. In an emergency the dump tank can also receive some of the lithium from the loop.

The dump tank is cylindrical with a vertical axis. The tank is 32 cm in diameter and 33 cm high, and has a volume of 0.029 m^3 (25.4liters).The (completely filled) loop volume is 0.024 m^3 (22.7 liters). Since there is some lithium retained in the dump after the loop is filled, not all of the lithium from the loop could be drained into the dump tank unless some of the lithium were also transferred further into the shipping tank. The lithium is kept molten in the dump tank, although the dump valves are not kept above the melting point of the lithium. (This could be done, but has not in practice been done; the valves are heated to some extent but not usually kept hot enough for immediate flow.) The shipping tank and the transfer line between the dump and shipping tanks are not kept heated and the lithium inside them is frozen.

The dump tank is connected with the loop through 1.6 cm inside diameter pipe, with a 0.21 cm wall thickness, identical to the piping used in much of the loop itself. Two bellows-seal liquid metal type stainless steel valves isolate the dump tank from the loop. The valves are located on pipes leading to the two low points of the loop--the radiator outlet and the main heater inlet. All joints in the pipes and valves are welded.

A stainless steel (type 304) tube, 1.27cm outside diameter by 0.9 mm wall,connects the dump tank to a gas manifold, through a ball valve. This allows for pressurizing and vacuuming the dump tank. The connections of this tube to the dump tank and the ball valve are Swagelok fittings.

A second tube similar to the gas tube penetrates to the bottom of the dump tank and is used for transferring lithium from (or possibly back to) the shipping tank, which is situated just outside and behind the right end of the loop enclosure.

The shipping tank is 30.5 cm inside diameter and 71 cm high. It is stainless steel (type 316) with a welded bottom and a copper-wire gasketed, flanged-and-bolted lid.

Between the dump and shipping tanks there are, in order, a stainless steel bellows seal liquid metal valve,a 7 and a 15 micron stainless steel filter, another valve, and a tee leading to a lithium sampler port. The intertank tubing is type 304 stainless steel, as described above for the dump tank's gas tubing. The fittings are all type 316 stainless steel Swageloks. To accommodate the difference in the

heights of the two tanks, there is a dogleg in the tubing between the filters.

Both the shipping and dump tanks are heated by three external tubular heaters, held by stainless steel shim stock spot-welded to the tanks. The maximum heat to either tank is 7.5 kilowatts at 240 volts. One heater, run at around 50-60 volts, is sufficient to maintain the dump tank at about 250C.

The intertank tubes, valves and filters are wrapped with heavily insulated heating tape rated for operation at 800C in direct contact with bare metal. The tapes are 1.2 cm x 61 cm rated 144 watts at 120 volts, or 2.5 x 122 cm rated for 576 watts at 120 volts.

Due to overheating of the transfer tube between the two tanks during the initial filling of the dump tank, a film of lithium leaked from the swagelock fittings of the two filters. Some weeks later the heating tapes were unwrapped and found to be burned or shorted out. The slight leakage was shown by a thin yellowish salt crust along the tube near each filter fitting (and about 2 cm along the tube). The tubes had been overheated (pale red color) to ensure that the valves in the line would be above the lithium melting point. The thermocouples on the line were known to be reading low and the extra heating had been meant as a precaution against having frozen lithium in the transfer lines or valves.

Radiator

Heat added to the lithium at the main heater is rejected in the radiator, which is at the low temperature end of the countercurrent heat exchanger (economizer). The estimated cooling capacity of the radiator is about 20 kilowatts when run with an air flow rate of .4m^3s^{-1} (800ft^3min^{-1}). This air can be drawn from within the laboratory (outside of the enclosure) and forced through the radiator by a 1.5 kilowatt (2 hp) blower, with exhaust from the sheet metal housing of the radiator passing through a prefilter and a high efficiency particulate air (HEPA) filter, and thence outside the Engineering Research Building through an axial exhaust fan rated at 1.9 m^3s^{-1} (4000 ft^3min^{-1}). However, operation to date has shown that natural convection is more than sufficient to remove the rejected heat. The radiator must be dampered, even shut completely. Additional information on the heat transfer characteristics of the radiator is in Appendix Q.

Within the radiator, the air flows by four passes of finned 1.6 cm ID x 0.21 cm wall pipe. The (two-sided) area of the fins totals 2.6 m^2. The fins are carbon steel and are press-fitted onto the pipe. The outer diameter of the fins is 4.1 cm and the spacing (pitch) between fins is 0.25 cm. The fins are 0.4 mm thick.

The radiator housing serves as an oven to preheat the finned piping during startup and after the many times the lithium in these pipes freezes when the flow of lithium is stopped, as for stringer

servicing, or in a power failure, or other shutdown. Four strip heaters bolted to the inside of the radiator ductwork (housing) amidst the finned pipes serve for heating. A fifth heater located within the housing burned out and has been replaced with three strip heaters of approximately the same type, mounted on the outside of the housing (access to the inside of the radiator housing is almost impossible due to the outfittings, such as wiring, insulation, etc., which have been added to the loop.) In addition to providing heat to thaw the lithium when necessary, the radiator heaters are used to control the radiator temperature during flow operation of the loop. If the loop scrams, the radiator heaters are the only 200+ volt heaters which remain on. The damper is closed in a scram.

Even with continuous heating of the radiator in a scram, and with the air circulation retarded to some extent by the closed damper, the radiator pipes generally freeze rapidly when lithium flow ceases. In a scram, therefore, the pump is kept on, but a servo motor reduces its speed from 10% to 2%. False alarm scrams are thus easier to recover from. In a genuine emergency the pump can be shut off remotely by flipping breaker switch #16 in the box in the hallway outside the laboratory. Flipping this switch releases a holding relay which was added to the pump control circuit.

Main heater

The main heater is a stainless steel pipe 1.37 long, and is 7.3 cm in diameter. It has a 0.5 cm wall thickness. Three pairs of ceramic-potted "clamshell" heaters provide a maximum rated heat input of 10 kilowatts when powered at 220 volts. The corresponding heat flux is 32 kilowatts m^{-2}.

The clamshell heaters are held away from direct contact with the steel pipe by ceramic "fish-spine" insulator beads (about .2 cm diameter) strung on 0.5mm diameter type 316 stainless steel wire looped around the pipe at 6 places. The clamshell heaters are controlled with two variable transformers and an automatic temperature controller which drives a silicon control rectifier (SCR). The controller proportions the SCR output to maintain the maximum lithium temperature, as sensed at a thermowell in the lower lithium manifold, at the desired set point.

The maximum temperature rating of the clamshell heaters is around 1000 C. To provide the large energy input needed at the main heater, these clamshells are often driven at near the maximum available voltage of 208V. They are rated 1.7 kilowatts each at 220 volts.

Economizer

The economizer is a type 316 stainless steel double-pipe countercurrent heat exchanger consisting of a 2.54 cm OD, 0.8mm wall tube coaxial within a 3.5 cm pipe. The economizer is formed in three straight sections, connected by 180° bends. The length of each straight section is 203 cm and the radius of the bends is 23 cm. The overall length of the economizer is thus 250 cm and the total flow path is 7.9 m. The economizer was made by the Mine Safety Appliances (MSA) Company(1975).

The inner pipe of the economizer receives lithium from the upper lithium manifold, cools it, and delivers it to the radiator. After the radiator cools the lithium further, the liquid metal is returned to the outer (annular) passage and is reheated and delivered to the electromagnetic pump. The economizer connections to the loop are with 1/2" Schedule 40 fittings.

Due to the configuration of the economizer within the loop, it cannot be completely filled (even under vacuum) and at least a small gas bubble will be present near the exit or in the radiator just downstream.

The economizer is used to cool and reheat the lithium in order to save energy and space. It is designed to be 90% efficient, that is, to transfer nine times as much heat as the radiator to which it is connected.

Trace heaters

Approximately 40 tubular resistance heaters run along the system piping as trace heaters. The output of individual heaters or small groups of heaters is adjustable through 20 dimmer-switch circuits. The trace heaters remain continuously on at settings determined by trial and error at the beginning of the experiment. Generally the trace heat is enough to maintain the associated piping above 250 C if no lithium is flowing in the loop. The tubular heaters are 0.6cm OD. Their heated lengths range from 80 cm to 260 cm. Most are bent hairpin-like to straddle the pipe which they trace heat.

The economizer tubular heaters are not hairpin-bent, but are in groups of three heaters set 120 degrees apart around the circumference of the economizer pipe. All trace heaters run parallel to their associated piping, following curves and elbows. Stainless steel (type 304) shim stock 0.07mm thick is wrapped around the pipe and the heater element to prevent insulation from getting between them. The tubular heaters are tightly fastened to the piping at intervals of 30 cm with power clamps or with 1.5 mm wire; these fastenings are stainless steel.

The surge tank is trace heated by a tubular heater wound in a spiral around the tank. The dump tank and the shipping tank are heated by tubular heaters (three on each tank) bent into form so that the elements run up and down the tank wall with approximately

5 cm spacing. The trace heaters on all three tanks are held on by stainless steel shim stock, which is in turn spot - welded to the tank wall.

The tubular heaters are rated at 1000 watts m^{-1} when operated at 240 volts. A maximum sheath temperature of 800 C is allowed for the heaters when the pipe temperature is 400 C. The sheath material is Incoloy. The tubular heaters on the loop are powered with 120 volts or less, less than 1/4 of their rated power, to prolong their life. Since each pipe has at least two heater elements tracing it (the economizer has three) the heat available with a driving voltage of 120 volts is 490 or 740 watts m^{-1}.

In addition to the radiator (heated by strip heaters) and the main heater (heated by clamshell heaters), one other zone of the loop is not trace heated. In the test section isothermal zone, strip heaters are used, as in the radiator, except that 5 cm of insulation is placed between the test section heaters and the test section pipes. This should provide a somewhat more even distribution of heat in the test section, where isothermal conditions are desired. Avoiding direct contact of the test section pipes with the heaters also minimizes thermal stresses in the tubing of the test section. Uneven stresses which might distort the test sections could prevent the removal of the stringers. Since the heaters are not in close contact

with the thermocouples in the test section, the accuracy of the temperature readings there is enhanced.

There are six strip heaters in the isothermal "oven" section of the test zone. They are placed in two banks of three horizontal heaters each, with the vertical test sections passing between the banks. The entire isothermal oven is well insulated.

All strip heaters have chromized steel sheaths rated for a maximum temperature of 650C. For the stagnant air in the radiator, a 500C air temperature is allowed, and in the totally insulated isothermal oven around the test pipes, a 370 C temperature is allowed, if the heaters are run at 240 volts. Since the oven heaters use 120 volts maximum, they can operate at a somewhat higher temperature because of the smaller heat flux.

The strip heaters are 3.7 cm wide with both terminals at one end. The radiator internal heaters are 95 cm long and the isothermal oven heaters are 58 cm long between mounting holes. The radiator external heaters are 85 cm long.

Argon cover-gas system

"Ultra-high purity" or Airco Grade 5 argon is the cover gas for the lithium loop. The argon is supplied from a standard (330 ft^3) cylinder, with an initial full-cylinder pressure of 2500 psig. A spare cylinder is kept available whenever the supply cylinder runs low. The argon is delivered from the cylinder through a two-stage regulator set at 10 psig to a biscuit-type low pressure (.5- 5 psig) regulator. A 6 psig safety regulator protects the cover gas system from higher pressures. The argon is delivered to the piping above the test sections (that is,the freeze standpipes under the ball valves) or to the surge tank through an upper gas manifold which has a number of valves to route the gas as desired. Argon can also be delivered to the dump and shipping tanks through a similar, "lower" gas manifold. Both manifolds are clamped to the loop enclosure frame. Copper and brass fittings are used to carry the argon up to the lithium containment vessels; the final connections into these vessels are made with stainless tubing. Both manifolds have ports for rough vacuum pumping, which is always done through a liquid nitrogen cold trap.

Electrical system

The electromagnetic pump is supplied with up to 30 amperes of single phase 480 volt power from a distribution board in the utilities room across the hall from the west end of the liquid metals laboratory. The conduit carrying this circuit crosses the laboratory about 4 m above the floor, just forward of the radiator ductwork. The 480 volt power is conditioned by a 15 kilovolt-amp variable transformer and a .5 farad capacitor to deliver up to 30 amperes at up to 270 volts to the pump primary winding. The pump secondary delivers a maximum of 1000 amperes at about 6 volts to the pump cell. The pump must be manually restarted by turning a switch on the pump control panel whenever the pump has been shut off. In a scram the pump is slowed down by a servomotor attached to the variable transformer's handwheel. Except for a shutdown due to a power failure, the pump will still continue to operate in a scram. It can be stopped manually at any time by tripping the switch on the pump control panel, or by turning off circuit #16 in the breaker box in the hall outside the double doors at the east end of the laboratory. Circuit 16 holds shut an enabling relay which has been added to the original circuit of the pump control.

The main heater and radiator heaters are powered with 3 phase 208 volt current, 30 amperes maximum per phase, from circuit #33 of the hall breaker box. The conduit delivering this power comes from an original outlet on the north wall of the laboratory. A

flexible conduit makes the final connection to the movable heater control panel.

The main heaters and the radiator heaters on circuit #33 are connected in an ungrounded delta. If each load phase receives 20 amperes, each feed phase will carry the maximum rated 30 amperes of current. Therefore, 20 amperes is the maximum current available for any load phase of circuit #33, when the loads are balanced. If one of the loads is not carrying a full 20 amperes, the other loads may carry correspondingly more current but the circuit will not be completely balanced. This imbalance sometimes occurs, especially during standby operation when the main heaters are receiving little power but the radiator is receiving much power.

Each of the three feed wires of circuit #33 is fused within the heater control panel to carry 30 amperes. Six pairs of distribution wires between the control panel and the heaters are also individually fused (10, 15 or 20 amperes). The three-phase 208 volt power to the main heaters and radiator heaters is carried through a 15 or a 25 ampere silicon control rectifier unit or through variable transformers rated at 8, 15 and 30 amperes. The 15 ampere SCR, controlled by a temperature controller, is used to control the main heater output temperature when pumped operation is underway. The SCR may be used for some of the radiator heating power during standby operation when there is no lithium flow. The 15 ampere variable transformer is dedicated to the radiator heating. The 8 ampere variable transformer is used for both the main and radiator heaters at

different times; the 30 ampere variable transformer may be used to control some of the radiator heat but is always at least partly used for the main heaters. During standby operation when no lithium is flowing through the main heater, the 30 ampere transformer is the only power source for the main heater, and must be turned down low to avoid overheating the main heater.

The 25 ampere SCR is driven by a time-proportioning temperature controller which senses a selected temperature in the loop with one of the chromel alumel (type K) thermocouples attached to the loop. Normally the 25 ampere SCR is devoted to controlling the radiator temperature. During flow operation, the controller senses the temperature just downstream of the radiator. During standby operation the controller is switched to a thermocouple within the radiator housing itself. At both times, current is about 12 amperes.

The 25 ampere SCR temperature controller can be used to back up the 15 ampere SCR which governs the maximum loop temperature, should the latter controller fail. The 25 ampere unit is only time-proportional, while the 15 ampere unit is true-proportional and has integral and derivative control features. Although the larger SCR is rated for 25 amperes, current through the control wires should be limited to their rated 20 amperes.

The trace heaters are powered by single phases taken from two three-phase circuits. Each of these circuits, denoted #21 and #27 in the hall breaker box, are 208 volt, 30 amperes per phase. Each of

the 6 feed wires on these circuits is fused within the control panel to carry 20 amperes. The trace heaters are wired in a "Y" with returns to appropriate neutral feed wires. Each of the "hot" wires delivers 120 volt current to three or four dimmer switches. The dimmers are rated 600 watts each at 120 volts, for a maximum of 5 amps per switch. A 20 ampere fuse is therefore the maximum size to be used on the feedwires. Each dimmer is itself fused and the dimmer loads return to the proper neutral of either circuit #21 or #27. Circuits #21 and #27 were added to the laboratory specifically for the lithium loop. The delivery conduit comes along the main air duct at the west end of the laboratory, in front of the loop. A flexible conduit makes the final connection to the heater control panel, allowing some movement of the panel.

Present trace heater settings require only about 50 amperes of the 180 amperes available as 120 volt power from circuits #21 and #27. (The dimmer banks can handle a maximum of 100 amperes.)

Circuits #21, #27 and #33 feed their respective dimmers, SCRs and variable transformers through relays which are controlled by the scram alarm system. For the trace heaters, served by circuits #21 and #27, to be on continuously, their relays are kept on manual "on" control. (Automatic control would turn the trace heat on only during a scram.) The main heater clamshells must be kept on automatic control since their heat flux to the insulated main heater is high enough to cause extreme overheating of the loop should the lithium flow cease. The radiator heaters, although they dissipate a great

deal of energy, are less likely to raise the radiator temperatures high enough to endanger the loop, since the radiator is not so well insulated as the main heater.

Since the feed circuits are all three-phase, the operator must use care when wiring heaters so that circuit #33 phases are not interconnected except through a 208 volt load. Phases are never interconnected in any way for circuits #21 and #27, since the dimmer switches in these circuits are limited to 120 volts.

It is a good policy to turn on circuit #27 first when switching on the heater circuits #21, #27 and #33. Circuit #27 powers the controllers as well as a fan which cools the 20 dimmers in their two mounting boxes. With the fan off, the dimmers will overheat.

Wiring inside the control panel and between the control panel and heater terminal box is plastic insulated. The main feed circuits are wired with #10 TW, capacity 30 amperes. The main and radiator heater distribution wiring is #12 TW, capacity 20 amperes. The trace heating circuits are #14 TW, capacity 15 amperes. Control circuitry (not delivering power to heaters) is largely #16 and #18 wire, capacity 10 or 5 amperes. The #10, #16, and #18 wire is stranded copper. The #12 and #14 wire is solid copper.

Between the control panel and heater terminal box is a 1 -1/2" conduit containing 15 #12 wires and 30 #14 wires. Code maximums for a 1-1/2" conduit are 47 #12 or 60 #14 wires.

Connections of the control circuits to the heaters are made on

terminal barrier strips in the heater terminal box, a NEMA enclosure attached to the loop at the lower right front of the loop enclosure. Each control circuit has a pair of terminals in the NEMA box. The six circuits for 208 volt loads each have a double pole, double throw center-off switch for selecting either the main heater or other (primarily radiator) heaters. These switches should not be opened or closed under load.

Each of the loop heaters is connected to the NEMA barrier strips in the same box with the power delivery wires. Appropriately sized (#12, #14 or #16) removable wires are used to connect the control (delivery) circuits to the load (heater) terminals. It is fairly easy to change the circuitry. Fanning strips are used to switch the radiator connections from standby to operating hookups.

Wiring within the loop enclosure is #14 SF-2 fiberglass-on-silicone-rubber insulated stranded copper wire. The insulation is rated for operation at 200 C. The wires are exposed to higher temperatures at some places. Wherever possible, heater power wiring is run near the bottom or rear of the loop enclosure, away from the thermocouple wires which are generally placed upward and to the front of the enclosure.

The 1-1/2" rigid conduit connecting the control board to the NEMA heater terminal box lies on the floor and pivots at both ends to allow limited movement of the control board. The electrical power to the control board comes via flexible overhead conduits,as previously noted.

Temperature measurement and control

There are more than 100 thermocouples on the loop. These are chromel-alumel (type K) grounded junction couples made by joining 18 gauge bare wires with tungsten-inert-gas (TIG) welding. The bead of metal formed at the welded junction is peened to give a flat disk of metal and is then spot-welded directly onto a pipe or vessel wall with a capacitor-discharge spot-welder, using a setting of about 200 watt-seconds. Fish-spine ceramic beads are used to insulate the bare thermocouple wire. Outside the piping insulation, type K glass-on-glass insulated duplex (paired) thermocouple wire is crimp-spliced onto the beaded thermocouples to carry the signal from 100 of the thermocouples to a thermocouple junction box. Thermocouples on the isothermal zones of the test sections differ in being made entirely from double-glass insulated type K 20 gauge or 22 gauge wire (the same kind of wire used to carry the thermocouple extensions to the junction box). Fish-spine beads are again used to insulate the last two or three inches of the thermocouple near its attachment to the tube wall.

The double-glass insulated wires from the thermocouples lead to phone jacks in a junction box on the left rear of the loop enclosure. Up to 30 of the 100 thermocouples can be selected for recording on three multipoint strip chart recorders.

The connection between the junction box and the recorders is made with phone plugs and PVC insulated type K extension wire.

Wherever possible, thermocouple wiring is run near the front or top of the loop enclosure to avoid crossing the heater power wiring which is generally placed at the back or bottom of the enclosure.

One thermocouple at a time can be monitored with a digital thermocouple readout accurate to $\pm$ 1 degree C. One thermocouple on the exit of the main heater is monitored by a control switch for safety against overheating. If possible, two such thermocouple/switch safeties should be used on the main heater for additional security.

A timing device automatically turns on the recorders for a few minutes of every two hours in order to obtain a running log of the loop temperatures. The entire set of thermocouples should be logged every few weeks using the digital thermocouple readout.

The temperature distribution around the loop is governed mainly by the energy input in the main heater and by the heat lost in the radiator; during flow operation the trace heaters have a smaller effect. When flow is stopped, the trace heating determines the temperatures which are eventually reached, and which are usually lower than the temperatures achieved during flow operation. The dimmer switches controlling the trace heaters are set at voltages found by trial and error during the initial preheating of the loop. With no lithium flow, the trace heaters maintain loop temperatures

around 250C . However, the upper part of the radiator is at about 400 C and the lower radiator is around 200 C.

When the lithium is flowing around the loop, the temperature profile is smoothed out between the maximum and minimum temperatures which occur at the main heater and the radiator, respectively. The maximum temperature is set roughly with one or two variable transformers and fine-controlled with a SCR unit driven by a fully proportional controller which monitors the lithium temperature in the lower manifold, just downstream of the main heater. The control thermocouple is an iron-constantan (type J) thermocouple in a lead-3% tin melt in a thermocouple well which extends radially into the center of the manifold pipe. The controller also has derivative and integral control actions. A proportional band of 5% and a 0.1 min integral time are used. No derivative action is used.

The temperature of the radiator must also be controlled, although in practice the control is not as precise as that of the main heater. Final control of the radiator temperature is by a time-proportioning controller driving heaters through a relay or solid-state switch (SCR). The time-proportioning controller uses one of the loop's chromel-alumel thermocouples as a sensing element. Any thermocouple may be selected. Usually a thermocouple outside and just downstream of the radiator (flow operation) or inside on the bottom finned pipe (non-flow servicing) is chosen. In an emergency this controller could serve the main heater, but it would not do a suitable job for fine control of the maximum temperature.

Pressure measurement

The pressure of argon in the expansion tank may be checked occasionally and brought to approximately 0.5 - 1.0 psig by adding argon to the tank or bleeding it off. The argon supply is not valved into the loop continuously due to the safety hazard of having the pressure maintained within the loop should a leak occur.

Pressure is measured by conventional Bourdon-tube gauges. The gauge on the upper manifold, which can be used to measure the surge tank argon pressure, is normally valved off from the surge tank and when measuring the gas pressure in this tank, the gauge is shielded from lithium mists by a stainless-steel-wool packed demister tube.

There are no automatic control features associated with the loop pressure. A safety relief valve, which is set at 5 - 6 psig, should prevent hazardous pressures of argon being delivered to the loop. However, this relief valve is on the supply cylinder, which is not normally valved into the loop.

In addition to the Bourdon gauge on the upper gas manifold, there is a similar gauge on the lower gas manifold at the dump tank. Both gauges read vacuum as well as positive gauge pressures.

The pressure in the lithium itself is not measured. It can be estimated knowing 1.) the height of lithium above a given point in the loop, 2.) the pressure in the surge tank, and 3.) the pressure drop due to flow in the loop.

Flow measurement

Permanent magnet flowmeters monitor the lithium flow rates in each of the four parallel test sections. The magnets have flux densities of approximately 4 kiloGauss, and are installed to have the 1.3cm ID type 316 stainless tubing of the test section passing between the magnet poles. Type 316 stainless steel wire electrodes with a diameter of .5mm are spot-welded onto the tubing at right angles to the magnetic field. A capacitor discharge welder was used to spot weld the wires onto the pipe. Ceramic fish-spine insulator beads are used to insulate the wires near the attachment to the tubing. For each of the four meters, two pairs of electrode wires are attached. One pair runs through fine teflon spaghetti tubing insulation up to the outside of the loop enclosure, where it connects with copper wires from a multipoint 0-10 millivolt recorder. The other, spare, pair of electrodes is not extended out.

The four meters were calibrated by draining lithium by gravity through the test sections. The time necessary to drain a known volume of the surge tank, as measured with the level probes, was measured. Several trials were averaged to get a meter calibration factor for each meter. The drain tests agreed fairly well with thermal tests which included measuring the temperature rise of lithium pumped through the main heater under a known electrical energy input to the main heater. A computer program was used to perform least squares analyses to find the meter factors (Appendix O).

Power measurements

The power used by the electric heaters is estimated using the ammeter reading and a knowledge of the equivalent resistance of the heater circuit being supplied through the ammeter. The electromagnetic pump control panel includes its own voltmeter as well as an ammeter. (See also power information, Appendix E).

Lithium level measurements

The lithium level in the dump tank can be measured with a removable inductive probe which slides into a dead-end well in the tank. The probe is reportedly accurate to within 3 mm. (Mine Safety Co., 1973).

The lithium level in the surge tank is monitored with a continuous readout resistance probe, which, from a constant input current, generates an output voltage linear with the level of the lithium. Two short-out probes, which indicate when the lithium is above (or below) a single set level, are used for checking and calibration of the continuous probe. The continuous probe can also be checked approximately by comparing the output to the level of lithium on the fisher rod used to remove the coupon stringers from the loop. The fisher rod can also be used to check the level of the frozen lithium in the freeze standpipes and thus check against a second level in the surge tank. Such checks should be made with all the

precautions used when working with molten lithium. It should not be assumed that the lithium in the standpipes is ever frozen; the temperature should be checked by thermocouple and (if the thermocouple indicates a low temperature) by touch.

The short-out probes are driven with 6 volt a.c. and actuate relays which can be tied into the scram alarm system. Low voltage light bulbs give a visual indication of whether lithium has reached either of the short-out probes, which extend down into the surge tank about 18 and 32 cm.

The continuous level probe's output is around 15-20 millivolts for a full expansion tank and about 40 millivolts for a nearly empty tank. A millivolt potentiometric indicator monitors the continuous probe. Microswitches on the indicator are tied into the scram alarm system. The high and low level microswitches of the continuous probe are adjustable. The short-out probes are not adjustable. All three probes are held in Swagelok fittings on the surge tank.

During the first year of operation of the loop, the higher short-out probe shorted to a continuously-on condition, making this probe useless for further monitoring. This probe was later replaced with one of a design similar to the original continuous-type probe, which also shorted when lithium splashed against it while a vacuum was being drawn on the surge tank. This small diameter probe was replaced but immediately shorted; its port was then plugged with a fitting. A larger probe is now the continuous one.

Control panels

The heater control panel houses dimmer switches, variable transformers, and SCR power controllers, as well as the ammeters, fuses and switches for each control circuit. Within the panel are the heater power relays and much of the scram alarm circuitry. The main heater temperature controller unit and the radiator temperature controller unit are also in the control panel. The panel is framed with slotted angle steel and is covered with plywood panels.

A second control panel unit serves the electromagnetic pump. This commercially built panel houses a 15 kilovolt-amp variable transformer, a .5 farad capacitor, and the potentiometric recorder which monitors the continuous level probe. Along with the pump control wiring, the panel contains the constant current source for the continuous level probe and a capacitor-type temperature control switch for protecting the main heater against overtemperature.

A separate rack holds four potentiometric recorders. Three are used to log temperatures and the fourth logs the millivolt outputs from the flowmeters. The rack also holds the power and pilot light box for the short-out level probes, and the recorders' automatic timer unit. Nearby is a second temperature control switch to provide additional security against main heater overtemperature.

Precautions

Automatic instrumentation is provided to sense and take action against: 1.) main heater overtemperature, 2.) unusual increase or decrease in the lithium level in the surge tank, and 3.) leaks, as evidenced by smoke from a lithium fire. In such conditions, the loop is automatically scrammed to standby conditions by turning off the main heaters, reducing the pump power setting, and closing the radiator damper. The radiator heaters remain on.

At least one, and when possible two, thermocouples located on the exit end of the main heater are connected to temperature switches which will scram the system if the heater temperature rises above a selected limit temperature, usually set 50 degrees C above the desired maximum temperature of the experimental run. The main heater can overheat dangerously in a few minutes if the lithium flow is stopped or greatly reduced. A lockout relay prevents the heaters from being turned on in the automatic mode with the pump off. To lessen risks of overheating in the manual mode, a spring-loaded enabling switch is used which must be held shut to operate main heater circuits in the manual mode. The manual mode is used almost exclusively during stringer servicing, when much of the main heater power is switched over to the radiator. During such manual-mode usage, care must be taken to limit any heat delivered to the main heater clamshells and thus avoid dangerous and unchecked temperature rises. The main heaters should not be left unattended in the manual mode. Since during stringer

servicing operations, the pump will not be on, the lockout relay may be overridden with a shunt switch to permit automatic mode operation at these times, too.

The operator should be aware that the pump may be turned on yet not be moving any lithium. In particular, this may occur if a section of the radiator piping becomes plugged with frozen lithium. Prolonged non-flow operation of the pump at power settings above a few percent may overheat the pump cell. When the flow is very low or stopped entirely, a safety buzzer on the flowmeter recorder will sound. The buzzer should be disconnected only when the pump is turned off.

A pair of photocell smoke detectors were installed in the radiator ductwork to sense smoke and scram the loop; these photocells do not presently monitor the rest of the enclosure. (It was originally planned that forced airflow through the radiator would aspirate some of the air from within the enclosure past the photocells. Since forced airflow is not used currently to cool the radiator, this anticipated scavenging action is not available to help monitor the enclosure air for smoke.) The sensitivity of the smoke detection system is uncertain; it has been disconnected from the scram circuits for much of the experiment. It should be checked for reliability and reconnected. A conventional ionization type smoke sensor is installed on the laboratory ceiling and is connected into the building alarm and annunciator system. Perhaps a similar sensor for the scram system could be mounted in the loop enclosure.

There are three level probes in the surge tank. One monitors the lithium level from full to empty, in a continuous linear fashion. A calibrated potentiometric indicator performs the monitoring. The indicator has adjustable safety switches for high and low level. Two single - point probes also are in the surge tank. One extends 18 cm into the tank. The other extends 32 cm in, to near the bottom of the 44 cm tank. In conjunction with these two probes are relays which can interface the probes to the scram circuit. Pilot lights on the recorder rack show the status of the two single-point probes. One single-point probe, as noted previously, had to be replaced due to a lithium nitride nodule shorting the electrode to the tank lid. The original single-point probes were made from spark plugs, while the continuous probe and replacements use a fitting designed for vacuum-pass-through service.

After any scram, the safety circuits must be reset by manually closing an electrically latched relay. Only the trace heaters and radiator heaters are unaffected by a scram. These are on whenever the building power is on and the proper breaker switches are closed. The electromagnetic pump is usually slowed but never shut off completely in a scram (except if the scram is caused by a power failure.) The pump can be tripped off at the control unit in the

laboratory, or by turning off circuit #16 in the hall breaker box.

An ever-present experimental problem is the tendency of the lithium to freeze, especially in the radiator, if a power outage or scram occurs. As long as the pump keeps the lithium moving, it will stay fluid for a considerable time, but with flow stopped, the lithium within the radiator may freeze in less than ten minutes. No problems have been encountered in remelting the lithium in the radiator, except that the process is time-consuming (sometimes requiring a half day or more.) The radiator pipes are not in direct contact with heaters except for the U-bends and the entrance and exit piping. In general, the available heat input, used judiciously, is not enough to endanger the radiator (i.e., to rupture partly frozen pipes by thermal expansion of lithium) as long as temperatures are carefully watched. However, when necessary to use 208 volt power on the left-end U-bends' heater, particular attention should be paid to avoid overheating the U-bends. The right end U-bend heater is only rated for 120 volts.

If there should be widespread freezing, as might begin to occur during a power failure of more than 30 minutes, extreme care would have to be used in applying trace heat during the thaw. In particular, after an outage of such duration, an operator must be on hand when power is restored, so that the trace heaters can be monitored or turned off if freezing has occurred. The trace heaters are on whenever the power to the building is on; they are

not affected by the scram circuitry. This prevents possible freezing in a false alarm scram or after short power outages, but could cause trouble if a prolonged power outage occurs and the operators are not present to oversee the loop when the power is restored.

In the event of widespread freezing in the loop (which has not been experienced to date) rethawing must begin at the surge tank, where the volume increase during melting can be safely accommodated. Thawing must progress along such a route that a liquid path back to the surge tank is always open from any zone(s) where thawing is taking place, to prevent pipe rupture by the expansion of the melting lithium. The trace heaters are powered through 20 circuits to enable fairly selective heating of the loop. Temporary rewiring in the heater terminal junction box (between the control panel and the loop enclosure) would allow additional careful variations of the heat distribution.

Operating environment

The lithium loop is enclosed by 1/16" sheet steel panels fastened with standard 1/4"-20 x 1/2" long hexagonal head bolts threaded into a frame of two inch steel angle; the frame has struts made of 1-1/2 inch steel angle. The steel panels are partitioned for easier removal if it is necessary to access the inside of the enclosure for maintenance. Backup lips close the horizontal cracks between the panels. The frame or struts back up the vertical cracks. The enclosure is meant to protect the operator and laboratory in the event of a lithium leak. It is not gas tight. A window at the right end of the enclosure allows limited visual inspection of the interior. The bay doors at the pump can be easily opened (by loosening wing nuts) for additional inspection.

The "floor" of the enclosure is a 1/16" welded sheet steel pan with sides 10 cm high. The pan will contain lithium which might be spilled if a leak occurred. The pan volume is 0.2 m^3. The volume of the lithium loop is .024 m^3. An additional .014 m^3 of lithium is stored in the dump tank, as a reserve supply for lithium lost during sampling and stringer servicing.

The loop enclosure can be manually vented to a 1.9 $m^3 s^{-1}$ (4000 $ft^3 min^{-1}$) exhaust fan by pulling a trip wire hung across the laboratory to the far end of the room. The exhaust fan can be switched on from the hallway. Air exhausted through this large fan passes first through a prefilter and then through a high

efficiency particulate air (HEPA) filter. The HEPA filter is rated for operation at 540C.

General ventilation of the laboratory itself is by the building air conditioning system, and can be supplemented by the use of a fan serving a laboratory hood. Airflow through the room is, however, reduced to allow the radiator to attain higher temperatures. Reducing the airflow through the room apparently reduces the flow (leakage past damper, etc.) of air through the radiator.

Where possible, water and steam pipes in the laboratory have been shut off.

Operator clothing

For personal safety, protective clothing is available to the operators while working near the loop. This garb is especially advisable when operators are servicing stringers or are sampling lithium.. (Mausteller, 1967).

Chrome leather helmets with flip-open visors are on hand. Under these, goggles or safety glasses with side shields are advisable. Chrome leather jackets, aprons, spats, and gloves are provided. Leather shoes should be worn; steel-toed shoes are best.

For personal clothing, fire-resistant cotton or woolen garments are preferred over synthetic fabrics. Synthetic fabrics will smolder and melt, and lithium runs on them. Natural fabrics self-extinguish,but lithium may either bounce off or stick to them.

Lithium fires

At temperatures above 260C lithium can spontaneously ignite in air. The temperature of the burning metal may be above 800 C. In contrast to hydrocarbons which burn in the vapor phase, liquid metal will burn as a glowing mass, possibly without visible flames (Mausteller, 1967).

If burning lithium falls on concrete, the concrete may spall or shatter like shrapnel. The addition of fire extinguishants can splash the burning metal.

Most common extinguishants react violently with lithium. Carbon dioxide, water, sodium carbonate ("dry powder") all react violently with lithium! Carbon tetrachloride is of course not to be used as an extinguishant, as in addition to reacting with lithium it may generate phosgene gas. Only graphite powder and Ansul brand Lith-X (or Met1-X, with precautions) are to be used to fight a lithium fire. Sodium chloride-based extinguishants (Met1-X for one) are not very effective since much of them will sink in lithium. Salt-base extinguishants are also corrosive to equipment.

Lithium leaking from insulated pipes may smolder in the insulation. Sodium-chloride based extinguishants may be more effective than graphite powder on insulation since the salt will stick to the smoldering area. Graphite cloth could be used to smother smoldering insulation.

The lithium laboratory is presently stocked with 80 kg of graphite spheroids (some in a large can with a scoop), a carbon dioxide charged pneumatic extinguisher holding 14 kg of Met1-X, a spare CO_2 cartridge, and additional Met1-X.

In order to apply solid extinguishants, the enclosure of the loop would have to be opened. The bay doors at the pump can be opened, and with more effort the upper left panel of the enclosure can be removed, after unscrewing a half dozen thumbbolts. In the event of a fire it might be judged more advisable to let the lithium burn itself out inside the enclosure. The 4000 ft^3 min^{-1} fan could be used to exhaust smoke from the enclosure through the HEPA filter (rated for operation at up to 540C) to the outside of the building. Such action might, however, fan the fire. The enclosure would have to be vented into the radiator exhaust duct by pulling the emergency trip wire strung across the laboratory ceiling to the opposite end of the laboratory. The laboratory hood fan could be used to exhaust smoke from the room.

In addition to the solid extinguishants on hand, a 330 ft^3 cylinder of argon is connected to the loop enclosure through a 3/4" IPS pipe and a sparger inside the enclosure at the upper left end. A single ball valve can be manually opened to flood argon at a pressure of 10 psig into the loop enclosure in case of fire. Some loops elsewhere have operated in inert atmospheres, particularly if the containment metal

was easily oxidized. With the air-cooled radiator in this loop, routine maintenance of an inert atmosphere in the enclosure is impractical.

If a fire does occur, the scrammed loop may be manually drained or "dumped" into the dump tank. However, the advisability of such a dump is questionable. The loop could not at once be drained completely into the dump tank. Some of the lithium would have to be transferred over to the shipping tank. The shipping tank would have to be heated to thaw the lithium first, as would the transfer lines. This would take at least several dangerous hours. It might even be impossible to drain the loop completely because of the sluggish flow behavior of lithium. Pressure might be needed to drain parts of the loop. Frozen lithium, as in the radiator, might inhibit draining. Finally, a drained loop is quite prone to contamination. A more favorable alternative to draining, if the leak is not serious, is to freeze the lithium in the loop and try to make repairs without draining. Techniques are outlined in several references.(See, for example, Mausteller, 1967.)

Although the auxiliary tank and the transfer line between it and the dump tank is frozen, the dump tank is kept at about 250C and the dump lines and valves are kept near the melting point of the lithium. Cover gas lines and drain lines are in effect checked at each stringer service operation, when lithium is actually transferred to and from the dump tank and the loop.

Cleanup should immediately follow a lithium spill or fire. This will reduce the chances of further fire and will minimize the corrosion of equipment by lithium and extiguishants. Cleanup methods are outlined in the literature (Mausteller, 1967).

First aid

If lithium splashes on gloves or clothes the affected apparel should be removed immediately. Heat is rapidly conducted through gloves, fabrics, and so on. The lithium, if not yet burning, may ignite. Chemical burns may occur. Hydroxide penetration into tissues would make chemical burns difficult to treat. The alkali must first be neutralized before healing would be possible.

Skin contacted by lithium should be very quickly flooded with large amounts of water for at least ten minutes. (The metal should first be removed quickly, if possible.) A 3% acetic acid solution (vinegar) can be used on the skin to neutralize hydroxides. Acetic acid should not be used near the eyes. A ten to fifteen minute eye wash with cool water and boric acid rinses is recommended. High pressure water should not be used for long periods of time (30 minutes) since it can cause permanent damage to the eyes.

Plastic eye wash bottles of distilled water or commercial saline solution are provided in the laboratory. An eye wash and safety shower are in the hall outside the lab. Since there is no

drain for these fixtures, thresholds 3/4" high have been anchored in placed across both doorways to the laboratory, to prevent water from running into the lab from the hallway in case the eye wash or safety shower is used.

The smoke from a lithium fire is said to be the most annoying produced by any burning alkali metal fire. Although not systemically poisonous, lithium smoke will thermally and chemically burn the throat and lungs. Standard dust filters are stocked in the lab to provide some protection to the respiratory system. A portable five-minute self-contained air supply and hood are also stocked. As an added safety measure, Scot air packs should possibly be purchased, as the five-minute air supply would be of little use in fighting a fire.

While cleaning lithium from coupons, stringers or tools, one should protect face and hands against splashed caustic. A fine aerosol mist is often formed by lithium dissolving in water. This mist irritates the respiratory system. The mist can be minimized by dissolving the lithium under several inches of water.

Gloves and suitable containers should be used when handling items wet with hydroxide solution. The solution is rather irritating to the skin, even when quite dilute. Hands should always be rinsed well after being in contact with LiOH solutions.

The operator must use caution with the alcohol rinses during cleaning coupons. Breathing the fumes is unhealthy. Fire can occur.

Alarms

The lithium loop operates 24 hours a day. It is generally unattended at night and for long periods during the days. The scram alarm system is monitored at all times at the University Police and Security Department switchboard (110 N. Mills Street, phone 262-2957, business phone 262-4524). In case of an alarm, the police telephone a list of operators responsible for the laboratory. One of these persons carries a radio paging unit so that he at least can be reached at any time. This operator, if notified by the University police, must immediately go to the laboratory. A police or security officer will also be sent to the laboratory. Decisions as to appropriate action (whether to call the fire department) are generally made by the operator in charge of the laboratory, but an obvious fire would be reported to the officer, who usually would arrive before the operator.

During the first 14 months of operation there were several false alarms due to temperature switch malfunctions. In two cases an operator was not reached and the Madison Fire Department came to the laboratory. A short in the control panel wiring, which burned some wire insulation and scorched a small area of the panel, caused an alarm after a fuse blew and the loop cooled, whereupon the lithium level apparently dropped sufficiently to cause a scram. No serious damage has ever occurred to the loop in these situations.

NOTES

[1] The format of this section is taken from a similar report, System Design Description of Forced Convection Molten-Salt Corrosion Loops MSE-FCL-3 & 4, (ORNL/TM-5540), by W.R. Hundley and M. D. Silverman.

Much of the operating information contained here and elsewhere in this thesis is taken from the book Alkali Metal Handling and Systems Operating Techniques by J.W. Mausteller, F. Tepper, and S.J. Rogers; Atomic Energy Commission Monograph Series, Gordon and Breach, New York, 1967.

Another general book on liquid metals is the Na-K Engineering Handbook (4 volumes) edited by O.J. Foust, Gordon and Breach, New York, 1972. Also, Liquid Metals Handbook (3rd Edition), Na-NaK Supplement, edited by C.B. Jackson. TID 5277, Atomic Energy Commission, United States Navy Bureau of Ships. United States Government Printing Office, 1975.

[2] The electromagnetic pump is placed after the temperature rise (outer) pass of the economizer and before the main heater. The temperature of the pump cell is near the maximum loop temperature. Generally, the electromagnetic pump is placed in a cooler part of the loop (Mausteller, 1967). Since the loop here runs at lower temperatures than many liquid metal systems have customarily been operated with, the temperature of the pump should not be excessive.

CHAPTER IV. LIQUID PHASE MASS TRANSFER THEORY

The conservation equations which describe fluid momentum and mass transfer are

$$\frac{D\rho}{Dt} = -(\nabla\cdot\rho\underline{v}) \qquad \text{(IV.1)}$$

$$\rho\frac{D\underline{v}}{Dt} = -\nabla p - [\nabla\cdot\underline{\underline{\tau}}] + \sum_{i=1}^{n} \rho\underline{g}_i \qquad \text{(IV.2)}$$

$$\rho\frac{D\omega_i}{Dt} = -(\nabla\cdot\underline{j}_i) + r_i \quad i=1,\ldots n-1 \qquad \text{(IV.3)}$$

where the mass flux $\underline{j}_i$ is

$$\underline{j}_i = -\rho\mathcal{D}_i \nabla\omega_i = \underline{n}_i - \omega_i \rho\underline{v} \qquad \text{(IV.4)}$$

Equations (IV.3) and (IV.4) may be combined to give, for constant temperature and pressure,

$$\rho \frac{D\omega_i}{Dt} = \nabla\cdot\rho\mathcal{D}_i\nabla\omega_i + r_i \qquad \text{(IV.5)}$$

This set of equations can be solved for flow past fixed interfaces by using boundary layer theory. Axial diffusion is neglected, the fluid velocity in the boundary layer is assumed to be proportional to the distance from the interface, and the diffusion boundary layer is assumed to be thin compared to the curvature of the interface. Neighboring boundary layers must not overlap. Stewart(1963), for example, outlines solutions for laminar flows.

Boundary layer solutions are often presented for heat transfer; these can be modified to obtain the mass transfer analogs. For two-dimensional flow along a flat plate, or in the entrance region of a tube, the heat flux and wall temperature are

$$q_0 = \frac{1.1198\, k\, \chi^{1/3} \sqrt{v_\infty}\, x^{-1/4}}{(9\alpha)^{1/3}} \int_0^x \left[\frac{4}{3}\left(x^{3/4} - \xi^{3/4}\right)\right]^{-1/3} dT_0(\xi, z) \qquad \text{(IV.6)}$$

$$T_0(x,z) - T_\infty = \frac{\chi^{-1/3} \sqrt{v_\infty}}{(9\alpha)^{2/3}} \frac{\int_0^x \left[\frac{4}{3}\left(x^{3/4} - \xi^{3/4}\right)\right]^{-2/3} q_0|_\xi d\xi}{\frac{1}{3}\Gamma\left(\frac{4}{3}\right) \rho \hat{C}_p} \qquad \text{(IV.7)}$$

where $$\chi = \frac{0.332}{2}\sqrt{\rho/\mu} \qquad \text{(IV.8)}$$

The solutions for developed laminar flow in a tube are

$$q_0 = \frac{1.1198 k \left(\frac{8\langle v\rangle}{D}\right)^{1/3}}{(9\alpha)^{1/3}} \int_0^x [x-\xi]^{-1/3}\, dT_0(\xi, z) \qquad \text{(IV.9)}$$

$$T_0(x,z) - T_\infty = \frac{\left(\frac{8\langle v\rangle}{D}\right)^{-1/3}}{(9\alpha)^{2/3}} \frac{\int_0^x [x-\xi]^{-2/3} q_0|_\xi\, d\xi}{\left(\frac{1}{3}\right)\Gamma\left(\frac{4}{3}\right) \rho \hat{C}_p} \qquad \text{(IV.10)}$$

These forms can be applied to mass transfer through equations (IV.11).

$$q_0 \longleftrightarrow j_i \qquad \text{(IV.11)}$$

$$T \longleftrightarrow \omega_i$$

$$k \longleftrightarrow \rho \mathcal{D}_i$$

$$\alpha \longleftrightarrow \mathcal{D}_i$$

$$\rho \hat{C}_p \longleftrightarrow \rho$$

$$Pr \longleftrightarrow Sc$$

HEAT AND MASS TRANSFER COEFFICIENTS

The heat transfer coefficient h and the mass transfer coefficient $k_{\omega i}$ are defined

$$q_0 = h\,(T_0 - T_\infty) \tag{IV.12}$$

$$j_{i0} = k_{\omega i}(\omega_{i0} - \omega_{i\infty}) \tag{IV.13}$$

These coefficients are often presented as Nusselt numbers

$$Nu = \frac{hD}{k} = -\frac{\partial}{\partial(r/D)}\left[\frac{T_0 - T}{T_0 - T_\infty}\right] \tag{IV.14}$$

$$Nu_i = \frac{k_{\omega i} D}{\rho \mathcal{D}_i} = -\frac{\partial}{\partial(r/D)}\left[\frac{\omega_{i0} - \omega_i}{\omega_{i0} - \omega_{i\infty}}\right] \tag{IV.15}$$

which are the dimensionless temperature or concentration gradients at the interface.

Graetz (1885) presented a series solution of the boundary layer problem for a constant property fluid in fully developed laminar flow in a circular tube. For large values of the Graetz number (Gz) the Nusselt number approaches the asymptote

$$Nu = 3.656 \qquad \left(Gz \equiv \frac{x}{Re\ Pr\ D} > 0.025 \right) \tag{IV.16}$$

For small Graetz numbers ($Gz < 0.01$) the Nusselt number is given by the Lévêque (1928) solution

$$Nu = 1.62\ (Re\ Pr\ \frac{D}{L})^{1/3} \tag{IV.17}$$

The flat plate solution from Pohlhausen's results (1921)

$$\frac{h\ x}{k} = 0.332\ Re_x^{1/2}\ Pr^{1/3} \tag{IV.18}$$

also fits data for laminar heat transfer in the entrance of circular tubes (Cholette, 1948; Karim and Travers, 1949).

HEAT TRANSFER CORRELATIONS

Experimental heat and mass transfer data are often summarized by correlations of the Nusselt number with the Reynolds number and the Prandtl or Schmidt numbers. Two examples are Sieder and Tate's correlation for turbulent flow

$$Nu = 0.026\ Re^{.8} Pr^{1/3} (\mu_b/\mu_0)^{.14} \qquad (IV.19)$$

and Hausen's (1943) equation for the thermal entrance region in developed turbulent flows

$$Nu = 0.116\ [\ Re^{2/3} - 125]\ Pr^{1/3}\ [1+c(\frac{D}{x})^{2/3}]\ (\mu_b/\mu_0)^{.14} \qquad (IV.20)$$

c=1 for 1/3 for local, 1 for mean Nusselt number

Correlations such as these are useful for calculating heat or mass transfer following a step change in wall temperature or concentration. The solutions for variable wall temperature or concentration may be found by superposition (for example, see Eckert and Drake, 1959).

If the heat flux following a step change in wall temperature is

$$q_0(x) = \frac{k}{D} Nu(x)\ \Delta T_0 = h(x)\ \Delta T_0 \qquad (IV.21)$$

then the heat flux from a wall with a variable temperature is, by superposition,

$$q_0(x) = \int_0^x h(x,\xi)\ dT_0(\xi) \qquad (IV.22)$$

Superposition is particularly useful for laminar flows, where the boundary layers remain intact for long distances so that wall temperatures or fluxes have a major effect in the downstream boundary layer. The distance over which upstream conditions show direct influence on a turbulent boundary layer may be quite short

(Shaw and Hanratty, 1977) and superposition is consequently less often used, though still appropriate under the assumption of constant physical properties.

For flows in long tubes at Reynolds numbers ($D\langle v\rangle\rho/\mu$) greater than 2100, turbulence appears. For flat plate flows, turbulence begins at a length Reynolds number ($x\, v_\infty\, \rho/\mu$) of about 3×10^5. Theoretical descriptions of turbulent flow are not as exact as those for laminar flow, but heat and mass transfer can be predicted, for instance with semi-empirical equations which have been developed from data and dimensional analysis.

Figure IV.1a summarizes Sieder and Tate's (1936) results, which include transition region heat transfer. Sieder and Tate's transition region data are fitted by

$$j_H = \frac{j_H(\text{turb})}{[j_H(\text{turb})/j_H(\text{lam})]^{g(Re)}} \qquad \text{(IV.23)}$$

where the exponent g(Re) is $22.4 \times 10^6\, Re^{-2.2}$ (see Appendix S). The data for the surface average Nusselt number in the transition region are also fitted fairly well by the Hausen equation (IV.20).

All of Sieder and Tate's data include a thermal entrance region, and the complicated trends of the j factor in the transition region might be due to an averaging across an abrupt jump in the local coefficient with the onset of turbulence. The average friction factor for a flat plate with a laminar-turbulent transition at a length Reynolds number ($x\, v_\infty\, \rho/\mu$) = 5×10^5, as shown on Figure

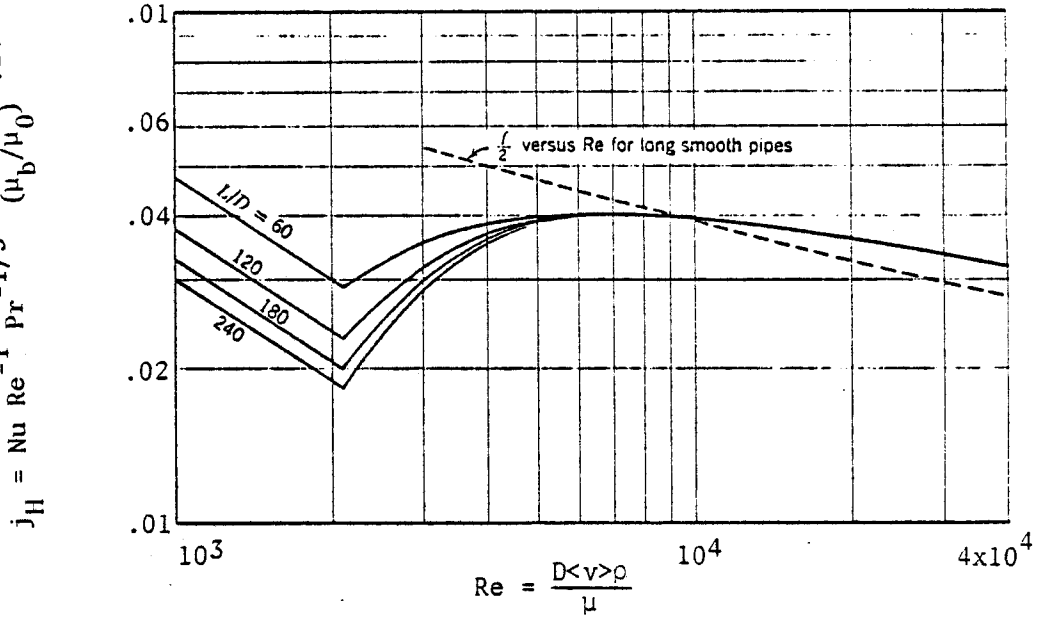

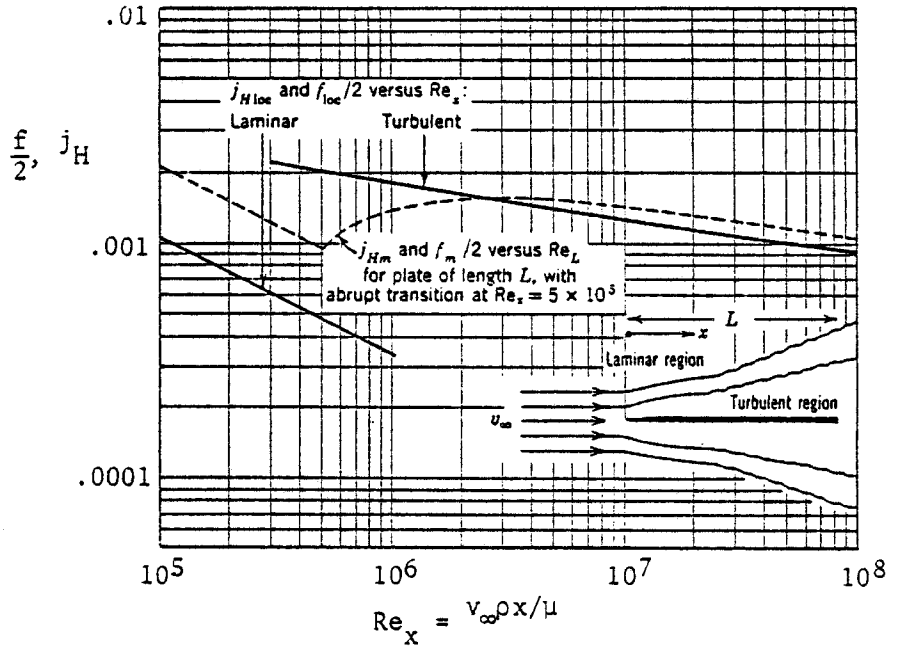

FIGURE IV.1. j factor charts showing transition region.
Top: Smoothed data of Sieder and Tate.
Bottom: Blasius and Pohlhausen theoretical results.
From Bird, Stewart, and Lightfoot (1960).

IV.1b, shows a trend with Re similar to that seen in Sieder and Tate's data. This curve, obtained by averaging over the entire length of surface, shows how an abrupt jump in the local j factor gives a gradual rise in the surface-mean j factor. Also, many of Sieder and Tate's data are for oils with strongly temperature-dependent viscosity; such fluids may undergo transition during heating or cooling even though the entering fluid was fully developed.

LAMINARIZATION

Turbulent flows undergoing a strong acceleration may revert temporarily to laminar flow. Relaminarization has been observed experimentally by Moretti and Kays (1965) and by Talmor and Weber(1970), among others. Kays (1966) reported that such a relaminarization would take place if an acceleration parameter K exceeded 3.5×10^{-6}, where

$$K \equiv \frac{\nu}{u_\infty^2} \frac{du_\infty}{dx} \qquad \text{(IV.24)}$$

A major result of relaminarization is a reduction in transfer coefficients in the relaminarized zone. The relaminarized flow is usually unstable and will revert to turbulence some distance downstream from the acceleration. Talmor and Weber (1970) reported that freestream turbulence, as well as the acceleration parameter, was a factor in determining whether relaminarization would occur. With 1.1% freestream turbulence, an acceleration parameter

$K = 10^{-6}$ would cause the reverse transition, while K must be 4.4×10^{-6} to effect relaminarization with 3% freestream turbulence.

Investigators of relaminarization have used converging rectangular or conical ducts to smoothly accelerate the flow without causing separation. Possible relaminarization following a sharp contraction apparently has not been studied to the same extent. Ede et al.(1956) studied heat transfer to water flowing in a circular tube following a sharp 2:1 reduction in the tube diameter. This geometry is similar to the test zones in the present research. Data from Ede and from Cholette (1948) are shown in Figures IV.2. Cholette's data are for air in a hydrodynamic entrance region downstream of a tube sheet. Exceptional behavior is observed by both Cholette and Ede at Re=4000, where the coefficient drops and then rises with increasing downstream distance (x/D). This might be evidence of a temporary relaminarization. Linke and Kunze's (1953) data have the same appearance over a range of higher Reynolds numbers.

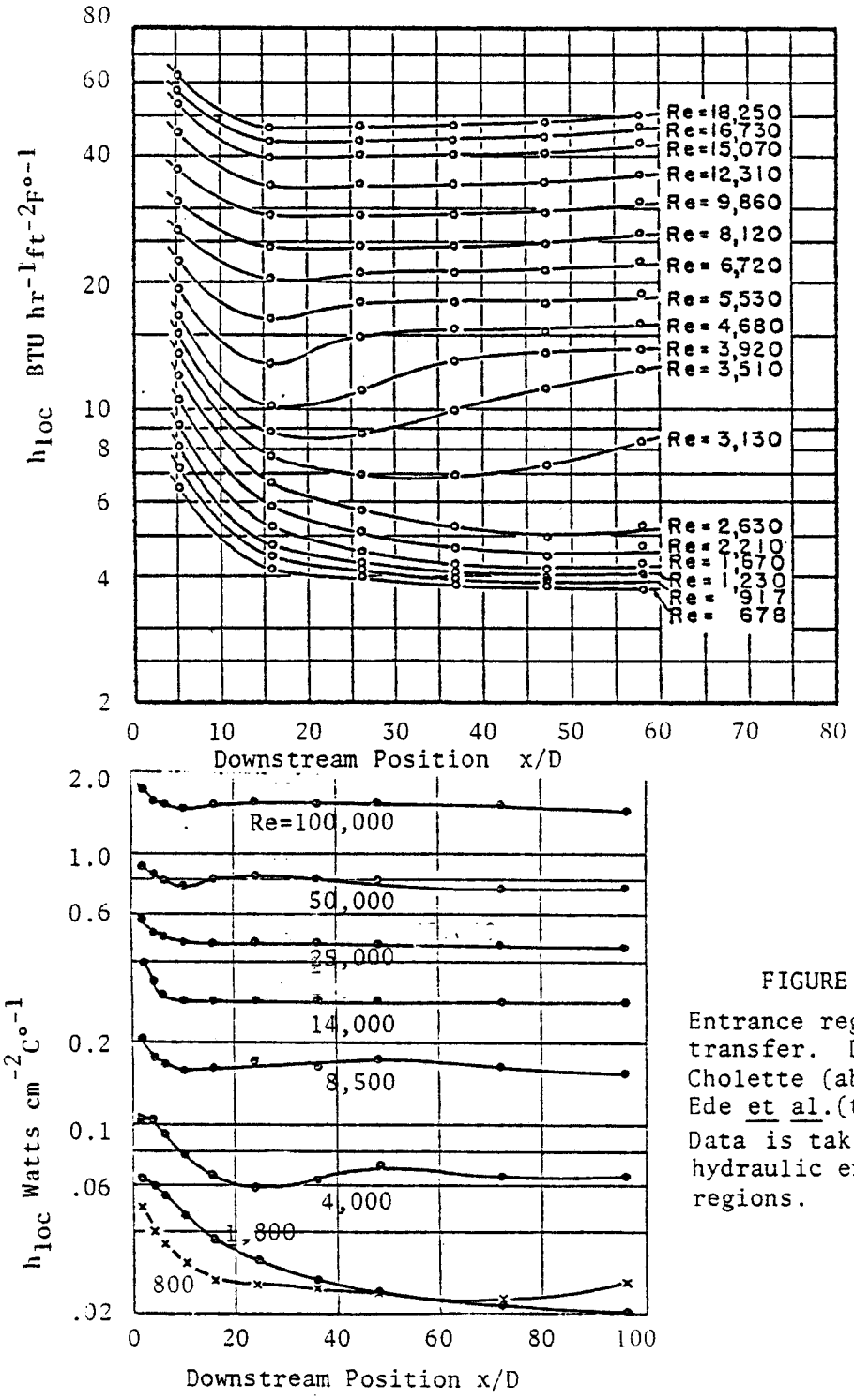

FIGURE IV.2

Entrance region heat transfer. Data from Cholette (above) and Ede et al.(to left). Data is taken in hydraulic entrance regions.

CHAPTER V. RESULTS AND DISCUSSION

RESULTS

MASS LOSS DATA

Data on mass loss versus time are shown in Figures V.1. The time scale of the graphs begins with the onset of operation at 440C coupon temperature, after a month of calibration tests at lower temperatures. The time scale for the 490C coupon temperature begins with the first exposure of these coupons to the lithium.

The data for the 440C coupon temperature are well-fitted by straight lines after the first time interval; the slopes of these lines give the long-term asymptotic mass fluxes. A faster mass loss occurs over the first time interval (with the calibration period neglected) and is also observed with replacement coupons which start out at the 440C test conditions.

This time pattern of mass loss is similar to that found by other workers (Whitlow et al., 1979; Tortorelli and DeVan, 1979). Tortorelli and DeVan attribute the rapid initial corrosion to depletion of nickel from the outer layer of the stainless steel.

Data for a run at 490C coupon temperature are also shown on Figures V.1. The earlier weighings at this temperature clearly show the higher initial corrosion rate.

Mass loss data were simultaneously generated (for x/D from 6 to

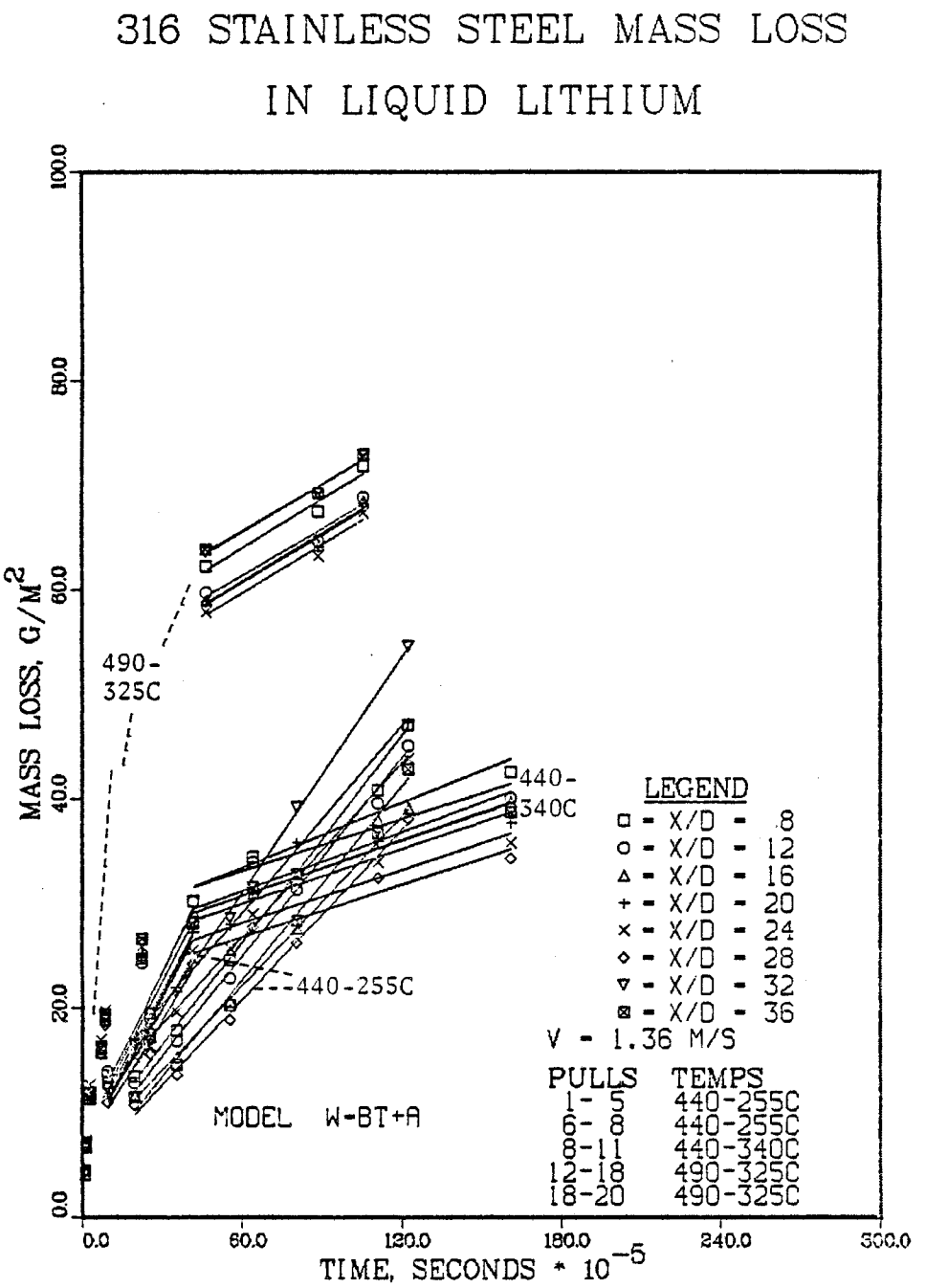

FIGURE V.1.a. Mass loss: upstream coupons, highest velocity.

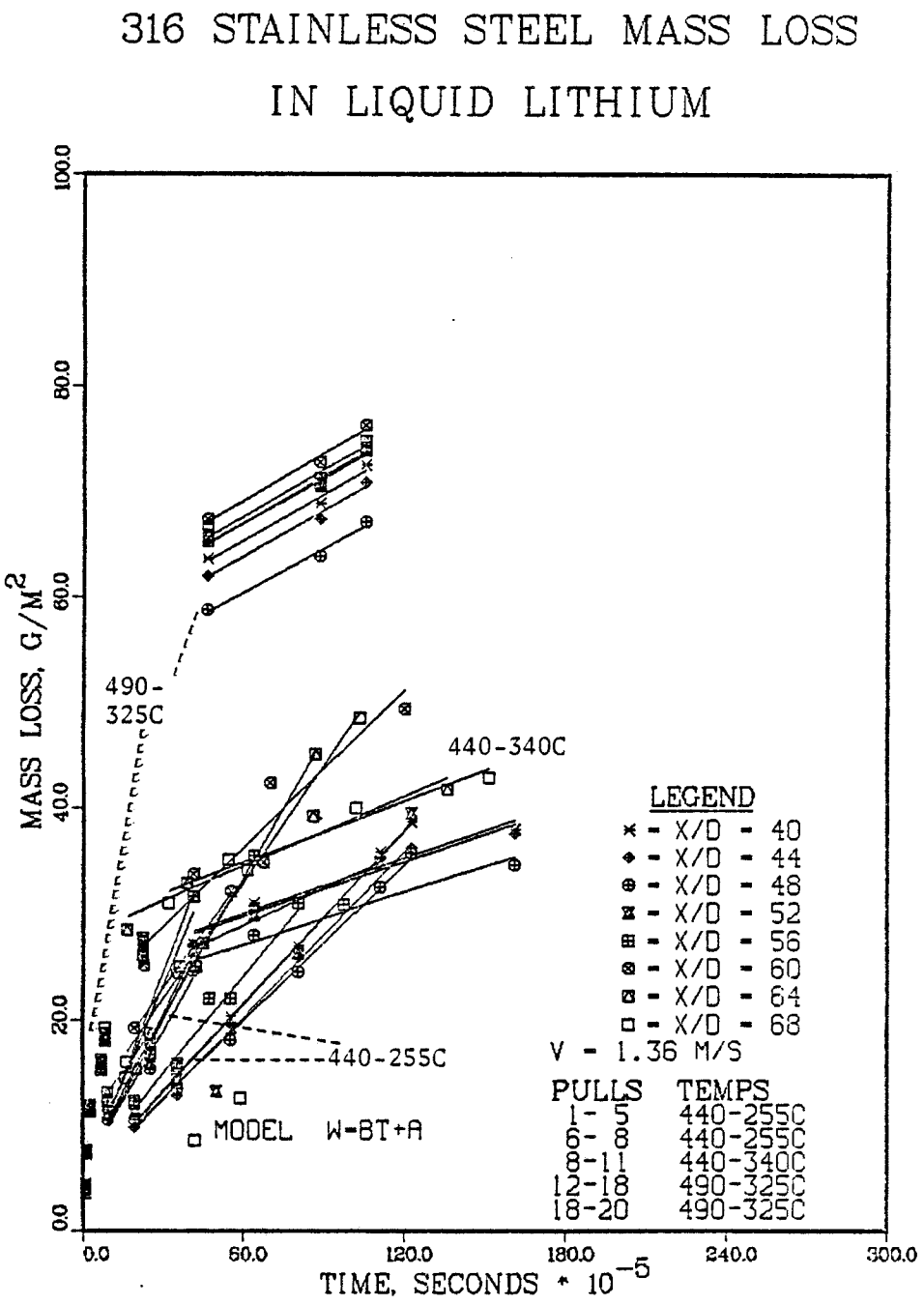

FIGURE V,1,b, Mass loss; downstream coupons, highest velocity.

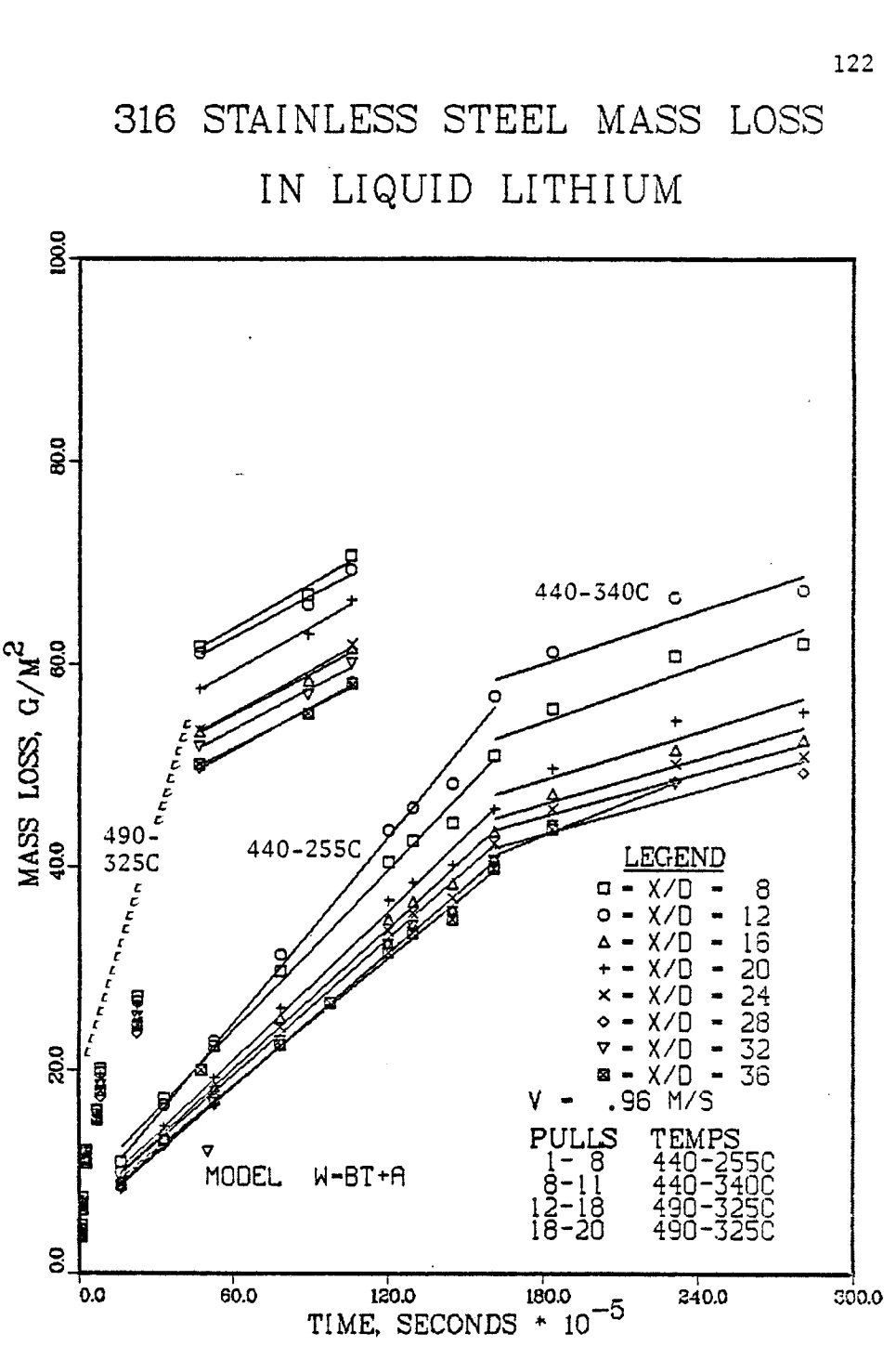

FIGURE V.1.c. Mass loss: upstream coupons, moderately high velocity.

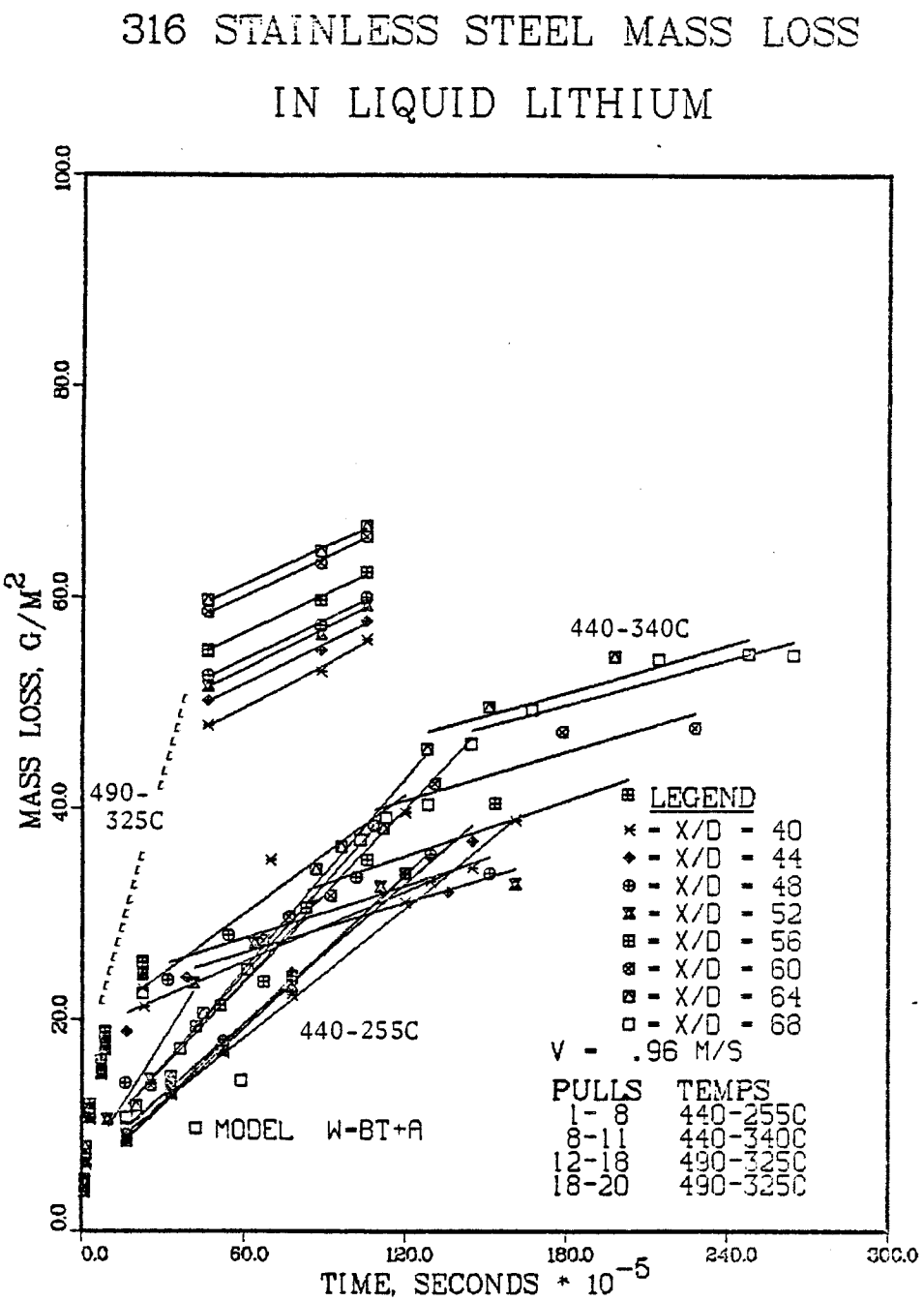

FIGURE V.1.d. Mass loss: downstream coupons, moderately high velocity.

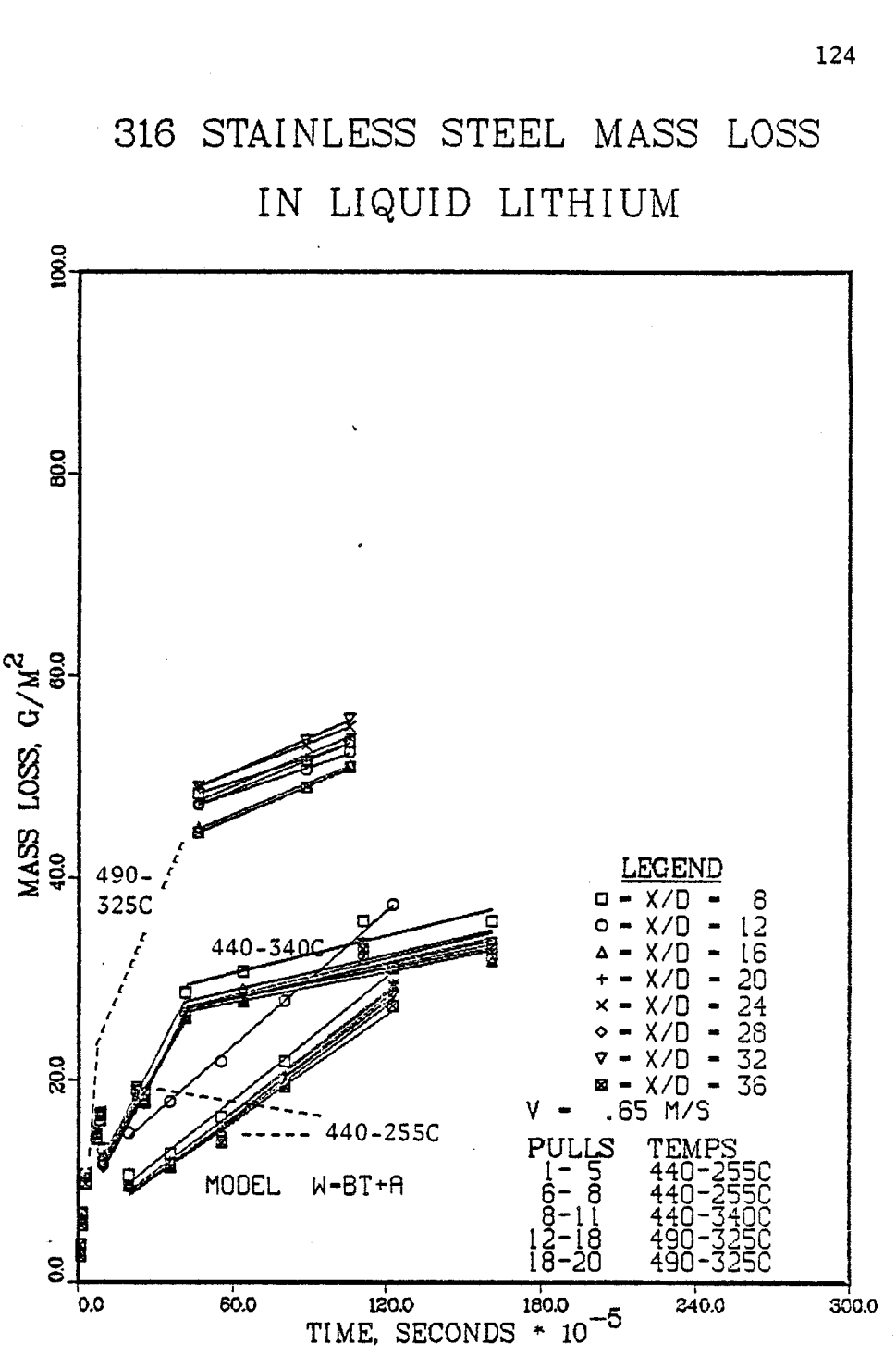

FIGURE V,1,e. Mass loss: upstream coupons, moderately low velocity.

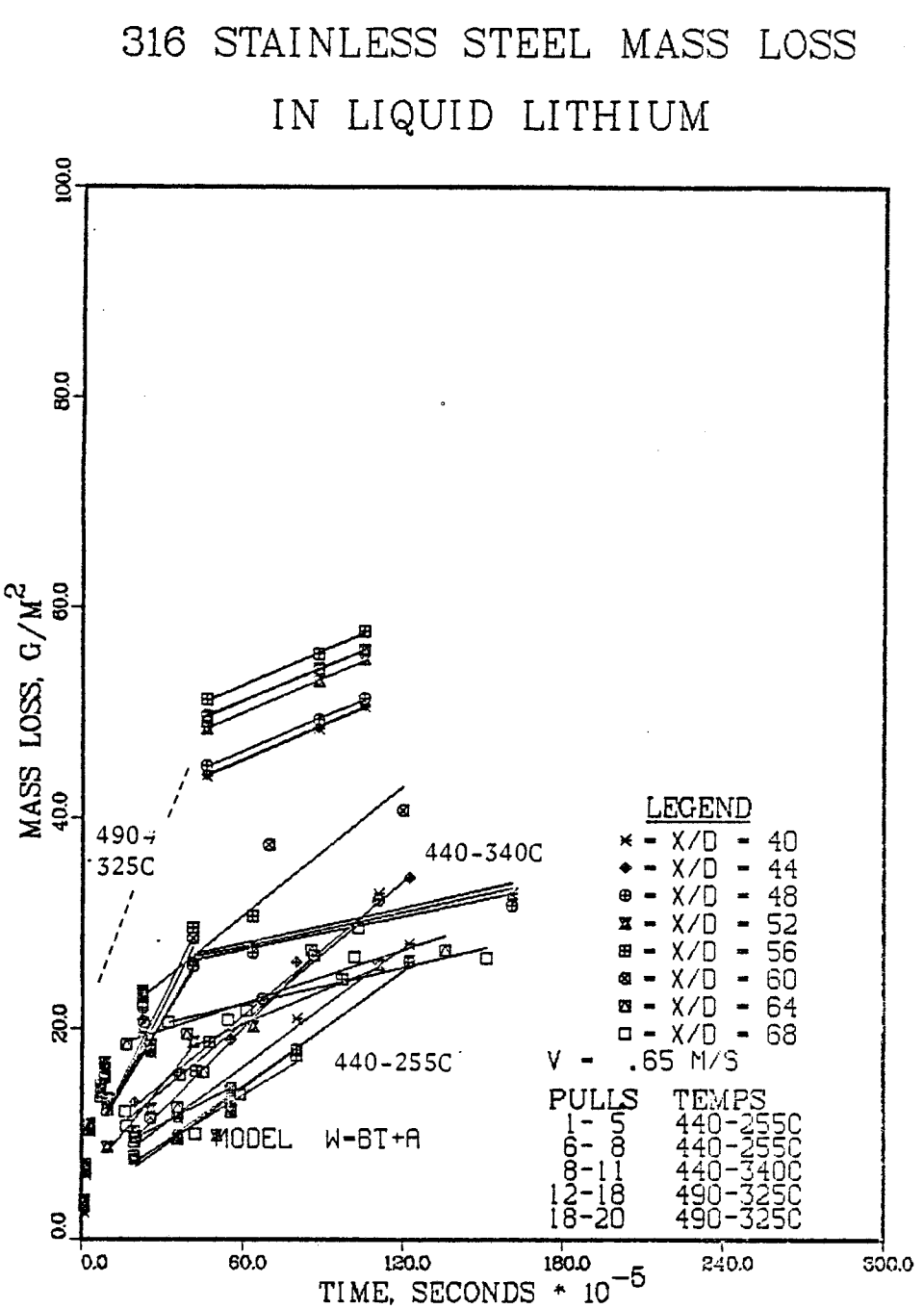

FIGURE V.1.f. Mass loss: downstream coupons, moderately low velocity.

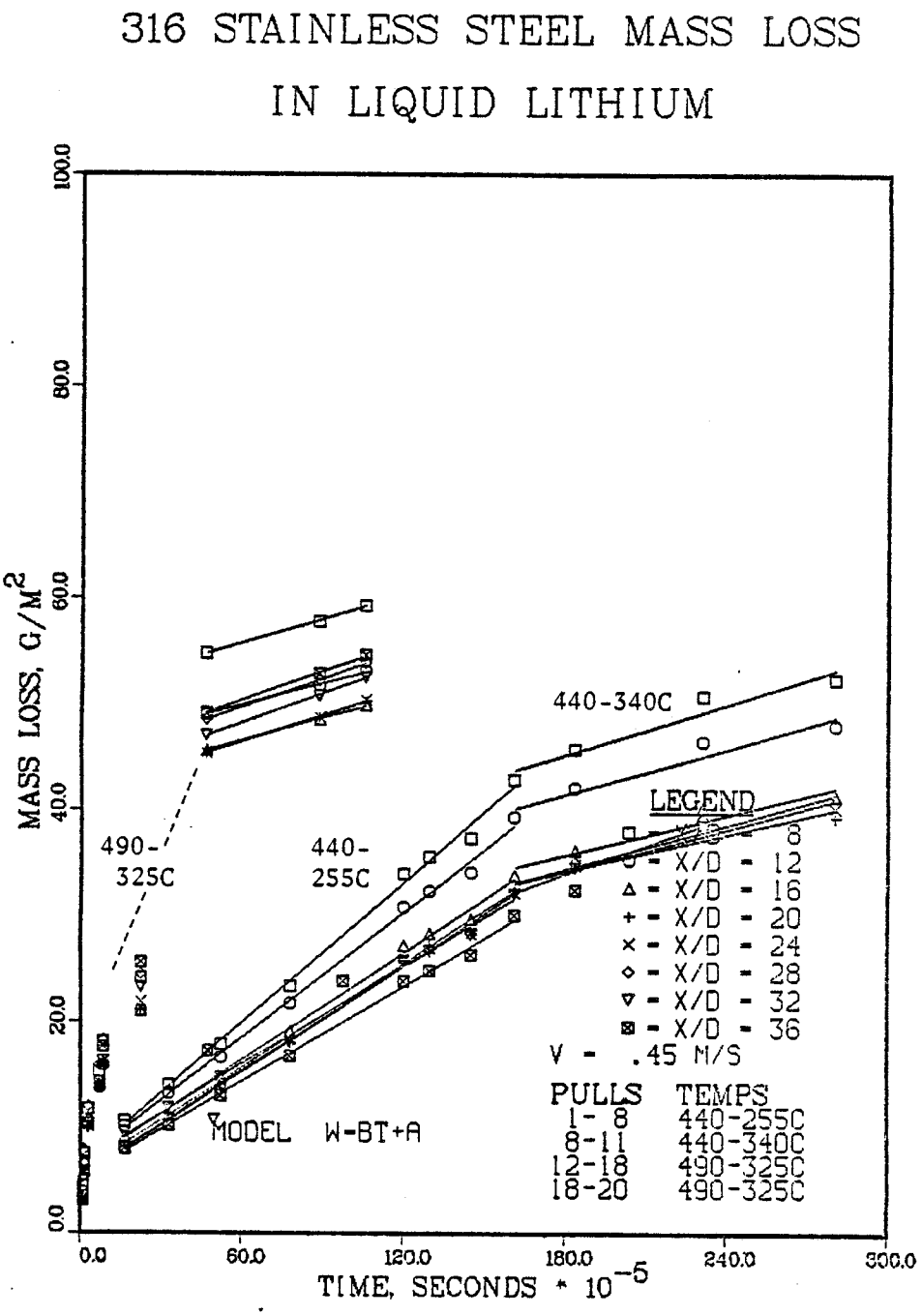

FIGURE V.1.g. Mass loss: upstream coupons, lowest velocity.

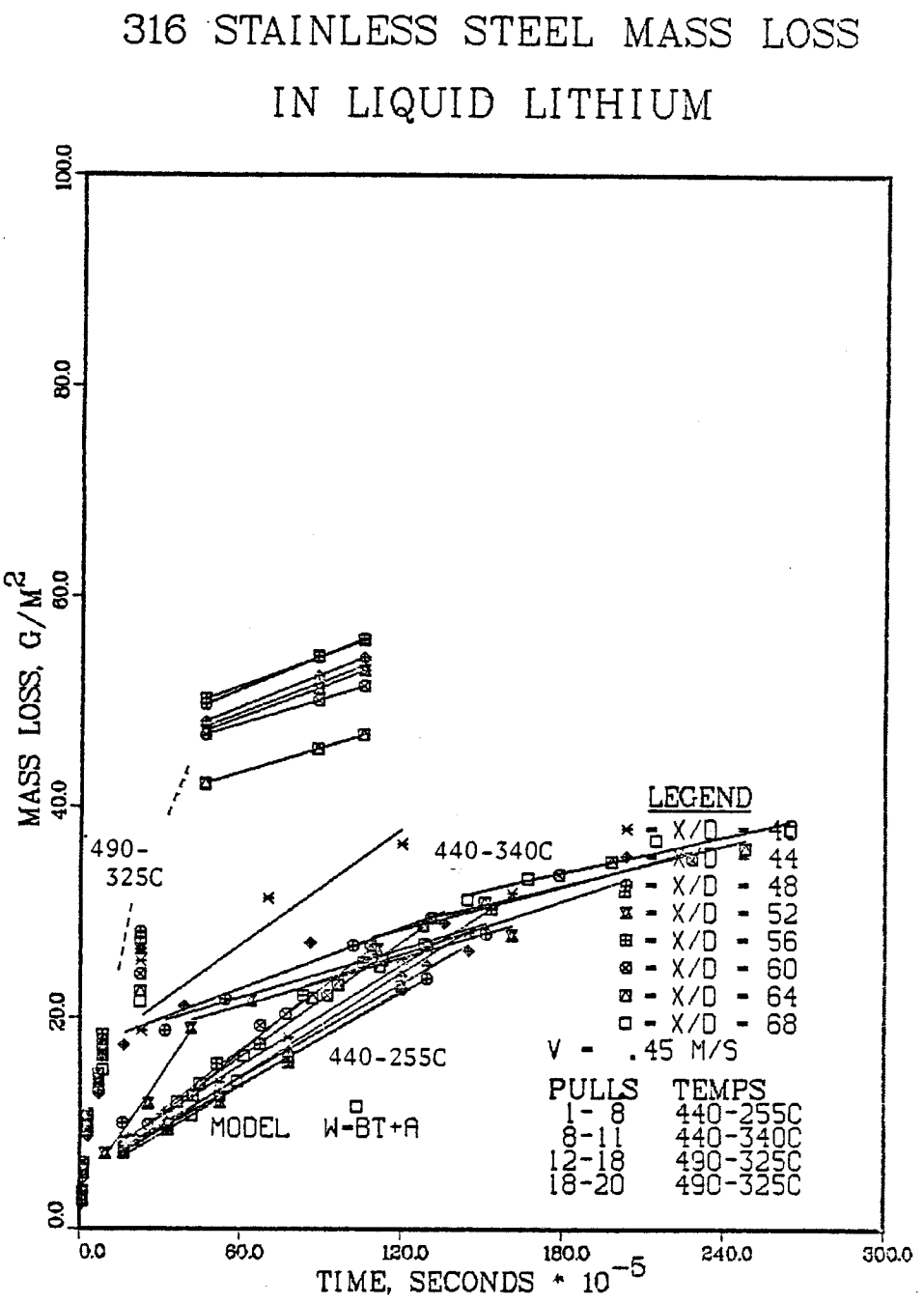

FIGURE V.1.h. Mass loss: downstream coupons, lowest velocity.

70) for four lithium velocities. Figures V.2 show the position dependence of the local mass fluxes. Each point is calculated by linear regression of the coupon weighings over intervals of several months. The fluxes are based on the inside area of the coupon. The dissolution mass flux generally decreases initially with downstream position (x/D) in each test section. This downward trend then gives way to fluctuations. In particular, on Figures V.2a and V.2d, for the two higher velocities, the point at which the fluctuations appear is at a length Reynolds number $(D\langle v\rangle\rho/\mu)(x/D)]$ of about 4×10^5. (At the lower velocities, this point is beyond the range of x/D studied. The Reynolds numbers $D\langle v\rangle\rho/\mu$ in the coupons range from 4000 to 12000.) This behavior suggests that the flow in the test sections is initially laminar, or is laminarized by the acceleration through the sudden contraction at x/D=0. The fluctuations beginning at $(x\langle v\rangle\rho/\mu) = 4 \times 10^5$ are attributed to the onset or resumption of turbulent flow.

Figure V.3 shows the influence of lithium velocity on the mean mass flux $\bar{n}$, for the region from x/D=6 to 30. This region, comprising the first six coupons of each set, lies in the laminar region according to Figures V.2a and V.2d. The data are fitted with lines according to the form

$$\bar{n} = a(T)\ v^{*m} \qquad (V.1)$$

where the flux is in $ug/m^2/s$, and v* is the velocity made dimensionless by dividing $\langle v\rangle$ by 1 m/s. The least squares results are shown on Table V.1.

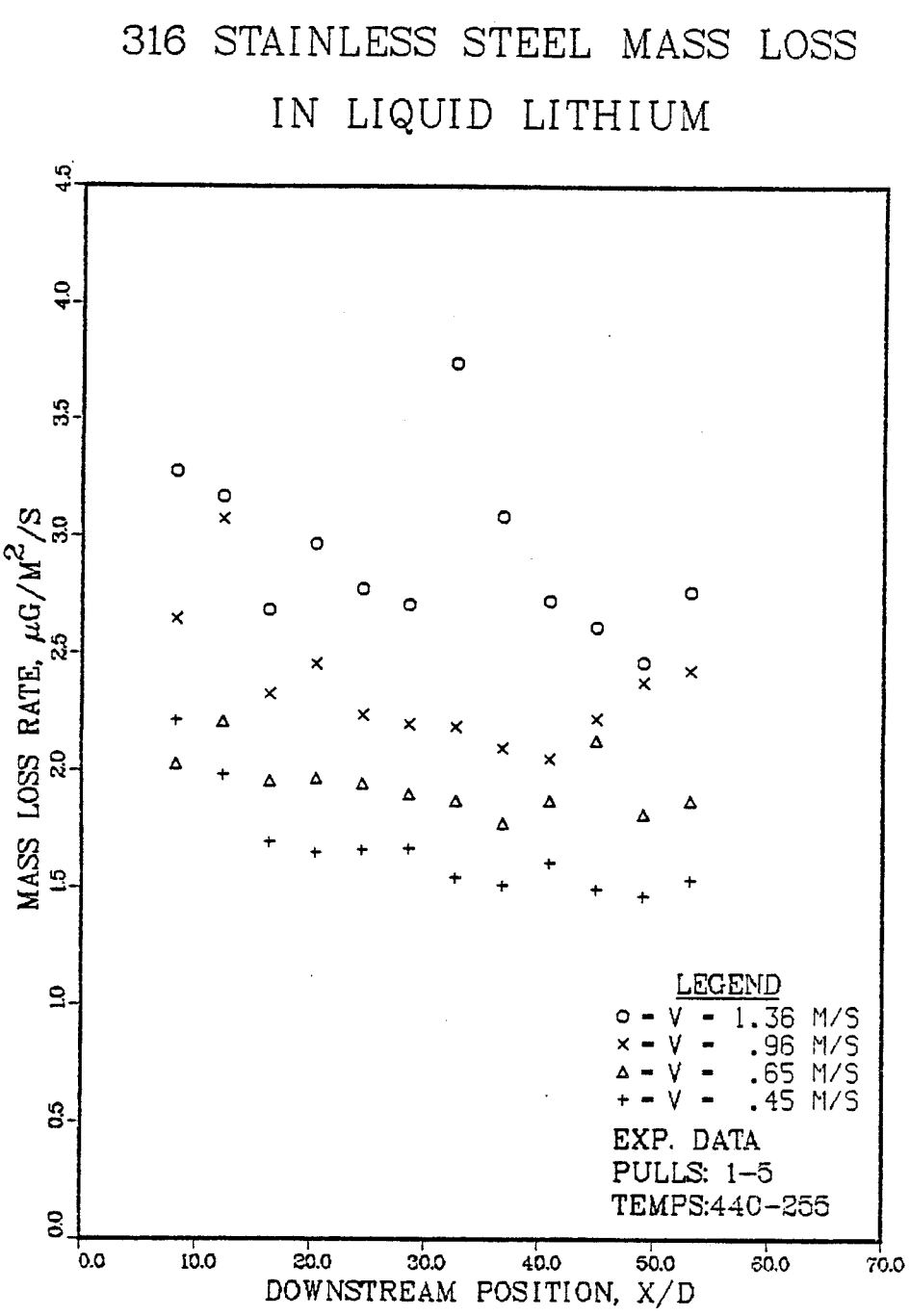

FIGURE V.2.a, MASS FLUX vs POSITION--440C coupon temperature, 255C radiator temperature.

316 STAINLESS STEEL MASS LOSS IN LIQUID LITHIUM

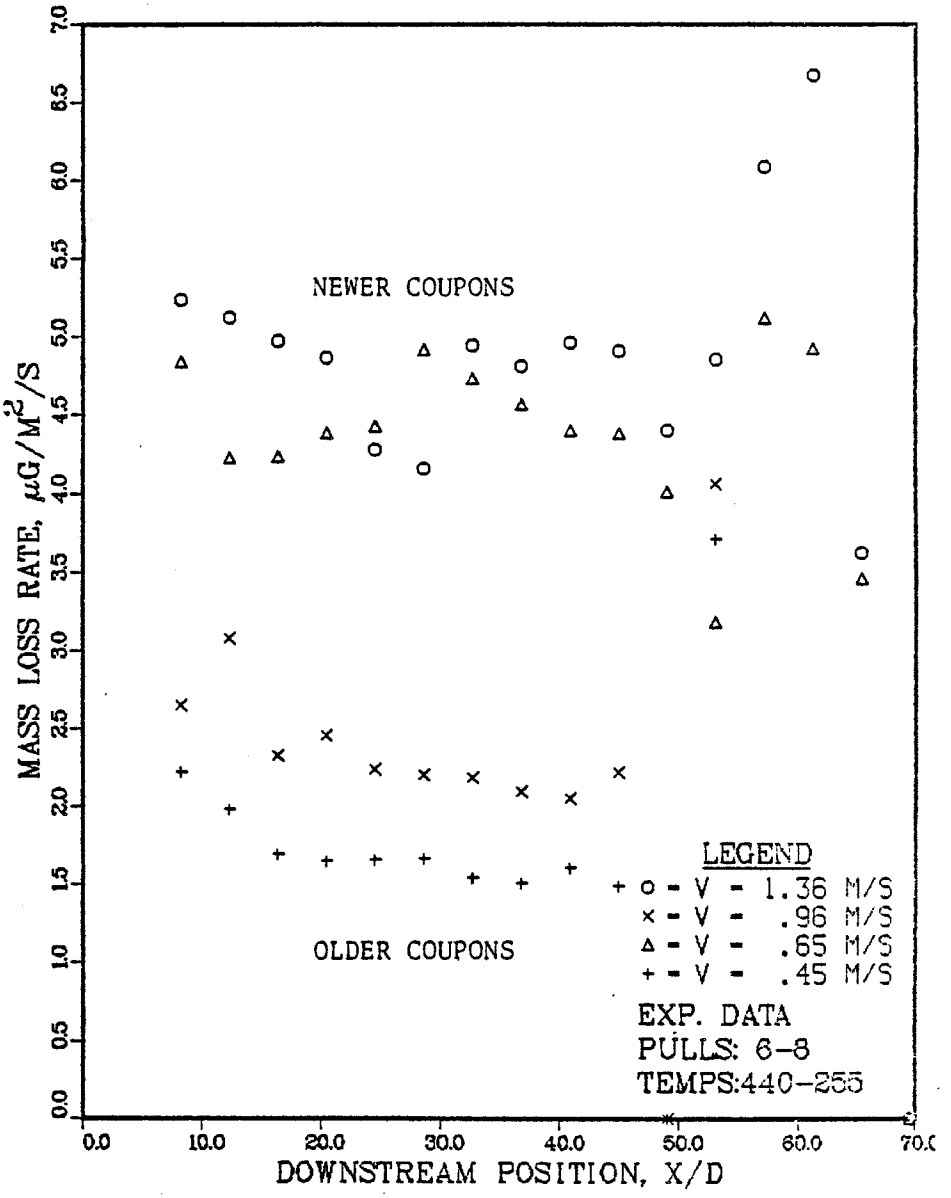

FIGURE V.2.b. MASS FLUX vs POSITION--440C coupon temperature, 255C radiator temperature. Coupons at 1.36 m/s are fresh set of original heat; coupons at 0.65 are fresh set of second heat.

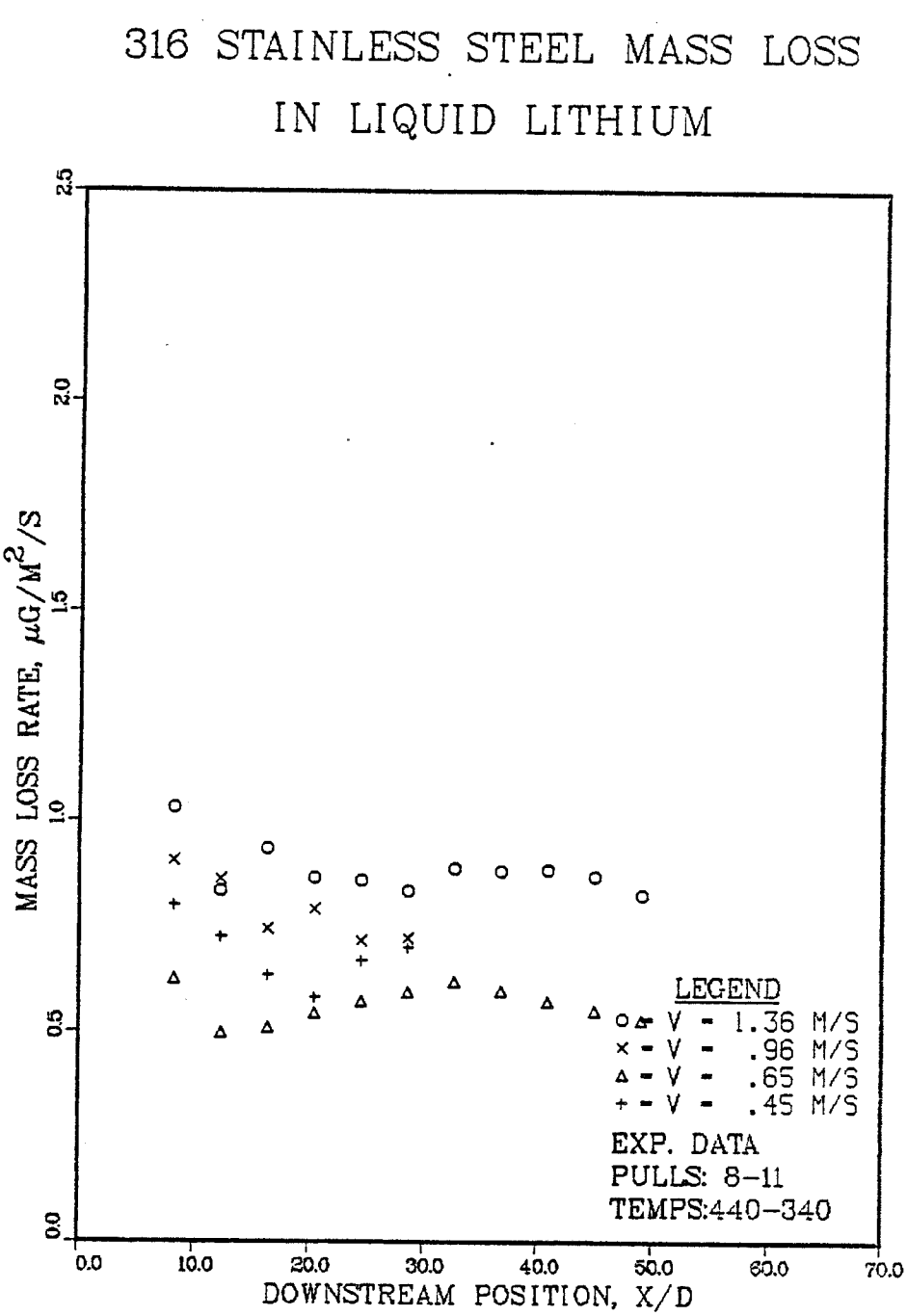

FIGURE V.2.c. MASS FLUX vs POSITION--440C coupon temperature, 340C radiator temperature. Coupons at 1.36 and 0.65 m/s have not been in loop as long as other two sets of coupons. (see Figure V.2.b).

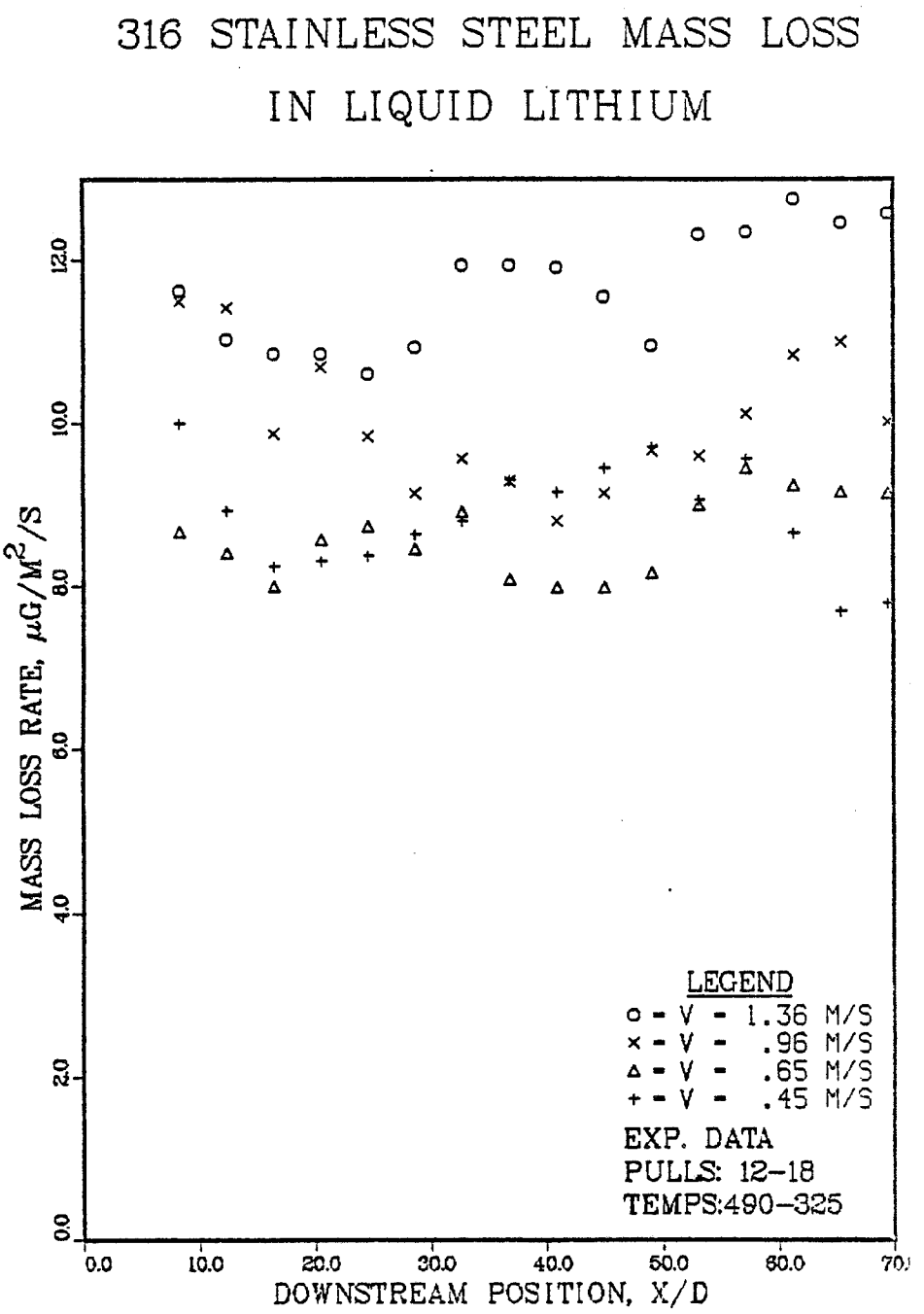

FIGURE V.2,d. MASS FLUX ys POSITION--490C coupon temperature, 325C radiator temperature, All coupons fresh; second heat.

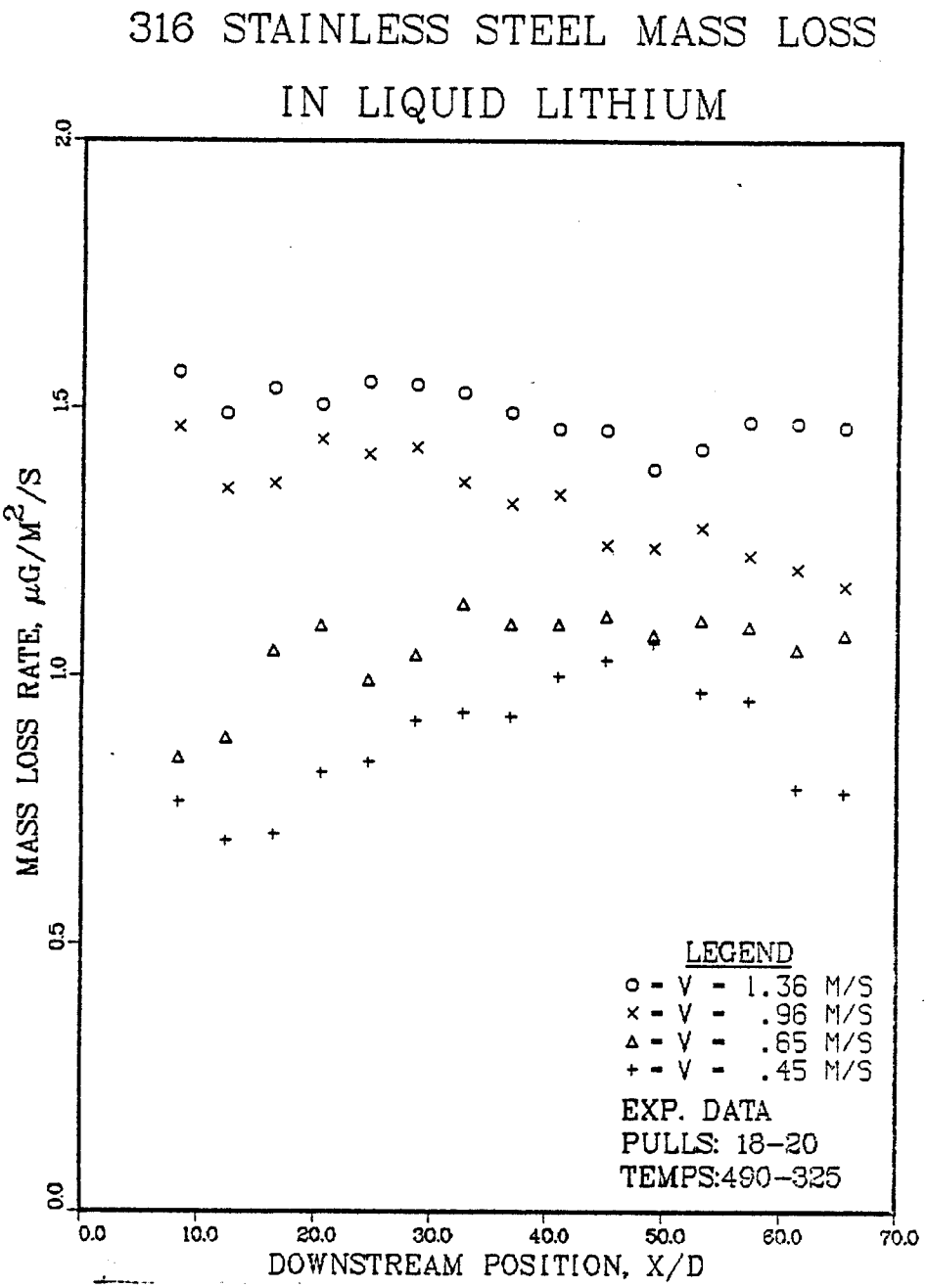

FIGURE V.2.e. MASS FLUX vs POSITION--490C coupon temperature, 325C radiator temperature, All coupons same age; continuing same conditions as Figure V.2.d.

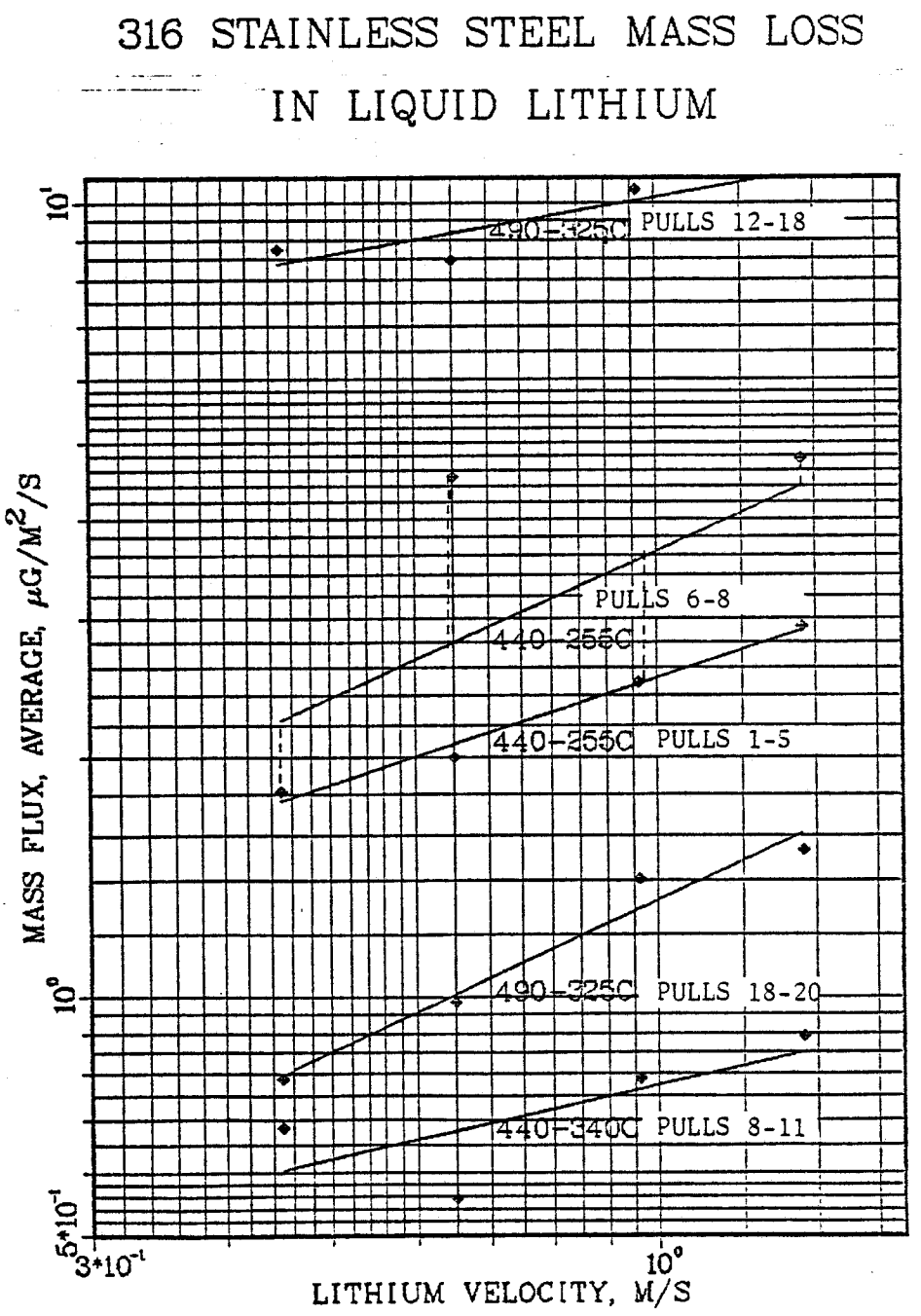

FIGURE V.3. Velocity Dependence of the Mean Mass Flux over the first 6 coupons (x/D=6 to 30).

TABLE V.1. PARAMETERS FOR EQUATION (V.1)

T_{coupon}	T_{min}	Time	m	a
440C	255C	0-3400hr*	0.45	2.53
440C	340C	3500hr**	0.31	.78
490C	325C	0-1300hr	0.24	10.2
490C	325C	1300-2900hr	0.64	1.33

*not including calibration time at lower temperature
**elapsed time; initial times 1200 and 4500hrs

$$\overline{n} = a(T)\ v^{*m} \qquad (V.1)$$

For fluid-diffusion controlled mass transfer in turbulent flow, the expected exponent m in equation (V.1) would be about 0.8. The appearance of significantly lower values of m here is further indication that the flows have been temporarily laminarized upon entering the test section. For developing laminar flow an exponent of 1/2 would be expected; the exponent for the data at 440-255C is actually 0.45 (see Table V.1). Mass transfer into a developed laminar flow would show a 1/3-power dependence on velocity.

MICROSCOPY DATA

Optical microscopy was used to examine several coupons. Typical micrographs are shown in Figures V.4. Microscopy procedures are described in Appendix N.

The coupons exposed at 490C have developed a porous ferrite layer about 30 microns thick. Such a layer is also reported by Tortorelli and DeVan (1979) and by Whitlow *et al.* (1979). The ferrite layer is not seen on unexposed coupons. All the coupons,

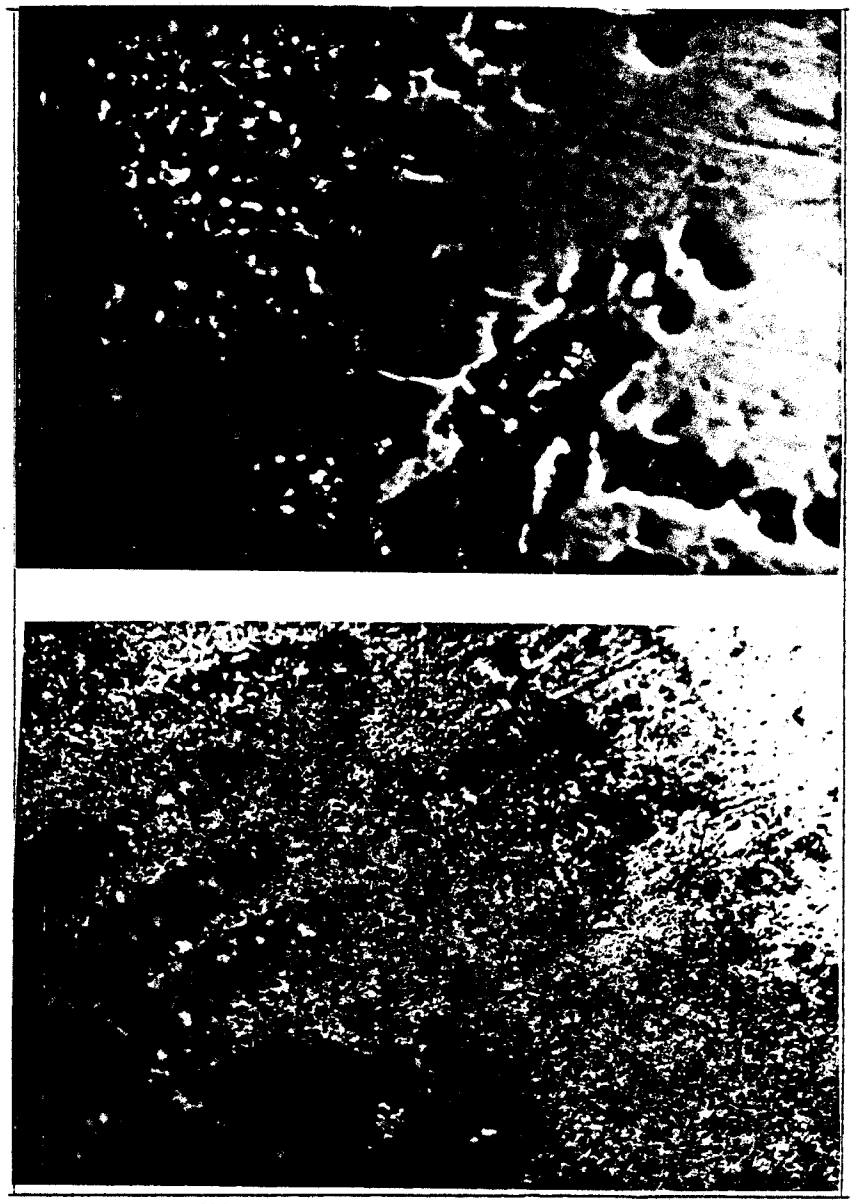

Figure V4a. Optical Micrographs of coupons.
Top: As-received-- Bottom: 1250 hrs exposure.
Coupon 12208X Lithium at 490C
0.6 m/s lithium velocity
Coupon 12215
Both coupons inside wall, polish factor 7:1,
Magnification 400X, Glyceregia etch.

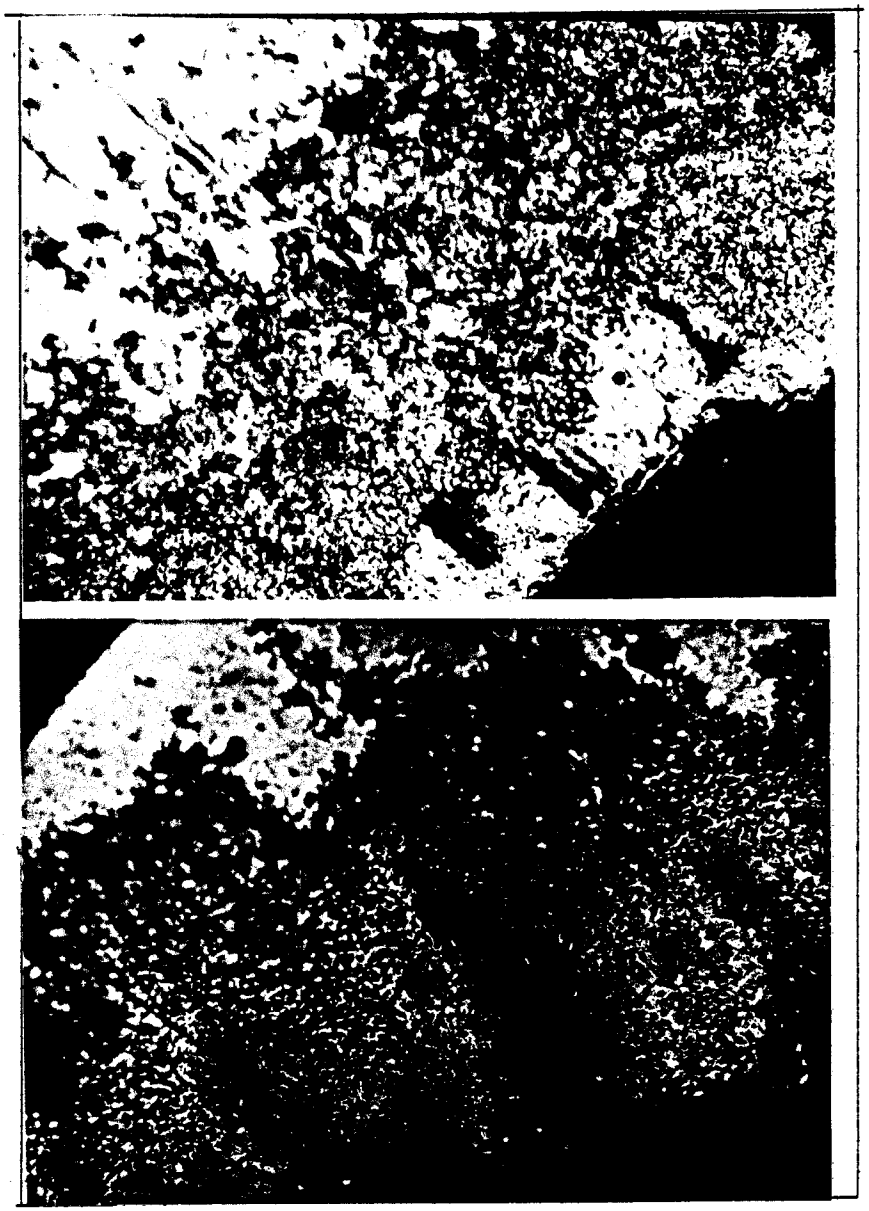

Figure V4b. Optical Micrographs of coupons
Top: 1250 hrs---Bottom: 3400 hrs exposure.
490C --- 440C Lithium temperature.
0.6 m/s --- 1.3 m/s Lithium velocity.
Nickel plated--Not plated.
7:1 --- 18:1 Polish factor.
12215 --- 10111 coupon number.
Both coupons: inside wall, magnification of 400, glyceregia etch.

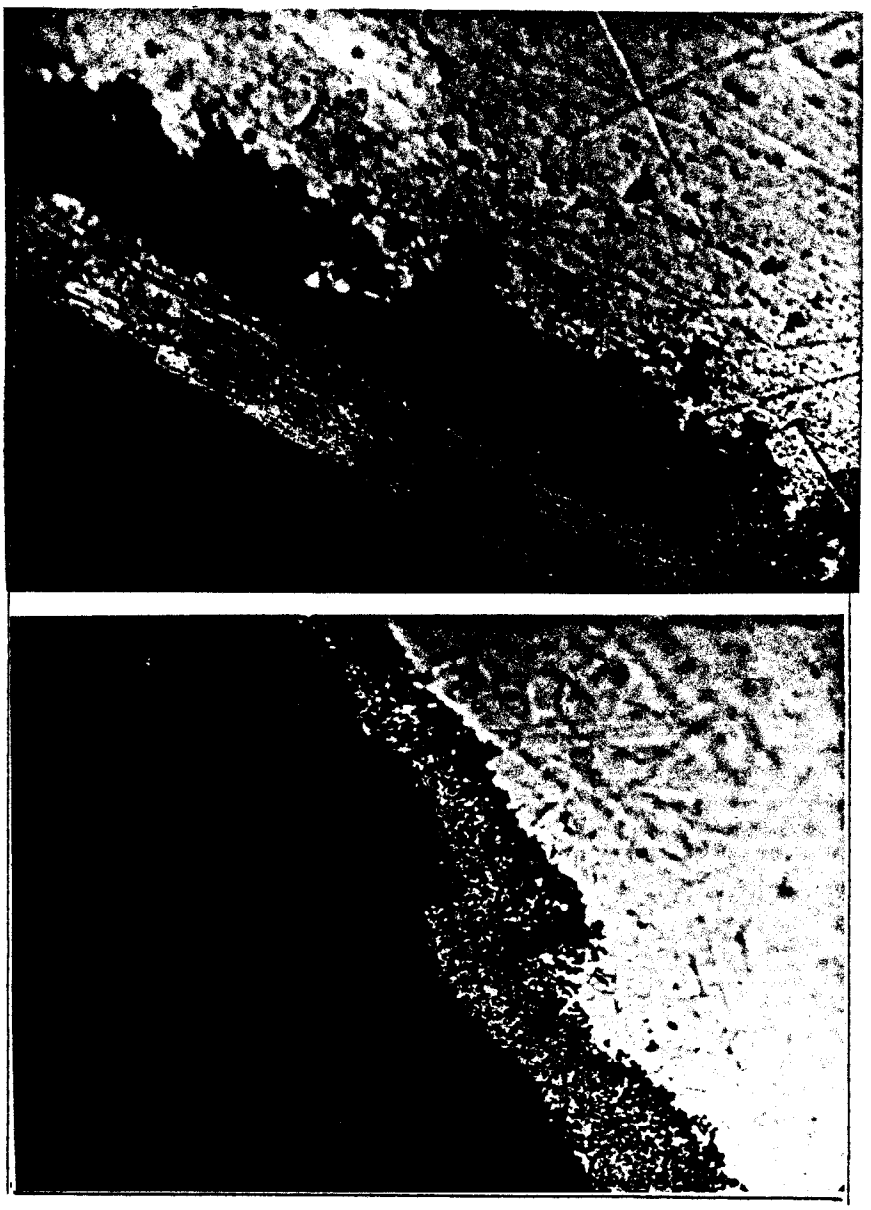

Figure V4c. Optical Micrographs of coupons.
Top: 1250 hrs---Bottom: 3400 hrs exposure.
490C --- 440C Lithium temperature.
0.6 m/s --- 1.3 m/s Lithium velocity.
Nickel plated--Not plated.
12215 --- 10111 coupon number.
Both coupons: inside wall, polish factor 2:1, magnification 400, glyceregia etch.

whether exposed to lithium or not, exhibit surface roughness of the order of 20-40 microns.

Figures V.5 show scanning electron microscope photographs of the outside of an as-received coupon and two coupons exposed to lithium at 490C. Figures V.6 show the inside surfaces of the same coupons. On each page the magnification is constant and the micrographs from top to bottom show an as-received coupon, a coupon exposed to lithium at 490C and 0.4 m/s, and a coupon exposed to lithium at 490C and 1.0 m/s. The 0.4 m/s coupon was in the test section for only 3 hours after the flow of lithium was stopped, but due to a blockage in the standpipe, the 1.0 m/s coupon remained in the cooling test section for 10 hours before it could be removed. The surface of the 1.0 m/s coupon appears to have a second phase of nodules or crystals up to 2 microns across, which are not seen on the 0.4 m/s coupon. This phase could be metal deposited from the cooling lithium.

The mass loss data recorded for the 1.0 m/s coupon (12415) did not appear unusual, but energy dispersive x-ray analysis (EDAX) of its surface showed high concentrations of nickel. The nickel content was lower in spots not covered by the second phase. The EDAX analyses are summarized in Table V.2. (See also Appendix N).

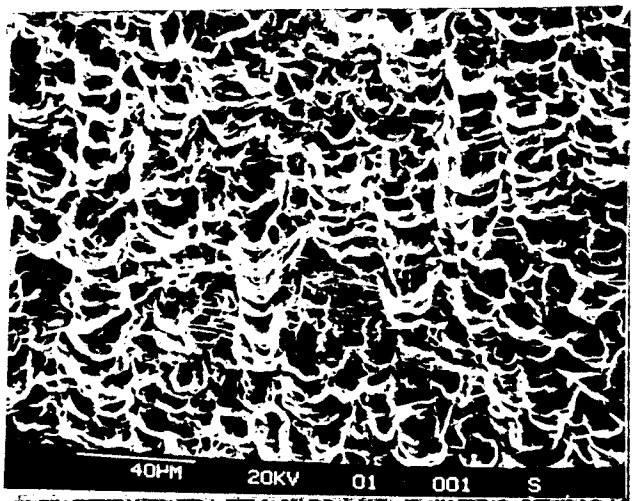

As Received.
Outside surface.
Magnification 375X.
Marker length = 40 microns.

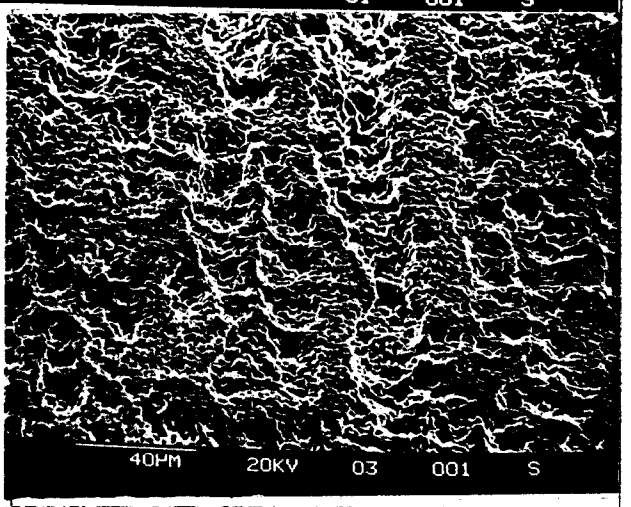

1250 hours in lithium
at 490C; 0.3 m s^{-1}.
Outside surface.
Magnification 375X.
Coupon # 12315.
Marker length = 40 microns.

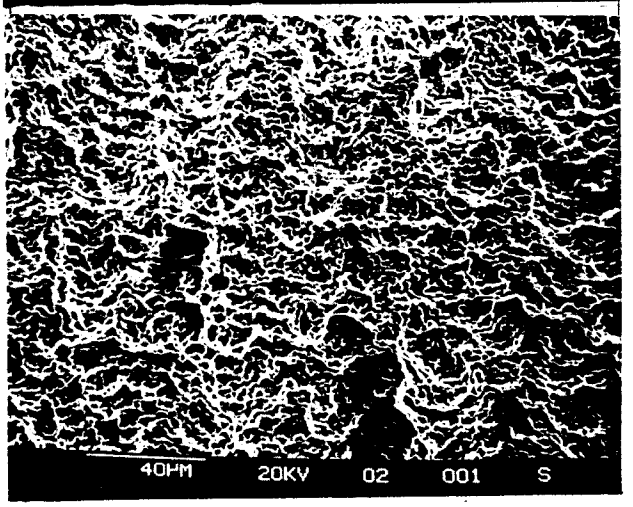

1250 hours in lithium
at 490C; 1.0 m s^{-1}.
Outside surface.
Magnification 375X.
Coupon # 12415.
Marker length = 40 microns.

Figure V5a. Scanning electron micrographs of coupons.

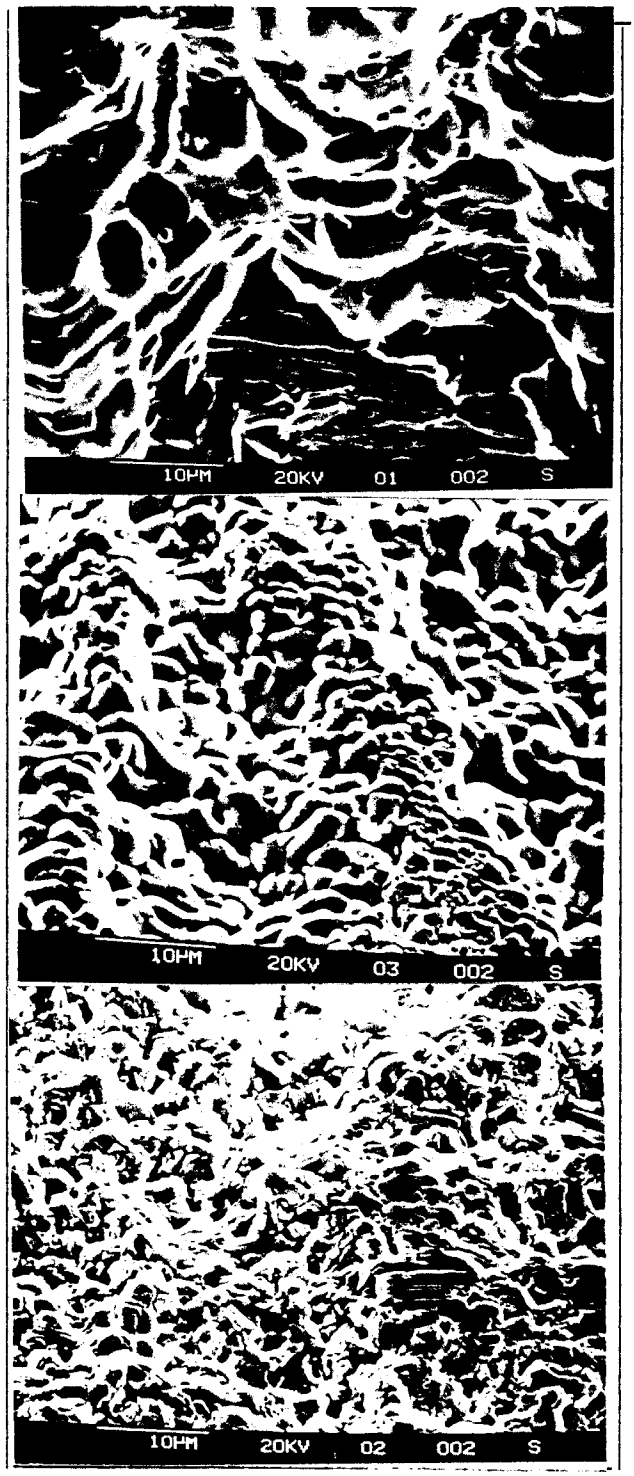

As Received.
Outside surface.
Magnification 1500X.

Marker length = 10 microns.

1250 hours in lithium
at 490C; 0.3 m s^{-1}.
Outside surface.
Magnification 1500X.
Coupon # 12315.

Marker length = 10 microns.

1250 hours in lithium
at 490C; 1.0 m s^{-1}.
Outside surface.
Magnification 1500X.
Coupon # 12415.

Marker length = 10 microns.

Figure V5b. Scanning electron micrographs of coupons.

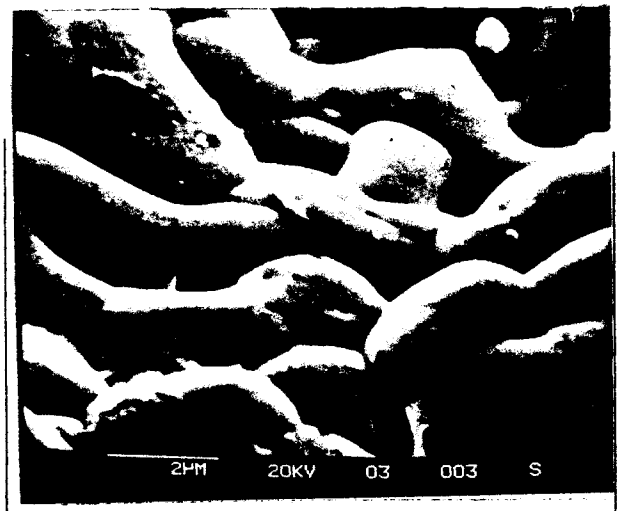

As-received coupon
not examined at
this magnification.

1250 hours in lithium
at 490C; 0.3 m s-1.
Outside surface.
Magnification 8000X.
Coupon # 12315.

Marker length = 2 microns.

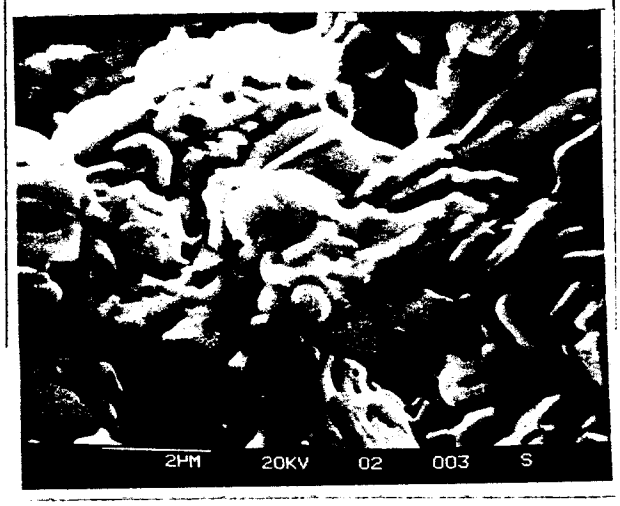

1250 hours in lithium
at 490C; 1.0 m s-1.
Outside surface.
Magnification 8000X.
Coupon # 12415.

Marker length = 2 microns.

Figure V5c. Scanning electron micrographs of coupons.

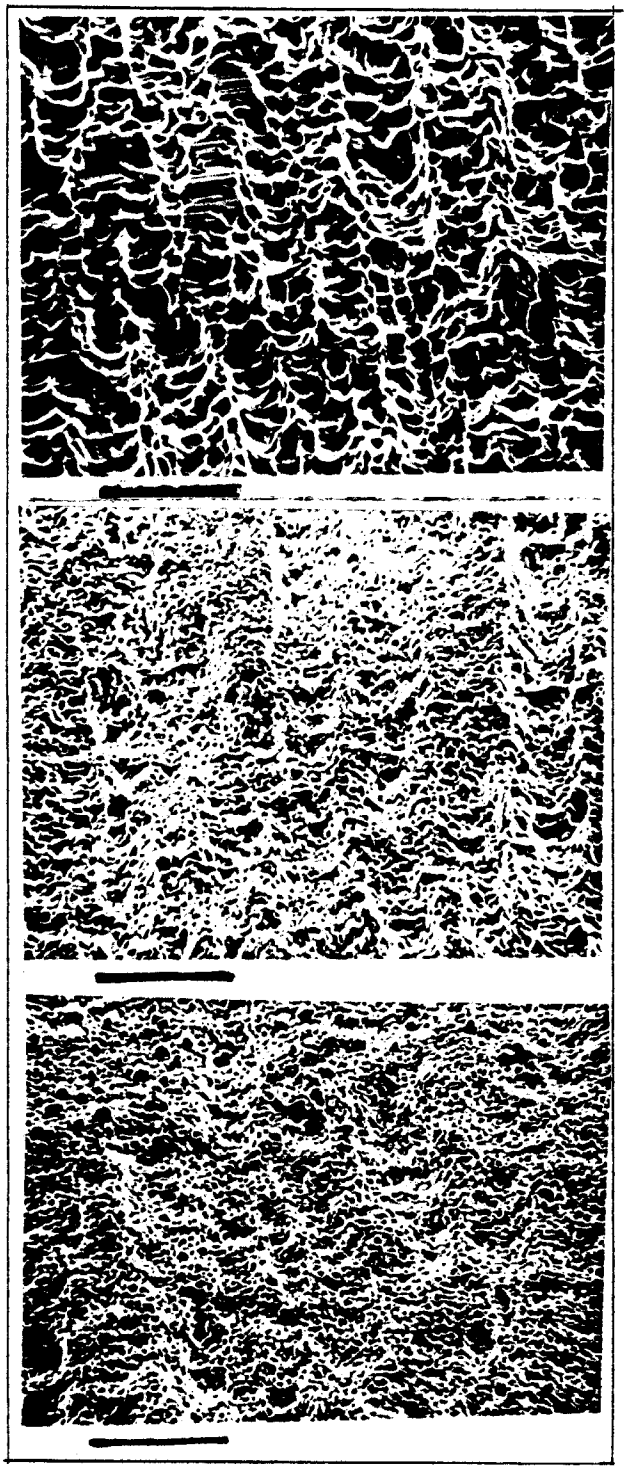

As Received.
Inside surface.
Magnification 375X.
Coupon # 12408x.

Marker length = 40 microns.

1250 hours in lithium
at 490C; 0.3 m s^{-1}.
Inside surface.
Magnification 375X.
Coupon # 12315.

Marker length = 40 microns.

1250 hours in lithium
at 490C; 1.0 m s^{-1}.
Inside surface.
Magnification 375X.
Coupon # 12415.

Marker length = 40 microns.

Figure V6a. Scanning electron micrographs of coupons.

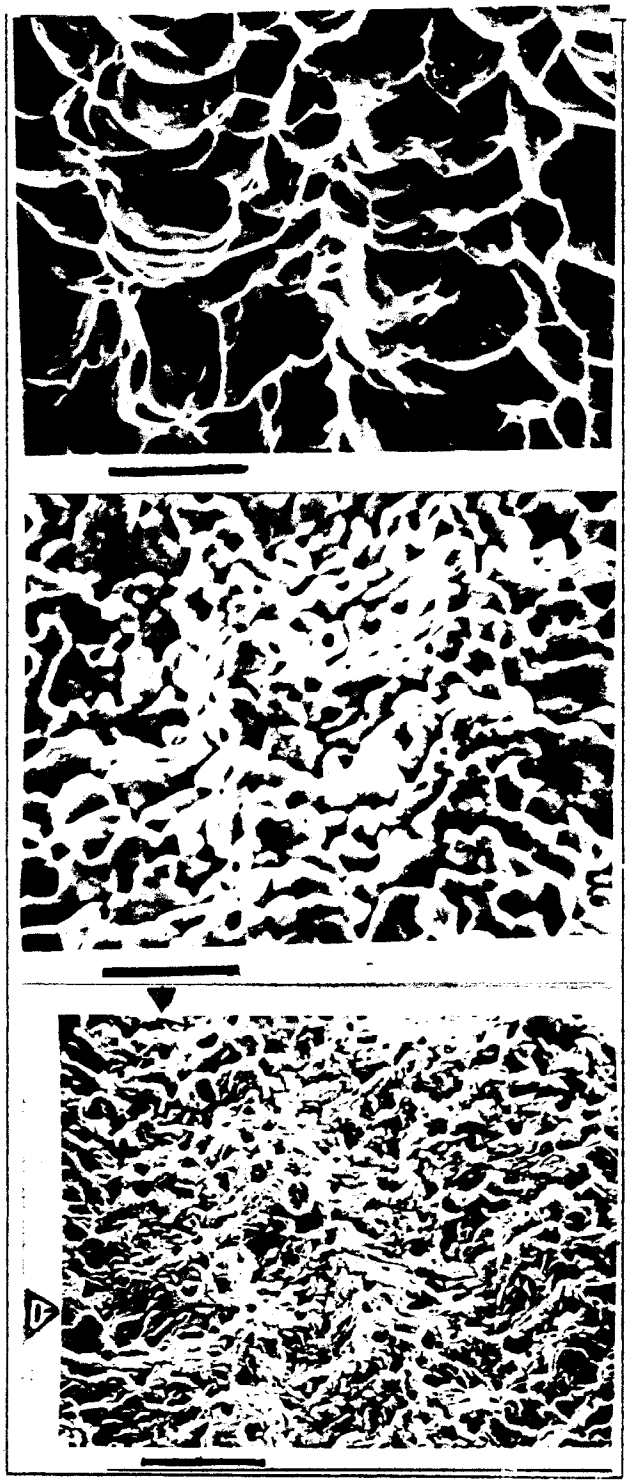

As Received.
Inside surface.
Magnification 1500X.
Coupon # 12408x.

Marker length = 10 microns.

1250 hours in lithium
at 490C; 0.3 m s^{-1}.
Inside surface.
Magnification 1500X.
Coupon # 12315.

Marker length = 10 microns.

1250 hours in lithium
at 490C; 1.0 m s^{-1}.
Inside surface.
Magnification 1500X.
Coupon # 12415.

Indicator points to
"spot 1", refer to
Table V.2. (Spot 2
is not shown.)

Marker length = 10 microns.

Figure V6b. Scanning electron micrographs of coupons.

TABLE V.2. EDAX ANALYSIS OF STAINLESS STEEL COUPONS

	Coupon Composition in Weight Percentages					
	Fe	Cr	Ni	Mn	Mo	Si
as rec'd OD	65.74	17.46	9.19	3.43	2.95	1.22
as rec'd OD	65.38	17.41	9.54	3.60	2.53	1.25
as rec'd ID	65.84	17.96	9.19	3.32	2.62	0.93
mfg analysis	---	16.36	11.75	1.65	2.39	0.63
0.4 m/s OD	84.99	11.32	1.04	1.50	0.49	0.66
0.4 m/s ID	88.58	7.50	1.71	0.60	---	---
1.0 m/s OD*	85.11	6.21	7.42	0.76	---	0.49
"" area ID*	72.04	10.65	14.05	1.01	---	0.22
""spot 1 ID*	87.47	7.83	2.18	0.74	---	0.24
""spot 2 ID*	86.02	8.71	2.02	1.04	0.44	0.25

*possible precipitation during prolonged exposure to cooling lithium

The inside surface of this coupon shows an average nickel composition of 14%, which is higher than the as-received nickel level. The outer surface had a lower nickel content of 7.4%. This was still higher than the nickel level of the other lithium-exposed coupons, and higher than spots on the same coupon not covered by the second phase. Deposition on the outside surface might be less because this surface is not open to the bulk of the lithium.

All of the exposed surfaces show a pattern of ridges and valleys with a "wavelength" of about 40 microns; the exposed coupons also have pores about one micron in diameter and of uncertain depth. The distance between pore mouths is about 5 microns. The roughness and porosity seen on the scanning electron micrographs confirm the similar features on the optical micrographs.

The electron microprobe was used to obtain semi-quantitative

composition profiles near the surfaces of several coupons (see Appendix N). Typical composition profiles are shown in Figures V.7. A ferrite layer on the exposed coupons is evident from the iron peak at the coupon surface. The peak concentration of about 80% iron is greater than the 70% bulk iron content. No iron peak is seen on the as-received coupons. Nickel and chromium show no definite peaks, but rise monotonically to their bulk composition levels. These levels are reached at the inner edge of the ferrite layer, that is, at the trailing edge of the iron peak.

The thickness of the ferrite layer appears to be in the neighborhood of 20 microns for coupons exposed 4 months to lithium at 490C, and 10 microns for coupons exposed 6 months at 440C.

LITHIUM ANALYSES

The lithium from the loop was analyzed several times during the experiment. A Kjeldahl method was used for nitrogen and both DC arc and ion-coupled plasma spectrophotometry were used for metals analyses. The analyses are summarized in Table V.3. Analytical procedures are described in Appendix N.

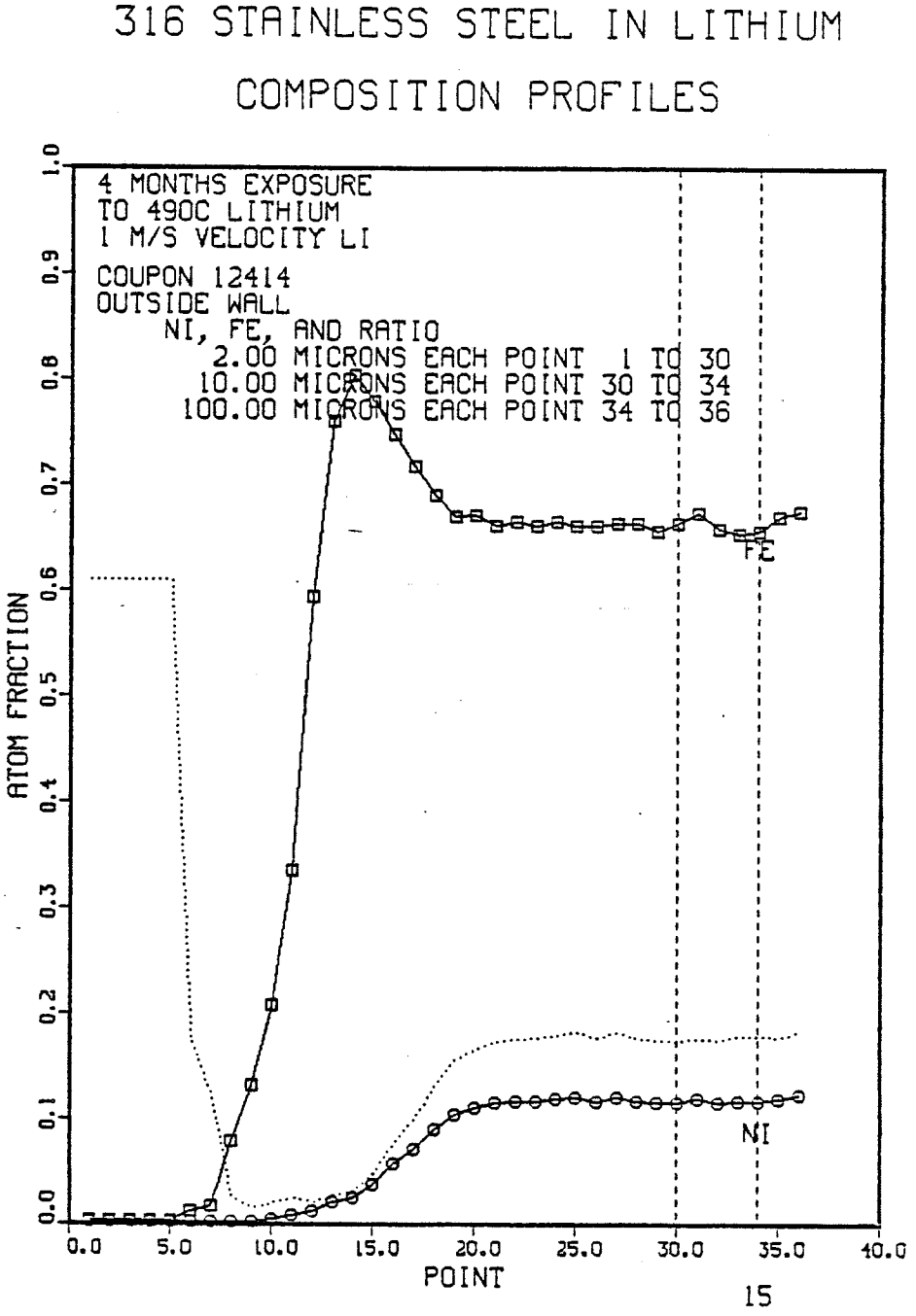

FIGURE V.7a. Iron and Nickel Profiles going into surface of stainless steel exposed to lithium. Additional microprobe profiles are in Appendix N.

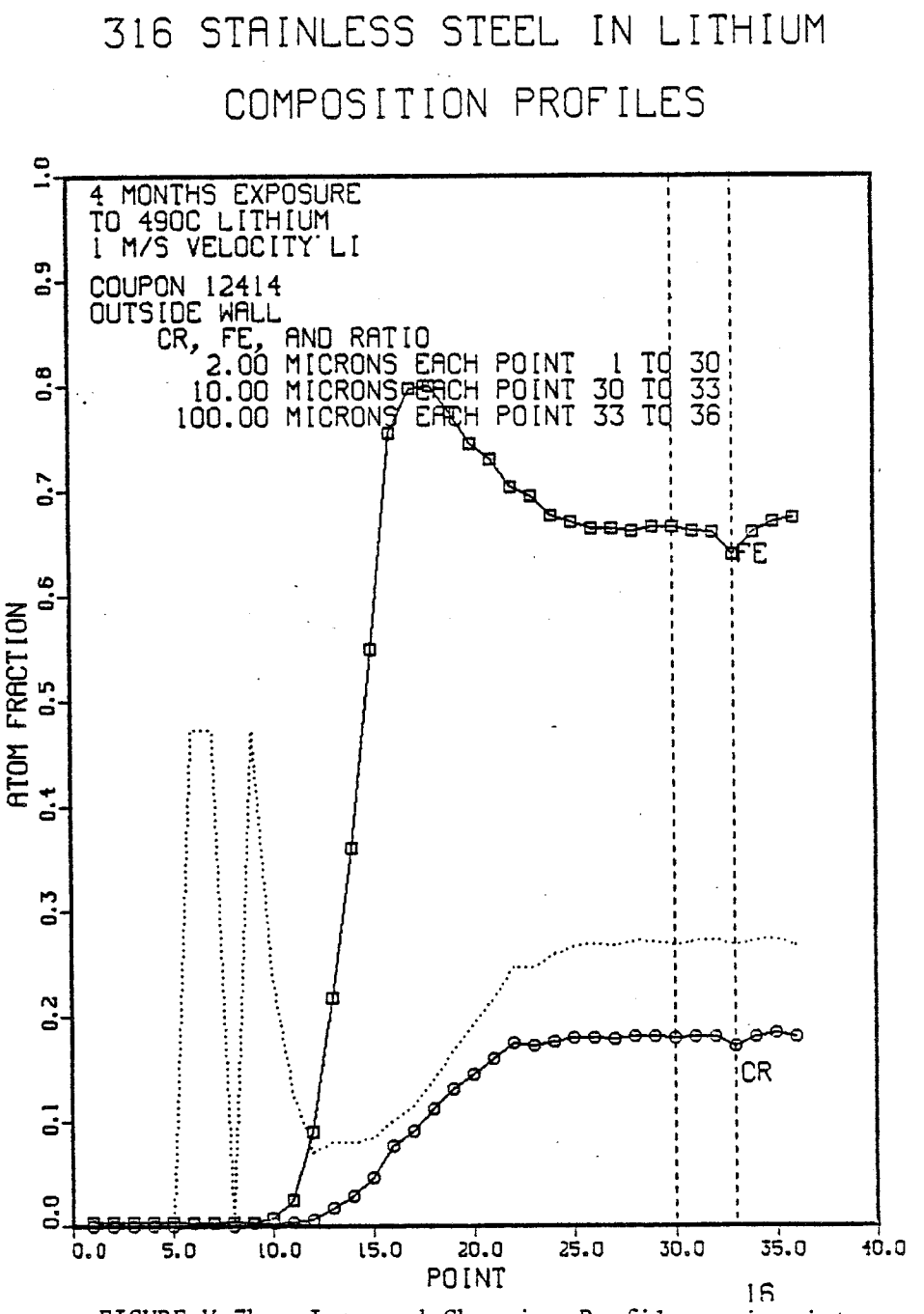

FIGURE V.7b. Iron and Chromium Profiles going into surface of stainless steel exposed to lithium. Additional microprobe profiles are in Appendix N.

TABLE V.3. LITHIUM ANALYSES

Date	Tmax	Tmin	Fe	Cr	Ni	N	O
6/78	—	—	—	—	—	422	—
2/79	449C	255C	—	—	—	50	275
7/79	449	340	—	—	—	101	—
8/79	449	340	30	<2	<5	—	—
11/79	500	325	5	10	<5	69	—
1/80	500	325	10	4	<5	—	—
1/80	500	325	4	3	8	99*	—
2/80	500	325	3	2	6	64	—
4/80	500	325	4	2	7	79*	—

*Bypass sample flow not achieved, or achieved for only short time.

DISCUSSION

MASS LOSS DATA

The data at 440C coupon temperature are generally well-fitted by straight lines, but pulls 7 and 11 fall below the apparent linear trend. The discrepancy in mass loss at these pulls is seen with all coupons, regardless of their exposure time in the lithium. No problems or unusual delays were encountered removing the coupons at pulls 7 and 11. The anomalous mass loss might be due to a temporary change in the lithium composition (Table V.3). There is no firm evidence to suggest such a change. Redeposition of solute from the lithium is a possible but unconfirmed explanation.

A valve blockage hindered pull 17 on the 490C run. Coupon sets 3 and 4 were removed after 7 hours in the cooling lithium. Sets 1 and 2 remained in the cooled lithium for 75 hours at 260-300C. It seems likely that the apparently lower mass loss at pull 17 was due to deposition on the coupons during this delay. The lower (upstream) coupons of sets 1 and 2 lost markedly less weight than the upper coupons, presumably due to their slightly lower temperature during the 75 hour delay. If any deposit was predominantly nickel or was loosely adherent, it might be rapidly dissolved away or spall off into the lithium when high temperature flow operation resumed. Subsequent mass loss data might therefore continue on the original linear trend. For instance, pull 8, following the anomalous pull 7, is on the same line as pulls 1

through 6.

During the preparations for pull 17, a bubble (presumably of argon) was accidentally put into the loop. The loop was shut down for four weeks before enough of the bubble was removed for operation of the loop to resume. Removal of the bubble required the freezing, for the first time, of the test sections and electromagnetic pump piping. It also involved several transfers of about one third of the lithium inventory to and from the dump tank. These transfers might have changed the lithium composition and could then affect the corrosion rate, at least temporarily.

The lithium composition might also have been altered by the month spent at the lower temperature shutdown conditions. Some of the metals dissolved in the lithium during higher temperature operation might have precipitated onto the pipe walls. Restoration of these solute metals to levels of a few parts per million in the lithium would, however, require only about 100 mg of metal. Each coupon lost from 10 to 20 mg during the 4 weeks of the next test period.

PARABOLIC MASS LOSS

The early mass loss at 490C (pulls 12-16) appears parabolic; the total mass loss seems to be proportional to the square root of the exposure time. When the data are fitted with

$$M = b \; t^{d} \qquad (V.2)$$

the values of d range from 0.48 to 0.74. Of the 64 values measured,

47 are between 0.48 and 0.60. This supports a square root dependence on time for the early mass loss at 490C; d is probably larger than 0.5 due to a simultaneous linear loss rate which becomes more apparent at longer times. The parabolic early mass loss, however, dominates the data in pulls 12 to 16. There is no apparent square root dependence for the data at 440C, possibly because none of the coupons (original or replacements) were weighed during the first 10 days of exposure to the lithium, when the parabolic loss would be most evident.

As noted above, the mass loss will not be a purely parabolic function of time (unless solid phase processes alone control the corrosion). Long-term linear mass loss rates are seen for all the experimental runs, indicating that a resistance outside of the solid controls the corrosion at long times. A combination of parabolic and linear mass loss behavior is indicated

$$M = b't + b''\sqrt{t} \qquad (V.3)$$

where b' is the long-term asymptotic mass flux, b" is representative of the initial parabolic mass loss rate, and both parameters depend on temperature, lithium velocity (and probably composition) and downstream position.

Presumably, equation (V.3) should fit all the data in the present research, with the exception of coupons exposed at two different ΔT values; in these cases, only the data up to the change in ΔT should be fit. Since none of the corrosion runs included

extensive early (parabolic) as well as long-term (linear) mass loss data, it is not possible to obtain good estimates of both parameters b' and b" from a single corrosion run.

All coupons in the loop up to pull 5 were from the same heat of stainless steel. At pull 5, the 1.36 m/s coupon set was replaced with a fresh set made of steel from the same heat. The 0.65 m/s set was replaced with coupons made of a second heat of type 316 stainless steel. The manufacturers' analyses of these steels are given in Table V.4.

TABLE V.4 MANUFACTURERS' ANALYSES OF STEEL

	Cr	Ni	Mo	Mn	Si	C	P	S
Heat 1	17.15	11.4	2.1	1.76	0.42	0.05	0.03	0.02
Heat 2	16.26	11.75	2.39	1.65	0.63	0.06	0.02	0.01

Heat 1 from Superior Tube; Heat 2 from Pacific Tube.

Between pulls 6 and 8, the fresh coupon sets experienced a higher corrosion rate than the similar coupons preceding them in pulls 1 to 5, although the temperature conditions were the same. This is best seen in Figures V.1a and V.1e. The mass flux for the coupons from the second heat, in the 0.65 m/s lithium, was markedly higher than for coupons from the first heat, exposed earlier in the experiment. Changes in the lithium composition could explain the difference in rates. Tortorelli et al.(1980) report that corrosion rates for stainless steel in lithium loops having a high initial nitrogen content are lower than rates observed in purer lithium. The nitrogen content of our loop apparently dropped from around

500ppm to 100ppm during the first 6 months of operation.

A second explanation for the higher rates in the two fresh coupon sets is that these coupons are still undergoing a transient faster dissolution during pulls 6-8. The original coupons in at 0.96 and 0.45 m/s maintain a linear mass loss from pull 1 to pull 8. The coupon sets put into the loop fresh after pull 5 are the only new steel exposed to the lithium, while both the coupons and the entire loop itself were uncorroded before the first test period. Therefore, the mass loss from the new coupon sets should not necessarily match that of the original coupon sets.

After pull 8, the radiator temperature was raised from 255C to 340C while maintaining the coupon temperature at 440C. By this time, the coupons at 1.36 and 0.65 m/s are apparently at pseudo-steady state. The mean fluxes from the four test sections again correlate fairly well with velocity (as seen by the better fit on Figure V.3). The correlation during pulls 6-8 was poor.

From pulls 1 to 11, coupons were also replaced one at a time in the downstream end of all coupon sets. The mass flux from the replacement coupons has not been thoroughly analyzed. Fluxes from these replacement coupons appear to be somewhat higher than for the original coupons, probably for the reasons noted above. After pull 11, all the coupon sets were replaced with fresh coupons from the second heat of type 316 stainless steel.

POSITION DEPENDENCE OF THE MASS FLUX

Figures V.2a and V.2d show rises in the mass fluxes at length Reynolds numbers ($x\langle v\rangle\rho/\mu$) of about 4×10^5; this suggests a transition from laminar to turbulent flow at those points in the test sections. Since the Reynolds numbers ($D\langle v\rangle\rho/\mu$) range from 4000 to 12000, the flow should be turbulent upon entering each coupon set. However, according to Kays' criterion, relaminarization may have occurred at the inlet to the coupons. Kays' (1966) criterion for relaminarization is

$$K = \frac{\nu}{u_\infty^2} \frac{du_\infty}{dx} > 3.5 \times 10^{-6}$$

The acceleration, du/dx, of the lithium can be estimated. If the velocity change is arbitrarily taken over a distance of 3 cm, then for the moderate velocity section where the lithium accelerates from 25 to 100 cm/s,

$$K = \frac{0.009 \text{cm}^2\ \text{s}^{-1}\ (100-25)\text{cm s}^{-1}}{(100)(100)\text{cm}^2\ \text{s}^{-2}\quad 3\ \text{cm}} \cong 225 \times 10^{-6} \qquad \text{(V.4)}$$

which is more than sufficient for relaminarization according to Kays' criterion.

The position dependence of the mass flux is similar to that seen by Cholette (1948) and by Ede (1956); Gill (1961) observed the same sort of effect for the dissolution of stainless steel tubular coupons in lithium. The increased flux presumably due to a laminar-turbulent transition is also evident in Cholette's and in Ede's data.

The flux decrease with x/D in the upstream coupons is much less than the inverse square root dependence expected in a developing hydrodynamic boundary layer (equation IV.6) or the inverse cube root dependence expected for a fully developed laminar flow (equation IV.9). This weak position dependence indicates that the diffusion boundary layer may already be partly developed at the contraction just upstream (x/D=0) of the coupons. (An alternate explanation is particulate solute in the lithium; this is discussed in a following section.)

BYPASS FLOW

Figure V.3 shows the velocity dependence of the mean mass fluxes. The velocities are calculated from the mass flow rates measured by the electromagnetic flowmeters. Some of the lithium passing through the flowmeters, however, bypasses the coupons. The lithium flow is primarily through the circular channel inside the coupons, but small amounts bypass along the outer surface of the coupons, along the outer surface of the stringer, and along the narrow longitudinal cut in the stringer. Bypass flow influences the coupon mass flux by reducing the amount of lithium flowing through the coupon, and by causing mass transfer from the outside surfaces of the coupons.

The lithium flow in each test section will divide between the four channels shown on Figure V.8. In each of these parallel

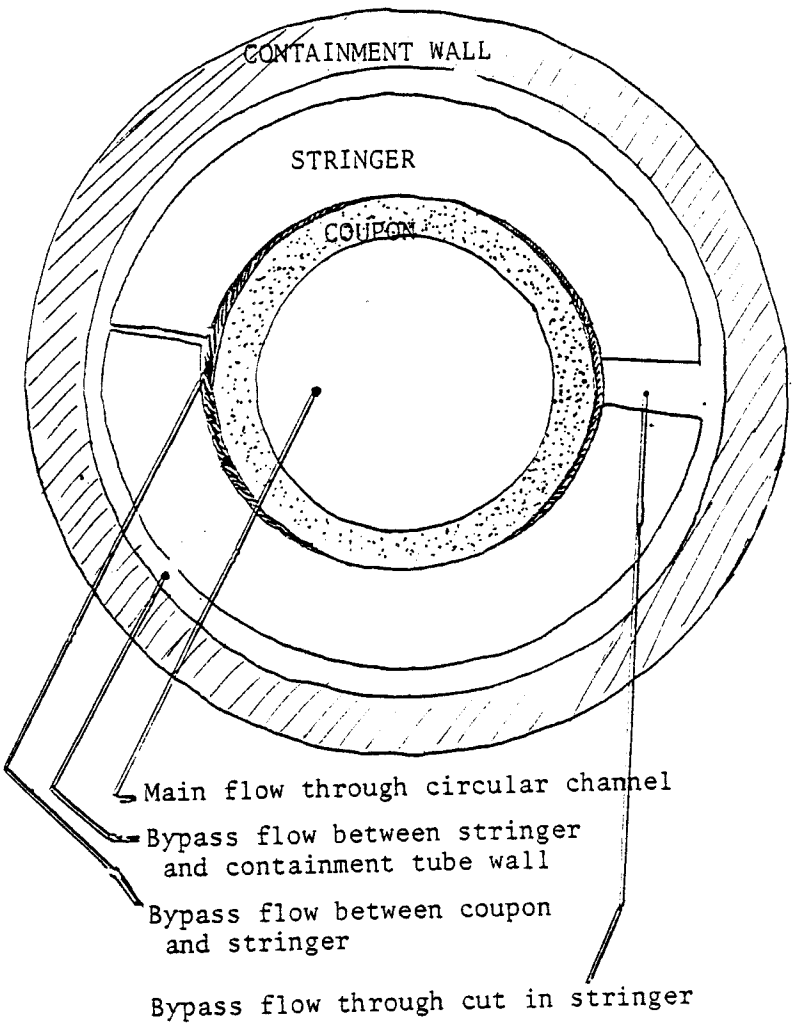

FIGURE V.8. Lithium bypass channels in coupon zone.

channels, the axial pressure gradient is assumed to be the same constant value. The product of the Reynolds number and the square root of the friction factor is (see, for example, Bird, Stewart and Lightfoot, 1960)

$$Re\sqrt{f} = \frac{D\langle v\rangle\rho}{\mu}\sqrt{\frac{(P_0-P_L)D}{2L\rho\langle v\rangle^2}} \qquad (V.5)$$

For length L of isothermal test section j

$$\frac{\rho}{\mu}\sqrt{\frac{P_0-P_L}{2L\rho}}\ D_j^{3/2} = Re_{ij}\sqrt{f}_{ij} \qquad (V.6)$$

$$B_i\ D_j^{3/2} = (Re\sqrt{f})_{ij}$$

where j represents the coupon interior flow or the bypass flow, and i represents the test section being considered.

$(Re\sqrt{f})$ is calculated for the flow on the inside of the coupon, assuming as a first approximation that all the lithium flow measured by the flowmeter is passing through the coupon. Since the hydraulic diameter of each bypass channel is known, $(Re\sqrt{f})$ may be calculated with equation (V.6). Once this value is known, the Reynolds number for each channel is determined, as follows.

$$\ln[f_{ij}] = -2\ln[Re_{ij}] + 2\ln[(Re\sqrt{f})_{ij}] \qquad (V.7)$$

Equation (V.7) is simply a logarithmic identity.

Next, the friction factor may be written

laminar flow in tubes	laminar flow in slits	turbulent flow in tubes
$f = \frac{16}{Re}$	$f = \frac{24}{Re}$	$f = \frac{0.0791}{Re^{1/4}}$

or, in general form

$$f = \frac{F}{Re^{E}} \qquad (V.8)$$

and, written with logarithms

$$\ln[f_{ij}] = \ln[F_j] - E_j \ln[Re_{ij}] \qquad (V.9)$$

Combination of equations (V.7 and V.9) gives

$$Re_{ij} = \frac{(Re\sqrt{f})_{ij}^{2/(2-E)}}{F^{1/(2-E)}} \qquad (V.10)$$

The flow rates in each channel j may now be determined from the Reynolds numbers (see Appendix S). The effect of bypass flow appears to be minor, as shown in Table V.5. The bypass flows all turn out to be laminar.

About half of the mass transferred into the bypass flows on the outside of the coupons is from the coupons' outside surface. This mass transfer was estimated as follows.

The fractional approach to saturation of the known laminar flow Q is

$$1 - \left[\frac{\omega_{i0}-\omega_{i2}}{\omega_{i0}-\omega_{i1}}\right] = 1 - \exp\left[-5.5\left(\frac{\mathcal{D}_i L}{Q_{ij}}\right)^{2/3}\right] \qquad (V.11)$$

A somewhat different form applies for turbulent flow. The

diffusivity may be estimated using the Stokes-Einstein equation

$$\mathcal{D}_i = \frac{KT}{6\pi\mu R_i} \qquad (V.12)$$

The atomic radius of iron, R =1.25 angstroms, is used.

The amount of mass transferred to the bypass flow, relative to the mass transferred to the flow in the inside of the coupon, is small. It is therefore appropriate to calculate steady state fluxes based on the inside area of the coupon. The extra mass loss is essentially independent of velocity. Bypass flows therefore do not explain the small velocity dependence. If the dissolution is not solely fluid-phase controlled, the relative loss to the bypass flow will be larger, and the apparent velocity effect will be smaller.

The foregoing analysis of bypass flow neglects entrance effects. The bypass calculations made here are simply estimates, and do not take into account the flow resistances, such as welds on the stringer, which should reduce the bypass flows while having little effect on the flow in the circular channel.

TABLE V.5. INFLUENCE OF BYPASS FLOWS

<v>	inside/total flow ratio	inside/total mass loss ratio	
1.4m/s	0.98	0.89	laminar
1.0	0.98	0.90	flow in
0.6	0.98	0.91	coupons
0.4	0.98	0.92	
1.4	0.89	0.95	turbulent
1.0	0.91	0.95	flow in
0.6	0.93	0.95	coupons
0.4	0.95	0.95	

MODEL FOR FLUID-PHASE CONTROLLED MASS TRANSFER

The mass transfer was modelled under the assumption that it is limited by fluid boundary layer diffusion. Axial diffusion and radial variations in the lithium properties are neglected. The resulting differential equation

$$\rho \frac{d\omega_{ib}}{dx} = \frac{4k_{\omega i}}{D<v>} (\omega_{i0}-\omega_{ib}) \qquad (V.13)$$

is solved by step-wise integration, which allows piping dimensions and lithium temperatures to be given in tables indexed by position, so that the variable coefficient can best be determined. The operating temperatures are taken from selected thermocouples around the loop. The lithium temperature is assumed to vary linearly between inlet and exit for the economizer, for the radiator, and for the heater. The temperature is assigned a constant value in the coupon zone. Lithium properties are written as functions of temperature (Maroni et al., 1973). The diffusivity of iron in lithium is found with the Stokes- Einstein equation (V.12), as suggested by Gill (1960) and Bonilla (1963).

SOLUBILITY OF IRON IN LITHIUM

Solubility data for iron in lithium (Figure V.9) show considerable variation. Jesseman's (1950) relatively high (1000ppm) values between 600C and 1000C are not included in Figure V.9. McKisson et al. discount the data because of the very low heat of solution indicated by the solubilities.

The most consistent data seem to be Leavenworth and Cleary's (1961) between 600C and 900C, and Bychov's (1962) from 900C to 1200C. (McKisson et al. (1966) report Leavenworth and Cleary's (1961) values 10 times lower than the actual data.) The Leavenworth and Cleary solubilities have heats of solution of about 14.2 kcal/mol (Kelly, 1961), which agree with Strauss' (1958) correlation relating the heat of solution ΔH to the ratio of the solvent to solute radii. An extrapolation of these data to 500C predicts a solubility of 4 ppm, which is consistent with the iron content of lithium in the present research, as measured by ion-coupled plasma spectrophotometry.

Beskoravaynyy and Yakovlev's iron solubility data (1962) for commercial lithium between 600C and 900C indicate a ΔH comparable to Leavenworth and Cleary's, but the solubility itself is 5 to 10 times greater. Beskoravaynyy's data for "pure" lithium shows lower solubilities in the same temperature range, but the ΔH is also lower. Sand's (1958) solubility "did not take into account a blank of approximately 60 to 80 ppm inherent in his method" (Mausteller, 1967); iron oxide on the test capsule walls apparently caused this

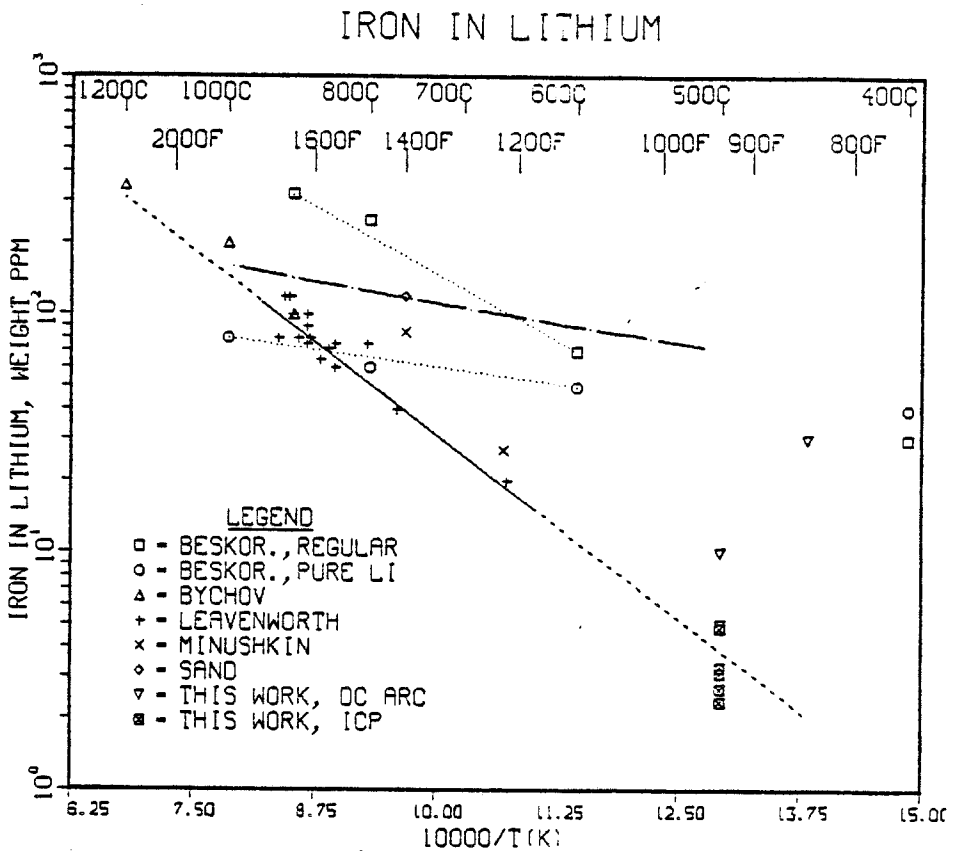

FIGURE V.9. Solubility of Iron in Lithium.

blank. If corrected Sand's data would agree fairly well with the Leavenworth and Cleary data.

Leavenworth and Cleary also measured solubilities for Ni, Cr, Ti, Nb, and Mo. Table V.6 shows the increases in solubility measured with increased nitrogen content of the lithium.

TABLE V.6. EFFECT OF NITROGEN ON SOLUBILITIES IN LITHIUM AT 1000K

solute	nitrogen ppm	solute ppm
nickel	146	2000
	220	20000
chromium	150	30
	790	70
titanium	55	6
	210	60
niobium	38	8
	70	100
	260	320

The effect of nitrogen on the solubilities of molybdenum and iron was not reported; the nitrogen levels used in the tests with these metals were 100ppm and 90ppm, respectively. The 90ppm nitrogen level in the iron solubility tests is comparable to the levels measured in the present research (Table V.3). Leavenworth's data for the other metals suggest that higher nitrogen levels might lead to higher solubilities; this is a possible explanation the higher values in Figure V.9.

An extrapolation of Leavenworth and Cleary's data was used in the mass transport model, in the form of a van t'Hoff solubility function with an heat of solution of 14.2 kcal/mol and a base solubility of 4 ppm at 500C. As a first approximation, only transport of iron is modelled, with a multiplying factor to account

for the alloying elements (predominantly chromium and nickel) in the steel. The iron, chromium and nickel contents are assumed to be 70, 18, and 12%w.

INTEGRATION OF DIFFERENTIAL EQUATION

Program METAL directs the solution of the loop differential equation (V.13). Subroutine CRUNCH adjusts the concentration level in the lithium by iterating until the periodicity condition on the concentration is achieved within $2 \times 10^{-12} g/cm^3$.

Once the periodicity condition is achieved, control returns to the main program. The mean modelled coupon fluxes can then be compared with the mean experimental coupon fluxes. As an option the solubility at the base temperature of 500C can be adjusted so that the modelled fluxes better fit the experimental fluxes. Here, the adjustment of the base solubility continues until the summation

$$\sum_{j=1}^{\text{runs}} \sum_{\text{sect}=1}^{4} \left(\bar{n}_{\text{theory}} - \bar{n}_{\text{experiment}} \right)^2 \qquad \text{(V.14)}$$

is reduced to a desired low value.

The numerical integration of equation (V.13) incorporating correlations to determine the mass transfer coefficient is used to traverse all of the loop except for the coupon zones, where superposition is used with equation IV.6 or IV.9 for the relaminarized flow between $(x\langle v\rangle\rho/\mu)=0$ and $(x\langle v\rangle\rho/\mu) = 4 \times 10^5$.

These equations are not used in the remainder of the loop because the flow elsewhere is turbulent.

PREDICTIONS OF THE MASS TRANSFER MODEL

The magnitudes of the measured mass fluxes are comparable to results of previous investigators (Gill et al., 1960-1961; Whitlow et al., 1979). However, the mass transfer model predicts dissolution fluxes 15 to 50 times greater than the measured fluxes. The fluxes predicted using the extrapolated solubility of iron (Figure V.9) are shown in Table V.7.

TABLE V.7 PREDICTIONS OF COMPUTER MODEL

Temperatures		Predicted Flux / Measured Flux			
Coupon	Min	<v>=1.4m/s	<v>=1.0	<v>=0.6	<v>=0.4m/s
440C	340C	26/0.9	22/0.8	18/0.6	15/0.7
440C	255C	33/2.9	27/2.5	23/2.0	19/1.8
490C*	325C	61/11.	52/10.	42/8.5	36/8.8
490C**	325C	61/1.5	52/1.4	42/1.0	36/0.8

* first 1300 hours
** 1300-2500+ hours

Experimental fluxes an order of magnitude lower than theoretical predictions are not unusual in liquid metal corrosion (Epstein, 1957). Mass transfer governed purely by liquid diffusion does not explain the results of the present research.

SOLUTE PARTICLES AND MASS TRANSPORT

Particles of solute circulating in the lithium have been suggested as a cause for low fluxes measured in sodium loops. Weeks and Isaacs (1973) noted that sodium taken from a loop usually contains as much or more iron than is soluble at T_{max}, using any of the available solubility data. When low fluxes are measured in liquid metal loops, the change in solute concentration between hot and cold zones should be correspondingly low (DeVan and Sessions, 1967). The liquid metal in much of the loop may accumulate solute in particles in order to relieve supersaturation. In-stream mass transfer (precipitation and dissolution of particles) would reduce fluxes at the containment walls.

Particles might also be present in the non-flow capsule tests used to measure solubilities. This hypothesis could explain the wide variations in the solubilities reported for transition metal solutes in alkali metals. However, in solubility tests, the melt temperature is generally held constant for long times in order to allow equilibrium. In flow experiments, on the other hand, it is possible and even usual for the liquid metal to be heated or cooled 200C degrees in less than one minute. Because of the high thermal conductivities and consequent low Prandtl numbers of liquid metals, the entire fluid cross- section is near the wall temperature. However, because of the high Schmidt number, mass transfer by diffusion to the wall is relatively slow and supersaturation is to be expected in regions where the liquid metal is being cooled.

Therefore much of the solute in a liquid metal flow loop might precipitate and subsequently redissolve in the lithium stream itself, reducing the wall flux. Isaacs and Singer (1970) have confirmed the presence of iron particles in sodium from a forced convection thermal gradient loop.

The flux measured in the present research at 490C is less than 10 $ug/m^2/s$. The hot zone pipe wall area is about 2 m^2. The lithium flow rate is 50 g/s. Assuming that the fluxes at the coupons are representative of the entire hot zone, the change in concentration $\Delta\rho_i$ between the hot and cold zones is

$$\Delta\rho_i = \frac{10\ ug}{m^2\ s}\quad 2m^2\quad \frac{s}{50g} = 0.4\ ppm$$

This change is about 10% of the extrapolated solubility of 4 ppm iron at 500C, or 20% of the 2-3 ppm measured in the loop. These numbers suggest that the lithium is supersaturated in the cooled zone (this by itself would cause a relatively high flux to the walls) or that particles are formed to relieve the supersaturation of the lithium each time it passes through the cooling zone.

An order of magnitude estimate of the particle mass transfer is made by adding a term to equation (V.13)

$$\rho\frac{d\omega_{ib}}{dx} \quad \frac{(\omega_{i0}-\omega_{ib})}{\langle v\rangle}\left[\frac{4k_{\omega i}}{D} + A_p\ k_{\omega pi}\right] \qquad (V.15)$$

where A_p is the particle surface area per unit volume of lithium, and $k_{\omega pi}$ is the particle mass transfer coefficient.

The area of a single (spherical) particle is πD_p^2 and its mass

is $\frac{4}{3}\rho_p \pi D_p^3$. If the weight fraction of iron particles in the lithium is ε , then with the densities of lithium and iron taken as 0.5 and 8.0 g/cm^3, the surface area A_p of particles in a cubic centimeter of lithium, is

$$A_p = \frac{3\varepsilon\rho_p}{4D_p\rho_p} = \frac{3\ \varepsilon}{64D_p} \qquad \text{(V.16)}$$

The mass transfer coefficients may be written in terms of Nusselt numbers

$$k_{\omega i} = \frac{Nu_i \rho \mathcal{D}_i}{D} \qquad k_{\omega pi} = \frac{Nu_p \rho \mathcal{D}_i}{D_p} \qquad \text{(V.17)}$$

The bracketed terms in equation (V.15) are then

$$\left[\frac{4Nu_i}{D^2} + \frac{3\varepsilon\ Nu_p}{64\ D_p^2} \right] \rho \mathcal{D}_i \qquad \text{(V.18)}$$

and the mass transfer contribution of the particles relative to the wall is the ratio of the second term to the first:

$$\frac{3\ \varepsilon}{256} \frac{Nu_p}{Nu_i} \quad (D/D_p)^2 \qquad \text{(V.19)}$$

The Nusselt number for the wall is about 100 in most of the loop. For stationary spheres, the Nusselt number is 2, and this is a lower bound on the value for the particles. The ratio (V.19) is therefore

$$\frac{3}{12800}\ \varepsilon\ (D/D_p)^2 \qquad \text{(V.20)}$$

With a pipe diameter of about 2 cm and an assuming an iron particle content ε =2ppm=$2x10^{-6}$, particles 0.1 microns in diameter would transfer 18 times as much solute to and from the lithium as would the pipe wall.

Weeks and Isaacs (1973) describe a computer model for particulate iron mass transfer in a steel-sodium system. Particles 1 micron in diameter are assumed to be present at a 20 ppm level. The diffusion boundary layer around each particle is assigned a thickness of 10 microns. The flux of iron from the particles is written

$$\mathcal{D}_i \, (\omega_{i0} - \omega_{ib}) \, \frac{F}{Z} \qquad \text{(V.21)}$$

where Z represents the diffusion boundary layer thickness and F is a "fudge factor" to account for the difference between the wall mass transfer rate and the particle mass transfer rate.

Inspection of equations (V.15) and (V.21) shows that $\mathcal{D}_i F/Z = k_{\omega pi}$. However, $k_{\omega pi}$ equals the diffusivity divided by the true boundary layer thickness. For a Nusselt number of 2, the boundary layer thickness for a sphere is one half of the sphere diameter. In the case cited by Weeks and Isaacs, the thickness Z should be 0.5 microns, not 10 microns. This is one reason why large "fudge factors" (100-1000) are needed to produce significant flux contributions from the particles in the example cited.

The size of the particles is unknown, but is of great importance, since the amount of particle mass transfer is inversely

proportional to the square of the particle size. Mass transfer to and from the particles will cause their size, and perhaps their number, to vary around the loop. These variations become particularly large in loops such as ours where the total iron content (dissolved and particulate) is near the solubility at the maximum temperature. In such cases, the particles might dissolve completely in the hot zone.

If virtually no particles return to the cooling zones, no instream deposition would occur despite supersaturation until nucleation sites have formed. Meanwhile the usual wall deposition will continue. Once nucleation begins, the wall flux will be reduced; it subsequently could be very low if nucleation proceeds rapidly.

For temperature-driven phase transformations in solid metals, a certain maximum degree of "subcooling" (or in a sense, supersaturation) can be tolerated before the unstable phase begins to transform to the new phase. This is called "spinodal decomposition." On the phase diagram (temperature vs. composition) a spinodal line will typically lie some variable distance ΔT below the coexistence line (Rundman,1973). Knowledge of an analogous curve showing the maximum degree of subcooling of iron-saturated lithium, would allow calculation of an upper bound on the amount of iron transferred to the wall before any particulate precipitation began.

While particles could give smaller corrosion rates, as observed

in the loop, their presence would not explain the weak velocity dependence of the corrosion. All four test sections are fed from a common manifold and are geometrically similar. Lithium, and any accompanying particles, travels slowest in the lowest velocity test section. Therefore the dissolution of the particles would presumably be more complete in the lowest velocity test section. The driving force for subsequent dissolution from the wall will be lowest in that section. Particles should therefore enhance the velocity effect.

Particles might have an effect on the position dependence of the flux. The usual decrease in flux with increasing downstream position is due to a thickening of the concentration boundary layer at the wall, which is normally the only solute source. If particles are present, each will generate its own diffusion boundary layer. Should a large number of particles supply solute into the mainstream itself, the mass flux at the wall might remain more nearly constant.

SOLID PHASE RESISTANCE

The foregoing discussion has considered only liquid-phase resistance to the mass transfer. In the cooled zone, interfacial or solid resistance is considered unimportant, but in the heated zone interfacial or solid resistances might be significant.

The electron microprobe profiles (Figures V.7) show that the exposed coupons develop ferrite layers 10-20 microns thick, which are depleted of nickel and chromium. This substantiates the optical micrographs (Figures V.4) and suggests that the ferrite layer itself

could be a significant resistance to diffusion.

If a pseudo-steady state is ultimately reached, with the iron, chromium, and nickel being removed from the steel at rates proportional to their percentages in the bulk alloy, then at least for nickel there must be a resistance besides the fluid boundary layer. If this were not so, the iron and nickel at least could not be removed in the proper proportions, since the lesser constituent (nickel) is much more soluble in lithium.

After an initial period in which nickel and perhaps chromium are preferentially removed from the surface of the steel, the exposed surface becomes nearly pure iron. In such a case the concentration of iron at the wall is constant. Assuming that there is no solid or interfacial resistance for iron, the flux of iron into a developing laminar boundary layer is given by equation (IV.6). Stoichiometric removal of nickel requires that the nickel flux be proportional to the iron flux; this in turn means that the nickel concentration at the lithium- steel interface must be constant. The concentration driving force for the nickel dissolution will be divided between the liquid boundary layer resistance and a solid or pore diffusion resistance. In order for the surface concentration of nickel to remain constant, the ratio of the liquid and solid resistances must be constant. In particular, if there is a sharp interface between the nickel-depleted surface ferrite layer and the parent austenite further within the coupon, then the thickness of the ferrite "boundary layer" will have the

same position dependence as the thickness of the liquid boundary layer.

If nickel is depleted from the surface of the coupons; one may assume that nickel atoms reach the surface by some sort of solid phase diffusion, most likely facilitated by some pore structure, since the solid phase diffusion coefficient is very low.

INTERFACIAL RESISTANCE

If interfacial dissolution of iron is not rapid compared with liquid diffusion of the dissolved iron, then a significant interfacial resistance will exist in series with the liquid boundary layer resistance. The apparent mass transfer coefficient, provided that the interfacial step is first order, is

$$k_{apparent} \cong \frac{1}{(1/k_{\omega i}) + (1/k'')} \qquad (V.22)$$

At a given temperature, the interfacial coefficient k" is constant, while the mass transfer coefficient k_{ω_i} varies with the fluid velocity. Figures V.10 show the effect of the series interfacial resistance on the velocity effect observed for k_{app}. Laminar developed, laminar entrance, and turbulent flows are considered, that is, $k_{\omega i}$ is varied as the 1/3, 1/2 and 8/10 power of the velocity. The interfacial rate constant k" is assigned values ranging from infinity to 1/4 of the mass transfer coefficient $k_{\omega i}$ for the lowest velocity. On a logarithmic plot the velocity

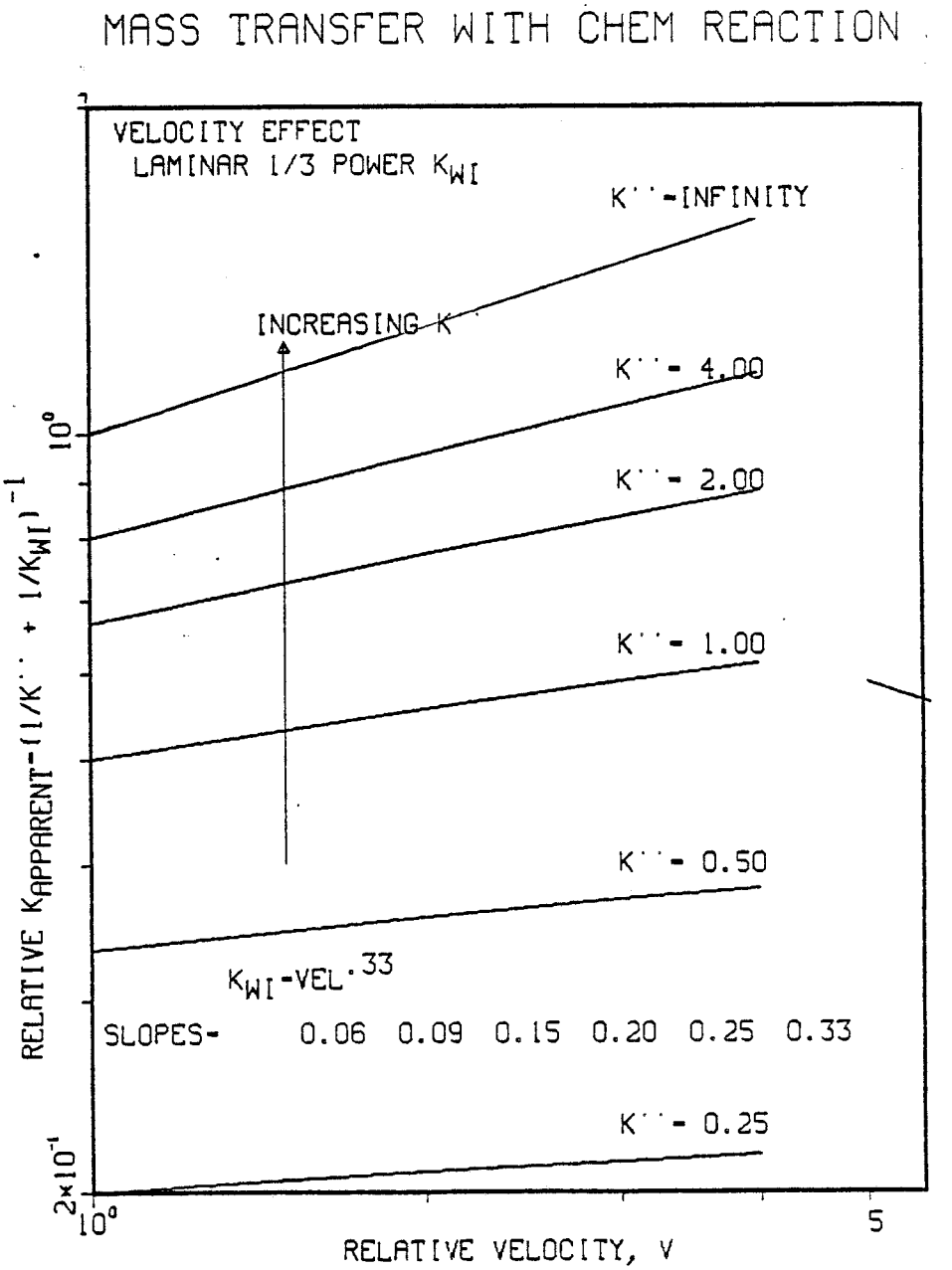

FIGURE V.10a. Interfacial resistance: effect on velocity dependence of overall dissolution rate constant.

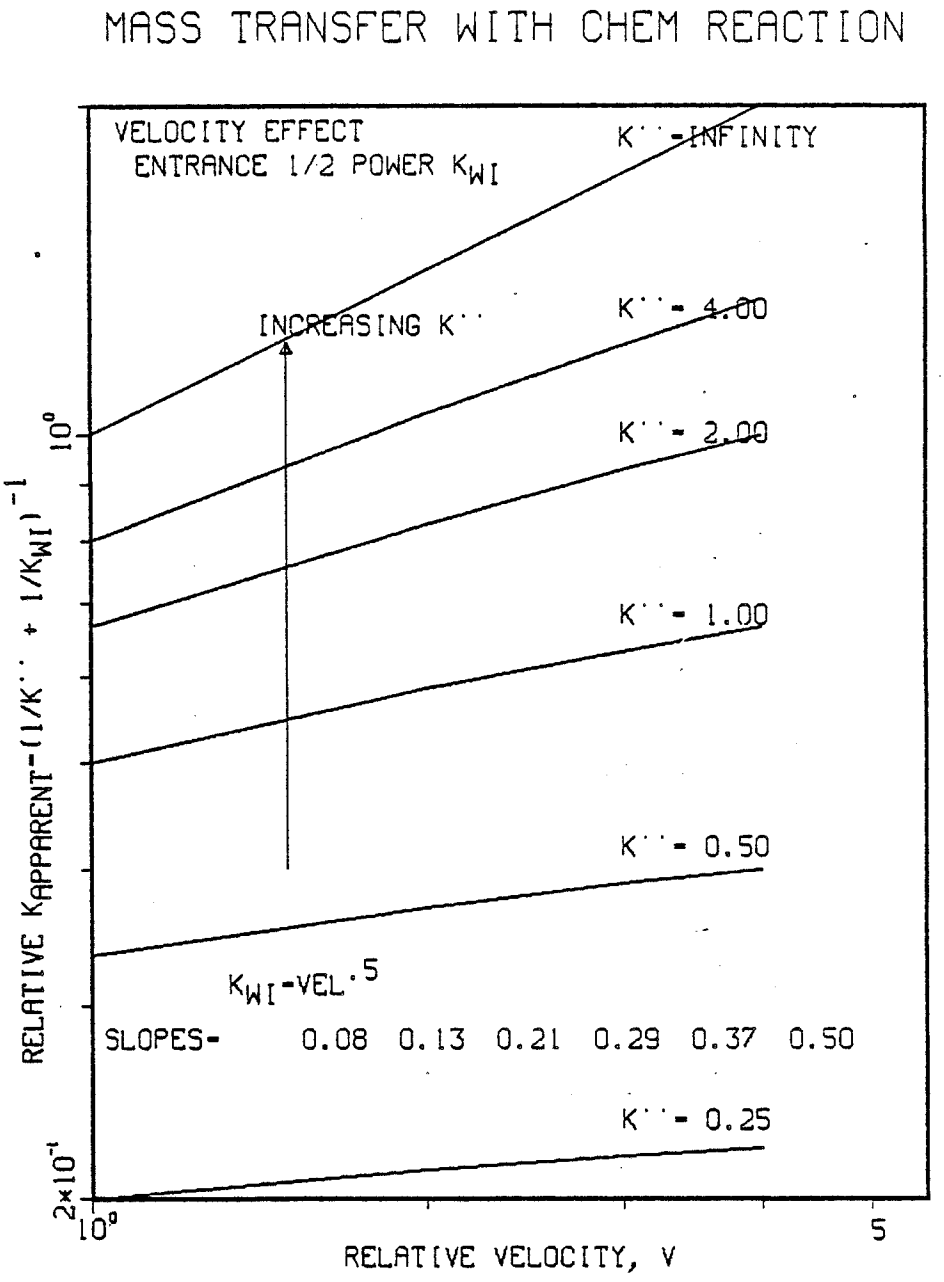

FIGURE V.10b. Interfacial resistance; effect on velocity dependence of overall dissolution rate constant.

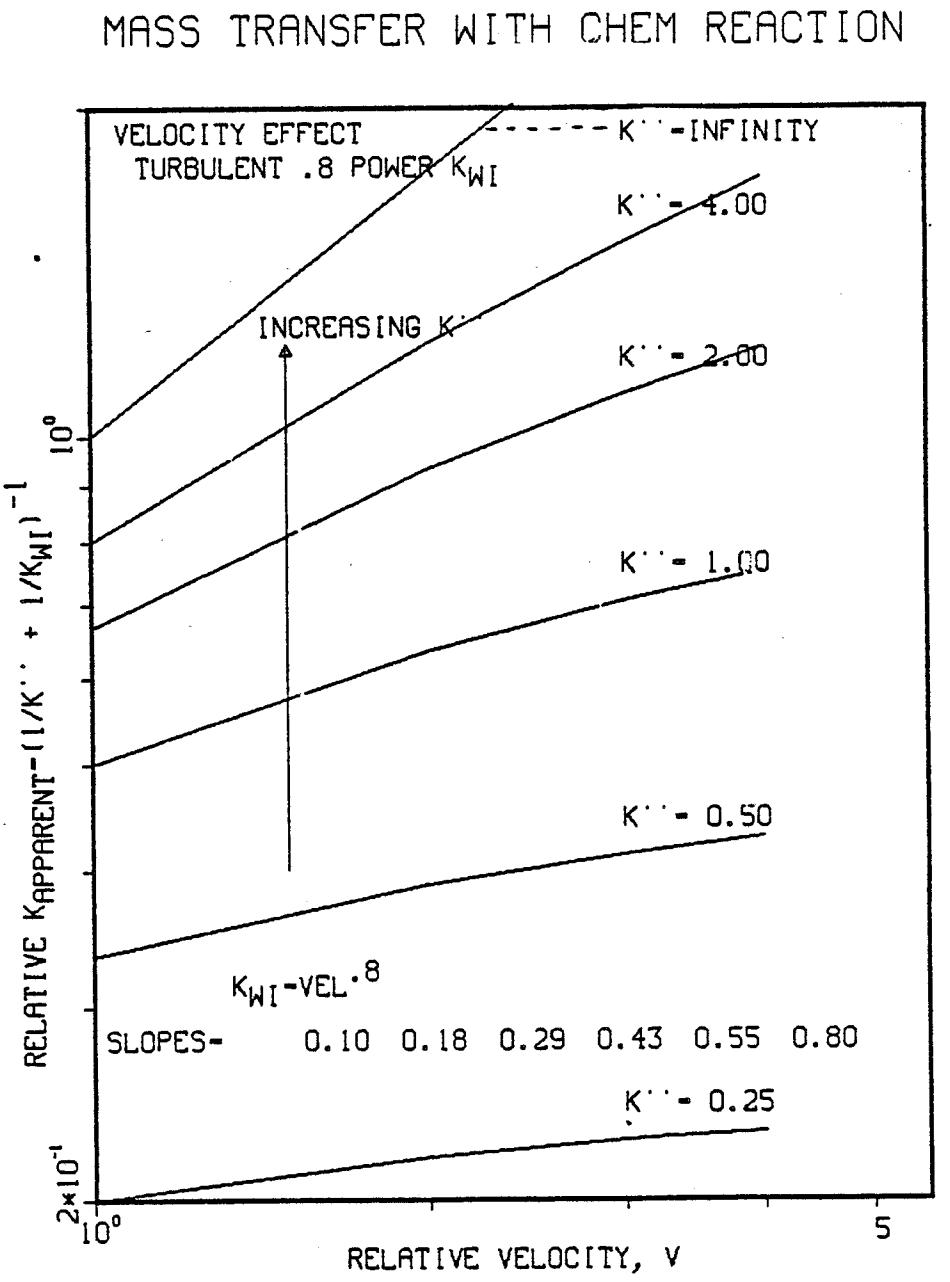

FIGURE V.10c. Interfacial resistance; effect on velocity dependence of overall dissolution rate constant.

dependence of k_{app} is almost linear even for finite values of k". Depending on the type of flow considered, apparent velocity exponents from 1/4 to 1/2 (as seen in the present research) require that k" be from 1 to 4 times the mass transfer coefficient for the lowest velocity. The interfacial resistance would also weaken the position dependence of the mass transfer.

The development given above considers the mass transfer coefficient to be independent of the interfacial coefficient. This is only an approximation. A more rigorous treatment of mass transfer with a surface reaction is given, for instance, by Acrivos and Chambre (1957).

AUSTENITE-FERRITE TRANSFORMATION

The austenite-ferrite transformation may also affect the corrosion rate. The diffusivities of nickel and chromium in ferrite are as much as 100 times greater than in austenite. Once transformation to ferrite begins, the nickel should leave the steel more rapidly, destabilizing the austenite further and hastening the transformation to ferrite. However, since ferrite is more stable than austenite at 500C, it might be less soluble in lithium. Indeed, Whitlow et al. (1979) show that ferritic stainless steels were attacked only 1/3 as rapidly as austenitic stainless steels during a 1000 hour test in lithium at 538C. Part of the difference may be due to the rapid dissolution of the nickel from the austenitic steels.

EFFECT OF TEMPERATURE ON DISSOLUTION RATE

The data for 440C coupon temperature show an apparent effect of temperature difference ΔT on the mass flux. The dissolution rates measured with a ΔT of approximately 200C degrees are 3 to 4 times greater than the rates for a ΔT of 100C (see Table V.1). Presumably the overall driving force for mass transfer in a temperature gradient loop such as ours is the difference in solubilities between the hot and cold zones. This solubility driving force differs by about 20% between the two runs with 440C coupon temperature. The measured fluxes, however, differ by a factor of three or four.

The long-term mass loss rate observed at 490C is lower than that seen at 440C, despite the fact that the solubility is about three times higher and the mass transfer coefficients (and any interfacial rate constant) should be greater at the higher temperature. A change in the lithium composition during the month-long shut-down is a possible reason for the reduced rate. Perhaps the nitrogen level was raised by the repeated draining and filling during the downtime. Tortorelli et al. (1980) noted that in their thermal convection stainless steel loop, high initial levels of nitrogen in the lithium decreased the corrosion rate. However, the lithium analyses before and after our shutdown do not seem to differ significantly.

If the lithium composition does not explain the reduced long-term corrosion rate at the higher temperature, then a change in

the steel surface must have occurred to reduce the rate. Transformation of the less stable (and therefore presumably more soluble) austenite to ferrite might explain the reduced rate. The rate of diffusion of nickel through the steel, relative to the rate of iron removal from the steel surface, may be faster at higher temperatures, which could cause the austenite-ferrite transformation to occur sooner at the higher temperature. If the transformation has occurred at 490C but did not occur at 440C, then the smaller rate at 490C is understandable because the condition of the steel is different. The linear mass loss observed at 440C may have been taking place before the austenite-ferrite occurred, in which case the long term rate at 490C is not directly comparable to the rates at 440C.

The linearity of the mass loss curves at 440C at first suggests that a layer of ferrite, with a constant thickness, had been formed on the coupons after as little as 1000 hours of exposure to the lithium. The time of 1000 hours is mentioned by Tortorelli and DeVan (1979) as the time at which linearity was seen in their lithium loop at 600C. However, at the lower temperatures used in the present research, this development might occur at much later times.

The mass loss measured for pull 11 at 440C was unusually small (for some coupons, it was unexplainably negative), which might signal impending changes in the mass loss behavior. However, the 440C run was ended at that point.

The cumulative mass loss is the same at pull 11 (440C) as at pulls 16-17 (490C). Perhaps the austenite- ferrite transformation occurs after a critical amount of material has been removed from the steel surface. The cumulative mass loss in question is from 30 to 60 ug/m^2, equivalent to 4-8 microns of steel (density =8g/cm^2). If this were predominantly nickel and chromium (which make up ~ 30% of the steel) the subsequent depleted layer would be 12 to 25 microns thick. Unless this layer was completely free of Ni and Cr, removal of 30-60 ug/m^2would give a somewhat thicker layer. However, recession of the iron from the surface would at the same time reduce the depleted thickness.

Optical micrographs (Figures V.4) and microprobe profiles (Figures V.7) show a depleted layer about 10-20 microns thick on the coupons. This thickness agrees with the thickness calculated from the weight loss.

COMPARISON OF DISSOLUTION RATES WITH PREVIOUS INVESTIGATIONS

The mass fluxes observed here are compared on Table II.1 with results from previous investigations. All the data shown are fairly consistent, given the differences in maximum temperature, temperature difference, and velocity, each of which is shown in the present research to significantly affect the dissolution rate.

The present research is most similar to that of Whitlow et al. (1979). The initial fluxes measured here at a 490 C coupon temperature are slightly higher than Whitlow's values, despite the lower temperature used here. This difference may not be particularly important, given the marked reduction in our rates after the first 1300 hours of the run.

TABLE II.1 INVESTIGATIONS OF CORROSION OF STAINLESS STEEL BY LIQUID LITHIUM

LAB	MATERIALS	T max	T diff	VELOCITY	TIME	CORROSION RATE OR AMOUNT
Oak Ridge (Hoffman,1960)	310 SS 347 SS	732 C 538 C	280 C 212 C	2.4-3 m s^{-1} 2 cm s^{-1}	23-53 hrs 3000 hrs	1000 ug m^{-2} s^{-1} (high) 75 microns irregular
Col. Schl. Mines (Olson, 1974-5)	304L SS	800 C	static test	static test	150 hrs	0.7 ug m^{-2} s^{-1}
Oak Ridge (DeVan,1975-9)	316 SS	600 C	200 C	natural convection	2500-7500 hrs	3 ug m^{-2} s^{-1}
Syracuse U. (Gill, 1960-1)	304 SS	420-612 C	10-212 C	.16-.85 m s^{-1}	100 hrs	4 ug m^{-2} s^{-1} @ 500C
JAERI (Nihei,1974)	316 SS	600 C	100 C	natural convection	2500 hrs	3 ug m^{-2} s^{-1} @ 600C
Westinghouse (Whitlow,1979)	316 SS	538 C	165 C	1.82 m s^{-1}	900 hrs	8 ug m^{-2} s^{-1}
University of Wisconsin --current-- (nominal conditions)	316 SS	450 C	195 C	.4-1.4 m s^{-1}	4000 hrs	1.8-2.9 ug m^{-2} s^{-1}
		450 C	110 C	.4-1.4 m s^{-1}	3900 hrs	0.6-0.9 ug m^{-2} s^{-1}
		500 C	175 C	.4-1.4 m s^{-1}	1300 hrs 2900 hrs	~10 ug m^{-2} s^{-1} 0.8-1.5 ug m^{-2} s^{-1}

Corrosion rates are given in each case for coupons located in the hot zone of the loop.

CONCLUSIONS

The dissolution of type 316 stainless steel by lithium at 440C and 490C in a forced convection thermal gradient loop is strongly influenced by fluid diffusion. A definite velocity effect (pp.134, 135) is evidence of fluid phase control. Dissolution may be partly controlled by interfacial or solid phase resistances (pp. 174 ff).

The local mass fluxes in the isothermal test zone are weakly position dependent, and in some cases indicate that the lithium flow has been laminarized upon entering the coupons. The position dependence of the mass flux lends further support to the fluid-diffusion-control hypothesis.

The measured dissolution rates are 10 to 50 times lower than the rates predicted by boundary layer theory using an extrapolation of the available solubility data. Sub-micron-sized iron particles circulating in the lithium is a likely explanation for the smaller wall fluxes (pp. 167 ff).

The dissolution rate of type 316 stainless steel decreases toward a steady value during the first 1000 hours of exposure to the lithium. At 490C the eventual steady dissolution rate is less than the rate at 440C for the same ΔT. The transformation of the surface of the steel from the parent austenite to a more stable ferrite layer may explain the reduced flux. This transformation may be imcomplete at the lower temperature test conditions.

RECOMMENDATIONS

More extensive metallurgical studies should be made of the mass transfer coupons to explain the solud phase corrosion processes. A large number of lithium-exposed coupons are available for such study.

Additional work should be done to elucidate the role of fluid diffusion and particle mass transfer in the corrosion process. A smaller, simpler loop with better defined flow conditions would be especially useful for a more exact analysis of the fluid phase processes.

The present research equipment is in good condition and is well suited for further studies, using either lithium or another candidate reactor coolant, such as a lithium-lead eutectic.

NOTATION

A_p	surface area of particles per unit volume of fluid
a(T)	parameter in equation (V.1)
$\hat{C}_p$	heat capacity at constant pressure
D	diameter of pipe
D_p	diameter of particle
$\mathcal{D}_i$	mass diffusivity of species i in mixture
F	"fudge" factor, equation (V.21)
f	friction factor, equation (V.5)
$\underline{g}_i$	body force, equation (IV.2)
Gz	Graetz number, x/(Re Pr D)
ΔH	heat of solution
h	heat transfer coefficient
j_H	j factor, $Nu\ Re^{-1}\ Pr^{-1/3}$
$\underline{j}_i$	mass flux with respect to velocity $\underline{v}$
K	relaminarization parameter, equation(IV.24)
$k_{\omega i}$	wall mass transfer coefficient for species i, based on mass fraction
$k_{\omega pi}$	particle mass transfer coefficient,species i, based on mass fraction
k''	interfacial rate constant
k_{app}	apparent mass transfer coefficient (eqn. V.22)
K	Boltzmann constant
k	thermal conductivity

NOTATION (CONTINUED)

L	length of transfer section
M	total mass loss
m	parameter in equation (V.1)
$\underline{n}_i$	mass flux of species i based on fixed coordinates
$\bar{n}$	mean mass flux
Nu	Nusselt number for heat transfer hD/k
Nu_i	Nusselt number for mass transfer, $k_{\omega i} D/(\rho \mathcal{D}_i)$
p, P	pressure
q_0	interfacial heat flux
r	radius of pipe
r_i	homogeneous generation term, equation (IV.3)
Re	Reynolds number $D\langle v\rangle\mu/\rho$
Re_x	Reynolds number $xv_\infty\rho/\mu$ or $x\langle v\rangle\rho/\mu$
R_i	atomic radius of species i
T	absolute temperature
t	time
u_∞	velocity in free stream
$\underline{v}$	velocity vector
$\langle v\rangle$	velocity averaged over pipe cross section
x	axial position coordinate
Z	boundary layer thickness in equation (V.21)
z	circumferential position coordinate

NOTATION (CONTINUED)

α	diffusivity of heat, $k/(\rho\hat{C}_p)$
ε	mass fraction of particles in liquid
μ	viscosity
ν	diffusivity of momentum, μ/ρ
ξ	dummy x variable
π	3.14159...
ρ	mass concentration (density)
ρ_p	bulk density of particle
$\underline{\underline{\tau}}$	viscous stress tensor (equation IV.2)
χ	coefficient in equations (IV.6-8)
ω_i	mass fraction of species i
$\Gamma(n)$	gamma function of n

subscripts

b	conditions far from interface
i	species i
p	particle
0	conditions at interface
∞	conditions far from interface
1	conditions at inlet to transfer section
2	conditions at outlet of transfer section